

TRACK STIFFNESS Measurement System Evaluation Program



**FINAL REPORT
DECEMBER 1979**

This document is available to the public through
The National Technical Information Service,
Springfield, Virginia 22161

Prepared for
U.S. DEPARTMENT OF TRANSPORTATION
FEDERAL RAILROAD ADMINISTRATION
Office of Research and Development
Washington, D.C. 20590

NOTICE

This document is disseminated under the sponsorship of the Department of Transportation in the interest of information exchange. The United States Government assumes no liability for the contents or use thereof.

NOTICE

The United States Government does not endorse products or manufacturers. Trade or manufacturer's names appear herein solely because they are considered essential to the object of this report.

1. Report No. FRA/ORD-79/30	2. Government Accession No.	3. Recipient's Catalog No.	
4. Title and Subtitle Track Stiffness Measurement System Evaluation Program		5. Report Date December 1979	
		6. Performing Organization Code	
7. Author(s) G. Hayes, P. Joshi, J. Sullivan*		8. Performing Organization Report No. DOT-FR-79-30	
9. Performing Organization Name and Address Engineering Test and Analysis Division ENSCO, Inc. 2560 Huntington Avenue Alexandria, VA 22303		10. Work Unit No. (TRAIS)	
		11. Contract or Grant No. DOT-FR-64113	
12. Sponsoring Agency Name and Address U. S. Department of Transportation Federal Railroad Administration (ORSR) 400 Seventh Street, S. W. Washington, DC 20590		13. Type of Report and Period Covered Final Report	
		14. Sponsoring Agency Code	
15. Supplementary Notes * At the time he contributed to this report, Mr. Sullivan was employed by the Southern Railway System. He is currently employed by the FRA.			
16. Abstract This report describes a three-phase program to develop and evaluate an on-board, track stiffness measurement system. High correlation has been established between observed variations in track stiffness signatures and the actual conditions of track structures and subgrade. Track stiffness and track geometry were found to be independent and complementary measurements. A detailed study of long-and short-span bridge stiffness signatures was conducted. An analytical study of the relationship of the mid-chord-offset difference to absolute stiffness for bridge structures and continuous roadbed was made. Theoretical stiffness models were matched to actual short-span bridge stiffness signatures.			
17. Key Words Bridge stiffness signatures. Absolute stiffness. Mid-chord-offset. Theoretical stiffness models. Dual profile measurement system.		18. Distribution Statement Document is available to the public through National Technical Information Service, Springfield, VA 22151	
19. Security Classif. (of this report) Unclassified	20. Security Classif. of this page Unclassified	21. No. of Pages 166	22. Price

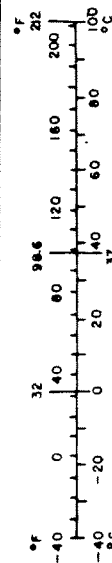
METRIC CONVERSION FACTORS

Approximate Conversions to Metric Measures

Symbol	When You Know	Multiply by	To Find	Symbol
LENGTH				
in	inches	2.5	centimeters	cm
ft	feet	30	centimeters	cm
yd	yards	0.9	meters	m
mi	miles	1.6	kilometers	km
AREA				
in ²	square inches	6.5	square centimeters	cm ²
ft ²	square feet	0.09	square meters	m ²
yd ²	square yards	0.8	square meters	m ²
mi ²	square miles	2.6	square kilometers	km ²
	acres	0.4	hectares	ha
MASS (weight)				
oz	ounces	28	grams	g
lb	pounds	0.45	kilograms	kg
	short tons (2000 lb)	0.9	tonnes	t
VOLUME				
tsp	teaspoons	5	milliliters	ml
Tbsp	tablespoons	15	milliliters	ml
fl oz	fluid ounces	30	milliliters	ml
c	cups	0.24	liters	l
pt	pints	0.47	liters	l
qt	quarts	0.95	liters	l
gal	gallons	3.8	liters	l
ft ³	cubic feet	0.03	cubic meters	m ³
yd ³	cubic yards	0.76	cubic meters	m ³
TEMPERATURE (exact)				
°F	Fahrenheit temperature	5/9 (after subtracting 32)	Celsius temperature	°C

Approximate Conversions from Metric Measures

Symbol	When You Know	Multiply by	To Find	Symbol
LENGTH				
mm	millimeters	0.04	inches	in
cm	centimeters	0.4	inches	in
m	meters	3.3	feet	ft
m	meters	1.1	yards	yd
km	kilometers	0.6	miles	mi
AREA				
cm ²	square centimeters	0.16	square inches	in ²
m ²	square meters	1.2	square yards	yd ²
km ²	square kilometers	0.4	square miles	mi ²
ha	hectares (10,000 m ²)	2.5	acres	
MASS (weight)				
g	grams	0.035	ounces	oz
kg	kilograms	2.2	pounds	lb
t	tonnes (1000 kg)	1.1	short tons	
VOLUME				
ml	milliliters	0.03	fluid ounces	fl oz
l	liters	2.1	pints	pt
l	liters	1.06	quarts	qt
l	liters	0.26	gallons	gal
m ³	cubic meters	35	cubic feet	ft ³
m ³	cubic meters	1.3	cubic yards	yd ³
TEMPERATURE (exact)				
°C	Celsius temperature	9/5 (then add 32)	Fahrenheit temperature	°F



*1 in = 2.54 (exact). For other exact conversions and more detailed tables, see NBS Misc. Publ. 286, Units of Weights and Measures, Price \$2.25, SD Catalog No. C13.10-286.

ACKNOWLEDGEMENTS

The success of this program was made possible through the dedication of members of the Southern Railway System, Eastern Division in Virginia and the Western and Alabama Divisions in Kentucky, Tennessee and Alabama. Preparation and operation of the R-1 and T-7 test vehicles were effectively accomplished by Southern Railway and ENSCO personnel. The initial tests and system concepts were the work of J. Corbin and G. Gunn of ENSCO. Continuity in the tests and much of the experiment design can be attributed to Dr. R. Owings and W. Szabo of ENSCO. Special thanks are reserved for W.S. Lovelace, Manager Research and Tests, Southern Railway System and Chairman, Track-Train Dynamics, Track Strength Characterization Working Group and Dr. A. Zarembski, Manager - Track Research, and Vice Chariman, Track Strength Characterization Working Group, Association of American Railroads (AAR) for their assistance in the field investigations.

TABLE OF CONTENTS

Section	Title	Page
1.0	INTRODUCTION	1
1.1	General	1
1.2	Background	2
1.2.1	Need for Track Stiffness Measurement	2
1.3	Report Organization	5
2.0	BASIC THEORY	7
2.1	Track Supported by an Elastic Roadbed	10
2.2	Chordal Measurement System	12
2.3	Profilometer Measurement System	14
3.0	TEST RESULTS	21
3.1	Phase I	21
3.1.1	Reasons for the Test	21
3.1.2	Test Zone	22
3.1.3	Test Results	22
3.2	Phase II	22
3.2.1	Reasons for the Test	22
3.2.2	Test Zone	23
3.2.3	Test Results	23
3.2.4	Test to Test Differences	23
3.3	Phase III	24
3.3.1	Reasons for the Test	24
3.3.2	Test Zone	24
3.3.3	Test Results	29
3.3.4	Test to Test Differences	30
4.0	CONCLUSIONS AND RECOMMENDATIONS	33
5.0	REFERENCES	39
APPENDIX A	Mathematical Modeling	A-1
APPENDIX B	Test Zone Descriptions	B-1
APPENDIX C	Data Processing	C-1
APPENDIX D	Instrumentation	D-1

LIST OF ILLUSTRATIONS

Figure No.	Title	Page
2-1	Base Stiffness Experiment	8
2-2	Beam on a Continuous, Elastic Supporting Foundation	10
2-3	Mid-Chord-Offset Measurement	13
2-4	Mid-Chord-Offset Measurement Using Three-Axle Truck	13
2-5	Track Stiffness Measurement Using Mid-Chord-Offset Measurement	14
2-6	Inertial Profilometer Measurement System - Schematic Diagram	15
2-7	Mid-Chord-Offset Constructed by Profilometer	15
2-8	Response of Track Stiffness System to Track Geometry	16
2-9	Measured MCO Displacement Versus Track Compliance	18
2-10	Response of Track Stiffness System to a Step Change in Track Support Modulus	19
3-1	Relative Stiffness on a Per Mile Basis	25
3-2	Signature of MCO-Difference for Short Spans ($11 \text{ Feet} \leq \ell \leq 22 \text{ Feet}$) with Flexible Supports. $\Delta/\ell = 0.423$	31
3-3	Solution for $EI/\kappa\ell^3 = 0.35$, $EI = 1.7 \times 10^{11}$, $\kappa = 9.01 \times 10^4 \text{ lbf/in.}$ Comparison with Field Data for Bridge at MP 87.50 MB	32
A-1	Inertial Profile of Loaded Track	A-2
A-2	MCO Measured by Beam System of Length 2Δ	A-3
A-3	Deflections Caused by a Three-Axle Truck	A-5
A-4(a)	Two Adjacent Simply Supported Spans of Equal Length	A-10
A-4(b)	Simply Supported Beam	A-10
A-5	Wheel Locations for a Long Span Bridge	A-11

LIST OF ILLUSTRATIONS (CONT)

Figure No.	Title	Page
A-6	Signature of MCO-Difference for a Simply Supported Span with Length $\ell \geq 4\Delta$	A-15
A-7	Signature of MCO-Difference for a Fixed End Span with Length $\ell \geq 4\Delta$	A-21
A-8	MCO-Difference Signature for Accotink Bridge	A-22
A-9	Wheel Locations for a Short Span Bridge	A-24
A-10	Signature of MCO-Difference for Short Spans with 11 Feet $\leq \ell \leq$ 22 Feet	A-28
A-11	Superposition of Deflections for an Elastic Beam on Flexible Supports	A-29
A-12	Case I for Flexible Supports	A-31
A-13	Signature of MCO-Difference for Short Spans (11 Feet $\leq \ell \leq$ 22 Feet) with Flexible Supports. $\Delta/\ell = 0.423$	A-35
A-14	Location of Absolute Zero Reference (All Quantities are Dimensionless)	A-37
A-15	Supports With Unequal Flexibility	A-39
A-16(a)	MCO-Difference for One Soft Support Among Infinitely Rigid Supports	A-44
A-16(b)	MCO-Difference for One Support Significantly Softer Than Other Supports of Equal Flexibility	A-45
A-17(a)	Example of Timber Bridge at MP 87.20 MB	A-47
A-17(b)	MCO-Difference Signature Averaged For Two Rails	A-47
A-18	Solution for $EI/\kappa\ell^3 = 0.35$, $EI = 1.7 \times 10^{11}$ $\kappa = 9.01 \times 10^4$ lbf/in -- Comparison with Field Data for Bridge at MP 87.50 MB	A-49
B-1	Test Consist Configurations	B-2
B-2	Test Zone Details of SRS for Manassas Bristow, and Gainesville Areas	B-2

LIST OF ILLUSTRATIONS (CONT)

Figure No.	Title	Page
B-3	Map of Test Zone on Southern Railway	B-5
B-4	Track Chart-Repeatability Test Segment	B-6
B-5	Test Consist	B-6
B-6	Topographic Map and Analog Stiffness Trace (MP 64 to 67) - Southern Railway	B-8
B-7	Topographic Map and Analog Stiffness Trace (MP 114 to 116) - Southern Railway	B-10
B-8	Topographic Map and Analog Stiffness Trace (MP 149 to 151) - Southern Railway	B-11
B-9	Configuration of Test Consist	B-12
B-10	Test Zones	B-13
B-11	Topographic Map and Analog Stiffness Track (MP 103) Southern Railway	B-15
B-12	Topographic Map and Analog Stiffness Trace (MP 92.4 to 94.8) Southern Railway	B-16
B-13	Topographic Map and Analog Stiffness Trace (MP 87.9 to 89.4) Southern Railway	B-17
B-14	MCO Difference Traces (Bridges at MP 80.9 and 87.2 on Southern Railway	B-20
B-15	MCO Difference Traces (Bridges at MP 87.5, 126.5 and 134.3 on Southern Railway	B-21
C-1	Mode 1 Processing at Turnout	C-3
C-2	Mode 1 Processing Comparing Northbound Versus Southbound Runs	C-5
C-3	Comparison of Average Compliance Values With WES Data on the Kansas Test Track	C-7
C-4	Mode 2 Processing Showing the Effects of Averaging for Extracting Meaningful Stiffness Information	C-8

LIST OF ILLUSTRATIONS (CONT)

Figure No.	Title	Page
C-5	Graph of Compliance Results Showing Repeatability for Different Sensor Positions and Direction of Travel on the KTT	C-10
C-6	Comparison of Computed Compliance with Physical Conditions on the KTT	C-12
C-7	Diagram of Data Flow	C-15
C-8	Data Flow for Post-Test Processing	C-17
C-9	Program T432 - Functional Block Diagram	C-19
C-10	Sample Analog Charts - Profile Mode	C-20
C-11(a)	Sample Analog Charts - Track Stiffness Mode	C-21
C-11(b)	Sample Analog Charts - Track Stiffness Mode	C-21
C-12	Frequency Response of Triangular Filter	C-23
D-1	Sensor Configuration for T-3 MCO and Chordal Alternatives When Wheels are Used as Sensors	D-3
D-2	Comparison of Compliance Values Obtained for Various Passes on the Kansas Test Track	D-4
D-3	Comparison of Average Compliance Values With WES Data on the Kansas Test Track	D-4(a)
D-4	Data Acquisition System--Block Diagram	D-6
D-5	Location of Test Instrumentation	D-7
D-6	Shock Test Assembly	D-20

LIST OF TABLES

Table No.	Title	Page
3-1	Track Stiffness System Evaluation	26
B-1	Summary of Data Processing Details	B-3
D-1	Field Calibration Summary (22 August 77)	D-11
D-2	Field Calibration Summary (26 August 77)	D-12
D-3	Adjusted Gains Accelerometer-Signal- Conditioning Electronics	D-21

1.0 INTRODUCTION

1.1 GENERAL

This report describes a three-phase program to develop an on-board, track-stiffness-measurement system. The first phase, implemented under Contracts DOT-FR-54174 and 64113, took place during the period December 1974 through December 1976. During the first phase, the following work was accomplished:

- The method for extracting track-stiffness information from track profile measurements was developed.
- Data processing systems were developed for extracting track-stiffness information.
- Preliminary tests were run to collect track-stiffness data.
- Instrumentation criteria were established.

The second phase, implemented under Contract DOT-FR-64113, took place during the period August 1977 through April 1978. During the second phase, the following work was accomplished:

- The accuracy and resolution of the instrumentation were improved to a point where they were adequate for track-stiffness measurements.
- Good repeatability was established in the collected data.
- High correlation was established between observed variations in track stiffness and the actual physical condition of track structures and subgrade.
- Track stiffness and track geometry were found to be independent and complementary measurements.

- At the rail level, it was established that rail structures and loose joints could be observed and studied.
- At the tie-ballast level, it was established that grade crossings and bridge approaches often exhibited distinctive signatures.
- At the subgrade level, it was established that the track-stiffness measurements reflected differences in areas of cuts and fills and differences between old and new construction.

The third phase, implemented under Contract DOT-FR-64113, took place during the period May 1978 through December 1978. During the third phase, the following work was accomplished:

- A detailed study of long-and short-span bridge stiffness signatures was conducted.
- An analytical study of the relationship of the mid-chord-offset (MCO) difference to absolute stiffness for bridge structures and continuous roadbed was made.
- Theoretical stiffness models were matched to actual short-span bridge stiffness signatures.
- Field testing was conducted for a short-span bridge involving locomotive loading and deflection measurements to verify the theoretical model.

A rigorous analysis of these four items is included in Appendix A.

1.2 BACKGROUND

1.2.1 NEED FOR TRACK STIFFNESS MEASUREMENT

Maintaining railroad track in a safe and functional condition so that it can efficiently carry train traffic, requires careful maintenance of all the elements of the track system - the rails, ties, ballast, subgrade, etc. Obviously, broken rails or split ties cannot be tolerated if the track system is to

be safe. Also, deterioration of the subgrade can lead to unsafe track conditions. A recent article in Railway Track and Structures [1] pinpoints the situation quite accurately.

"The problem created by soft subgrade has, of course, plagued trackmen ever since the railroads came into existence. Because water in the subgrade was identified as the main culprit, good roadbed drainage has always been given the highest priority in the minds of track engineers. It was for this reason that nearly every railroad has its annual ditching program in which side ditches were cleaned out and deepened and such other grading was carried out that was considered necessary to cause water to be drained rapidly from the right of way."

The commentary continues:

"But soft, unstable roadbeds continued to be a problem which even became more serious than before. Two reasons come to mind for the worsening situation. One is that many roads in recent years had been unable to pursue the annual ditching programs, and perhaps even had to cut back on the other measures they had been using for stabilizing roadbeds. The other is the increasing use of 100-ton cars which cause subgrades to break down more rapidly than before."

Having established the need for maintaining a proper subgrade, the question of the cost of this maintenance must be determined. In general, the exact costs are difficult to quantify because of the widely differing conditions that are encountered.

The same article in Railway Track and Structures [1] sums up the situation as follows:

"...At one extreme we have track that is supported on a well-drained subgrade consisting of a stable, well-compacted material. It is probably safe to say that the cost of track maintenance attributed to sub-grade deficiencies under such conditions is close to zero. At the other extreme are those situations where the track is supported on a material of low bearing power that has become saturated with moisture. Any trackman who has had the responsibility for maintaining track under these conditions is aware of the amount of effort required to keep it in surface and line."

Nevertheless, we do know that with the advent of continuous welded rail (CWR) a higher percentage of the maintenance costs are going into subgrade maintenance (as pointed out in [1]). Prior to the conversion to CWR, approximately 50 percent of maintenance dollars were expended on repair to the rail joints. Currently, CWR represents a sizeable capital expenditure. Poor subgrade conditions can cause bending of the rail and replacement costs are high. Consequently, a cost-effective scheme for maintaining subgrade in proper condition is of the utmost importance.

The dual-profile-measurement system developed in the first phase of this program is intended to measure track stiffness, a property directly related to the condition of track subgrade and ballast as well as to the condition of rails and ties. The dual-profile-system, which derives track stiffness data from measurements of track profile obtained from the standard mid-chord-offset and profilometer techniques, using a track-geometry-measurement car operating at normal speeds, is simple and economical. During the second phase of this program, the existing system was refined by improving the instrumentation and the processing algorithms to demonstrate the usefulness of the collected data relative to the maintenance of railroad track. The third phase of the program was conducted to examine the signature characteristics of bridge and roadbed anomalies.

1.3 REPORT ORGANIZATION

Section 2.0 of this report covers the basic theory of the dual-profile measurement system. Section 3.0 covers the three individual phases of the test emphasizing: reason for the test, test areas, actual results and test-to-test differences. The appendices included at the end of the report contain the detailed information concerning theory, instrumentation, electronics, data acquisition, testing, post-test processing and bridge structure signatures as well as topographic maps showing the test areas and corresponding stiffness signatures for each phase.

2.0 BASIC THEORY

The purpose of the Track Stiffness Measurement Program is to develop a mobile, automated track measurement system that can identify track support anomalies that cannot be detected using existing track-geometry-measurement systems. The absolute stiffness of a track support system is difficult to analyze. In theory, the following aspects of stiffness must be considered:

- There is a directional variance in stiffness in a plane normal to the longitudinal axis. Intuitively, there is a dependence of lateral stiffness on vertical stiffness but an independent measurement is required.
- Vertical stiffness is load dependent. Since track does not deflect uniformly under graduated loading, the stiffness is also non-uniform for a uniformly graduated loading condition.
- Under dynamic loading (a simulation of the pounding, rhythmic effect of the wheels of a passing train) the dynamic stiffness response will be different from the static stiffness because of plasticity or the recovery rate of the track after an applied load is removed.

In a theoretical study, the above considerations cannot be overlooked. The purpose of this program is not to establish a rigorous, absolute-stiffness measurement system. The purpose is to develop a system that can detect track-stiffness-related anomalies under survey conditions that cannot be detected with current track-geometry-measurement instrumentation.

Figure 2-1 shows the vertical-stiffness, base experiment which consists of measuring a maximum vertical deflection of the track support system at the applied load. If the

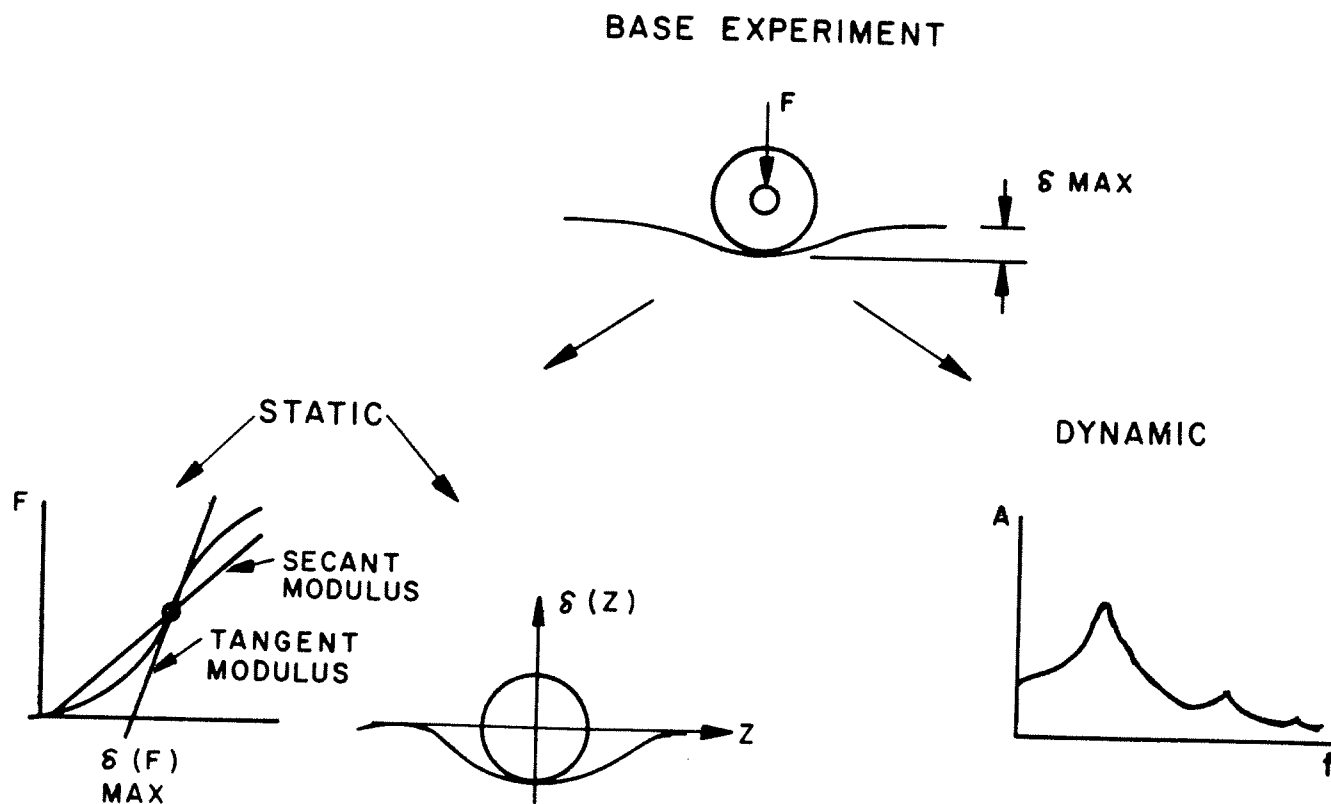


Figure 2-1. Base Stiffness Experiment

system were designed in this manner, some very important parameters would be overlooked. First, the deflection of the track support system is non-linear when graduated loads are applied. Therefore, the static load application yields a linear approximation of the actual force-deflection curve.

There are two basic linear approximations of the force-deflection curve; the tangent modulus is actually tangent to the curve at a point while the secant modulus passes through the origin and a point on the curve. When the track is loaded enough to take up the initial low-load deflection, the secant modulus is a close approximation to the tangent modulus. Determination of the tangent modulus requires two levels of force application with their respective deflections. Battelle

[9] has been conducting theoretical research in this area using a vehicle with three axle trucks modified to produce different force levels on the axles of the two trucks. ENSCO has been utilizing the secant modulus in its stiffness research.

There is also a spatial variation in the longitudinal direction on the deflection curve of the track support system. The curve forms a dish shape; ENSCO (utilizing the secant modulus) has conducted research into the form factors associated with the dish shape. The nature of a Winkler-type beam supported by a continuous elastic foundation is such that the spatial variation in the deflection is an important consideration in the overall integrity of the track support system.

Another consideration is the response of the track support system to periodic excitation. The periodic application of loads to a point in a track simulates a passing train. Battelle's [9] theoretical research indicates that there are some track structures with fundamental frequencies that fall within the range of interest and coincide with the range of speeds of passenger and freight traffic.

All of ENSCO's stiffness research has been conducted using a dual-profile, measurement system. Tests have been conducted on continuous track and on bridge structures.

The dual profile system measures the response of track to a distributed load. When mid-chord-offset is measured by a beam system attached to a three-axle truck (Figure 2-4), the load is stationary with respect to the three measurement points. When the output of an inertial device called a profilometer is converted to an equivalent MCO, the relative deflections are computed with the load in three different positions. As a result, the mid-chord-offset measurement is smaller than for the beam system. Subtracting the profilometer MCO from the

beam MCO yields a deflection that is associated with load only and not with track geometry.

2.1 TRACK SUPPORTED BY AN ELASTIC ROADBED

Railroad track can be described as long beams on a continuous, elastic, supporting foundation (Figure 2-2). When a point-load (P) is applied to such a beam, the vertical displacement (y) as a function of the distance (x) from the point-load is given by

$$y(x) = \frac{P\beta}{2\mu} e^{-\beta x} [\cos\beta x + \sin\beta x] \quad (2-1)$$

when $x \geq 0$ and

$$\beta = \left[\frac{\mu}{4EI} \right]^{1/4} \text{ (inches}^{-1}\text{)}$$

μ = track modulus (pounds/inch/inch)

E = Young's modulus of the rail
(pounds/inch/inch)

I = second moment of area (inch⁴)

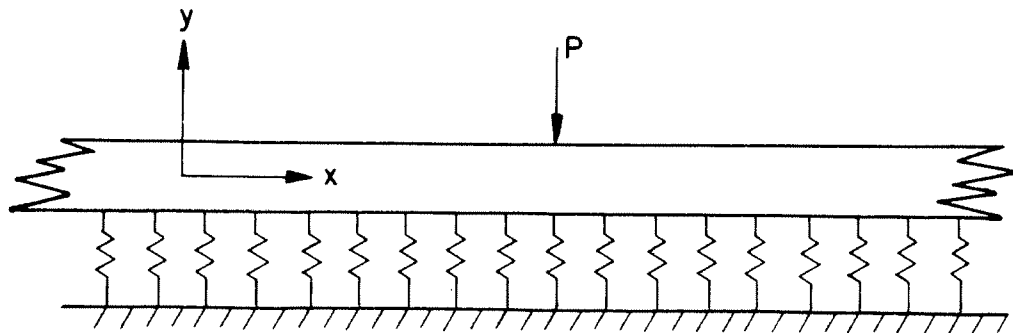


Figure 2-2. Beam on a Continuous, Elastic Supporting Foundation

At the point where the load is applied, $x = 0$ and

$$y_{\max} = y(0) = \frac{P\beta}{2\mu} = \text{maximum deflection.}$$

Track compliance (C) is defined as the maximum deflection of the beam divided by the applied load or

$$C = \frac{Y_{\max}}{P} = \frac{\beta}{2\mu}$$

Track stiffness is the reciprocal of track compliance. Therefore,

$$S = \frac{1}{C} = \frac{P}{Y_{\max}} = \frac{2\mu}{\beta}$$

The important point in this derivation is that Equation 2-1 for the deflection of the rail can be written as a function of the compliance or the stiffness of the foundation

$$y(x) = PCf(x) = \frac{P}{S} f(x) \quad (2-2)$$

where

$$f(x) = e^{-\beta x} (\cos \beta x + \sin \beta x) \quad (2-3)$$

which is called the rail deformation form factor.

In the case of multiple loads, i.e., two or three-wheel trucks, the superposition principle applies and the deformation at any point is the sum of the deformations due to each individual load. Thus, the rail deformation form factor will appear as a baseline term in the measurement of mid-chord offset.

2.2 CHORDAL MEASUREMENT SYSTEM

To make a mid-chord-offset measurement of rail profile, a chordal length is defined and a measurement is made at the mid-point of the chord to determine offset of the rail from the straight line between the two end points as illustrated in Figure 2-3. In the case of the R-1 research car, a three-axle truck at the rear of the car is equipped with an 11-foot, rigid beam suspended from the first and third axle and the mid-chord-offset measurement is made at the center axle as shown in Figure 2-4. The truck is weighted for equal loads on each axle and the entire truck will sit in the "well" caused by the deformation due to the superposition of the three loads as illustrated in Figure 2-5. A chordal measurement with this system will always be dependent on the shape of the rail deformation form factor as well as imperfections in profile. In the case of perfect track geometry (i.e., no variations in rail profile) only a baseline reflecting the shape of the form factor will be measured by the mid-chord-offset-measurement system. For the three-axle truck on the R-1 research car, from Equation 2-2, this baseline is given by the expression

$$d_{MCO} = PC \{f(66'') - f(132'')\} \quad (2-4)$$

when the track stiffness is constant.

Equation 2-4 relates the MCO measurement on perfect geometry track to track compliance. If one considers the case of imperfect geometry but constant track stiffness, the chordal measurement will be the sum of the above bias and the variations in track geometry as related through the chordal measurement. In an actual physical system, the track will have neither perfect geometry nor constant track stiffness. However, if an independent measurement can be made of track profile, the two measurements can be combined to yield track stiffness. One instrument which can be used to make an independent measurement of profile is the inertial profilometer.

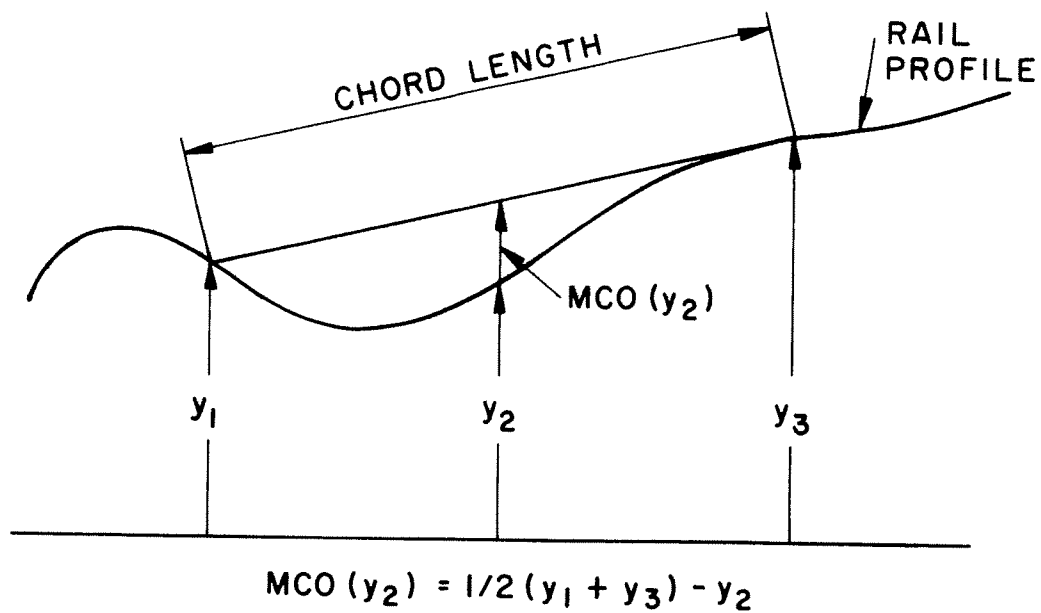


Figure 2-3. Mid-Chord-Offset Measurement

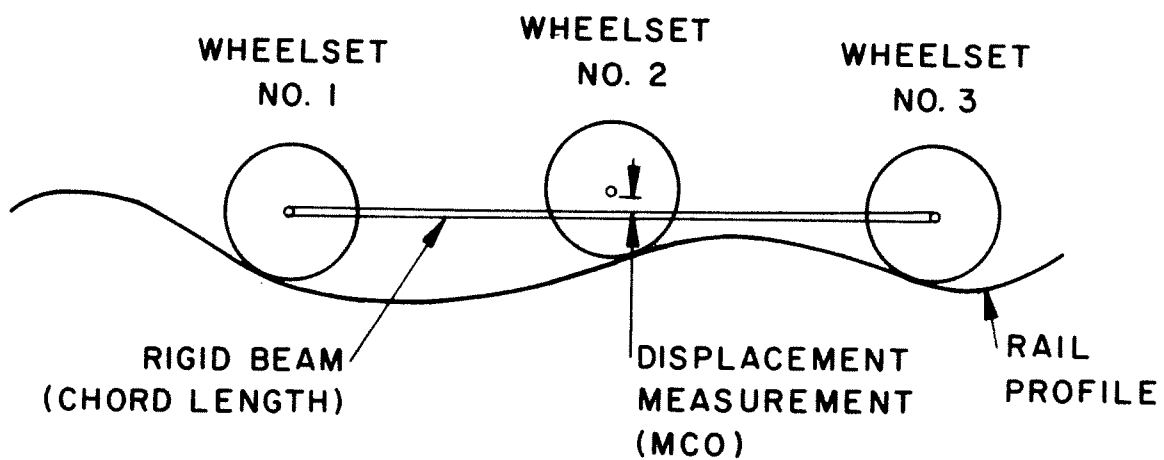


Figure 2-4. Mid-Chord Offset Measurement Using Three-Axle Truck

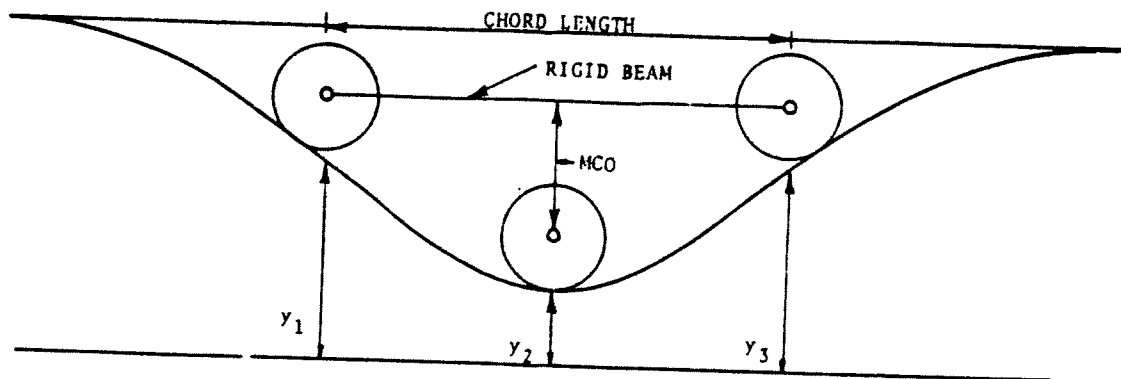


Figure 2-5. Track Stiffness Measurement Using Mid-Chord-Offset Measurement

2.3 PROFILOMETER MEASUREMENT SYSTEM

Figure 2-6 is a schematic diagram showing the operation of a profilometer. A massive platform is attached to the journal bearing of a truck axle using a spring and damper. An accelerometer is attached to the platform and a linear variable differential transformer is used to sense the displacement variations between the axle and the platform. These two signals can be amplified, filtered and combined to produce a displacement signal relative to some inertial reference. Since the profilometer output is a point-by-point measurement of displacement, a mid-chord-offset measurement can be developed from this data. The response of a profilometer to perfect track geometry and constant stiffness is shown in Figure 2-7. The profilometer is not sensitive to the deformation form factor. Thus, the chordal construction from the profilometer would produce an output of zero.

The way in which a profilometer can be used to eliminate the track geometry contribution to a mid-chord-offset measurement is illustrated in Figure 2-8. Assuming infinite track stiffness (zero track compliance), we have a rail surface with an imperfection of depth A . As the 11-foot, mid-chord-offset measurement is made by the moving test car, a chordal response

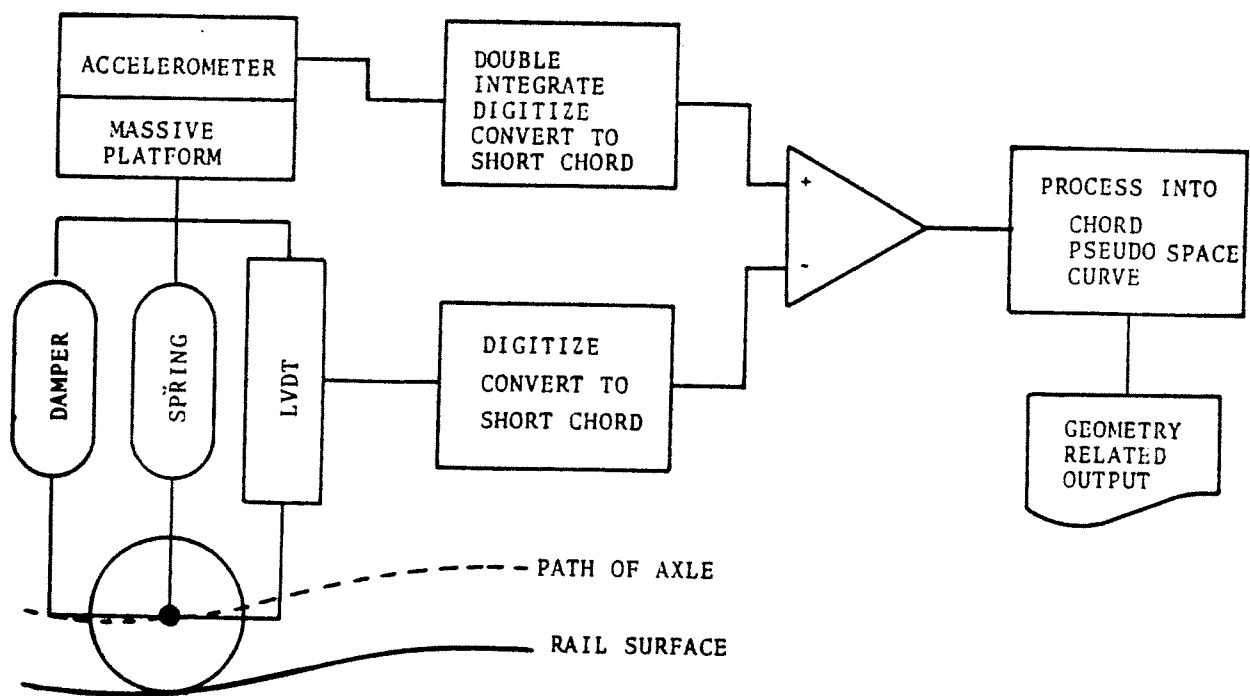


Figure 2-6. Inertial Profilometer Measurement System - Schematic Diagram

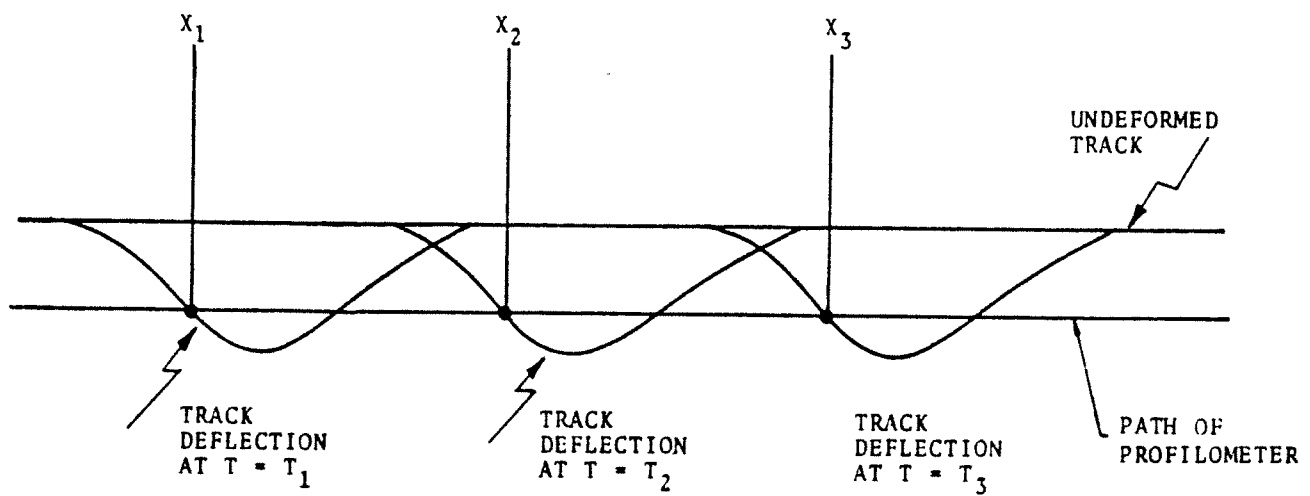


Figure 2-7. Mid-Chord-Offset Constructed by Profilometer

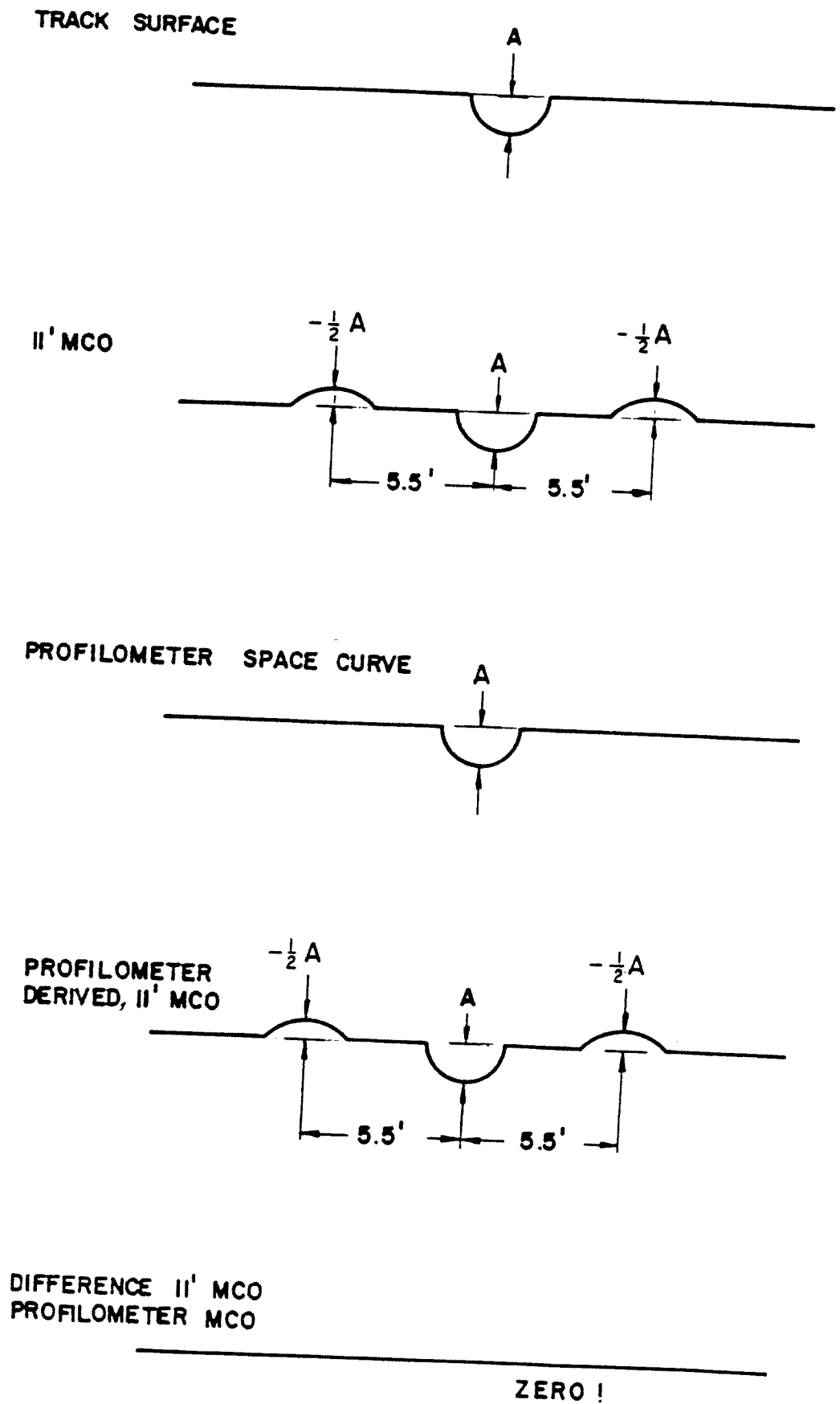


Figure 2-8. Response of Track Stiffness System to Track Geometry

profile results with the geometry defect reproduced, as well as two half-amplitude bumps which result as the first and third wheels fall into the defect. The profilometer will reproduce the actual track surface by generating a space curve trace from which we can construct an 11-foot, mid-chord-offset identical to the measured mid-chord-offset. The difference between these two signals is zero. Thus, for the case of imperfect geometry and constant stiffness, the difference between a digitally constructed profilometer mid-chord-offset and a measured mid-chord-offset will be the baseline expression, d_{MCO} of Equation 2-4.

These measured deflection values, being a measure of the deformation of the track under the truck, can be directly related through Equation 2-2 to track stiffness or compliance. Figure 2-9 is a plot of measured MCO displacement versus track compliance. The total range (from soft to stiff track) of the mid-chord-offset displacement is 0.15 inches, demanding that the measurement-accuracy be at least 0.02 inches to discriminate between significant changes in track stiffness.

Although variations in track profile have been eliminated from the measurement system, the response of the system to non-constant track stiffness has not as yet been discussed. Consider the case of perfect geometry and an abrupt change in track support modulus from a stiffer value (u_1) to a less stiff value (u_2) as shown in Figure 2-10. As the 11-foot, mid-chord-offset moves across the boundary, the baseline will change from that associated with u_1 to a new baseline associated with u_2 . The profilometer will generate a space curve reflecting the gradual change in its vertical position as the form factor under the truck changes as shown in Figure 2-10(c). The derived, 11-foot, mid-chord-offset (shown in Figure 2-10(d)) has a rather complicated shape but is zero away from the interface. The difference between the measured and profilometer-derived-mid-chord-offsets yields a trace which reflects the

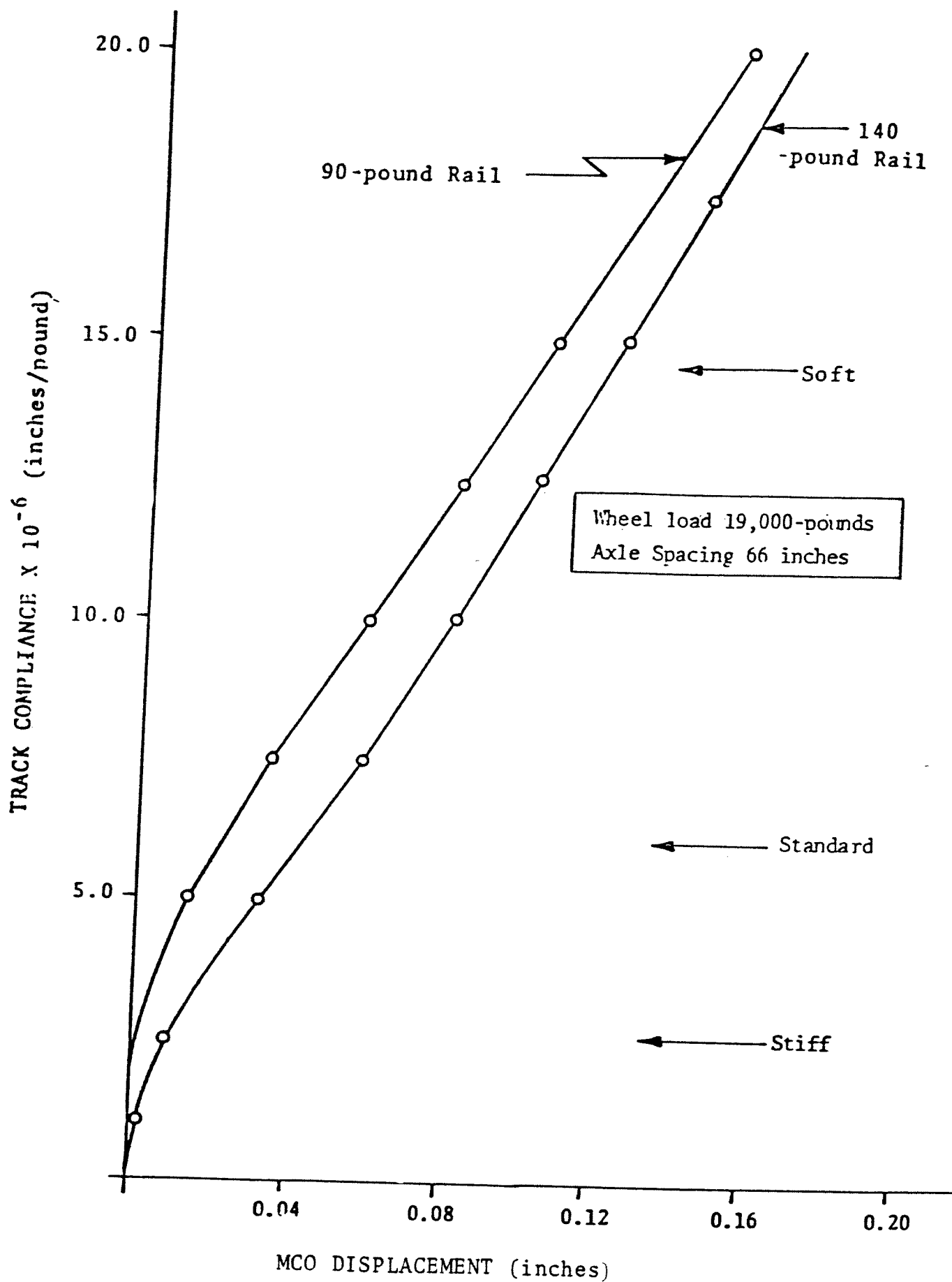


Figure 2-9. Measured MCO Displacement Versus Track Compliance
From ENSCO Report DOT-FR-78-15 [11]

TRANSITION BETWEEN TWO ELASTIC FOUNDATIONS

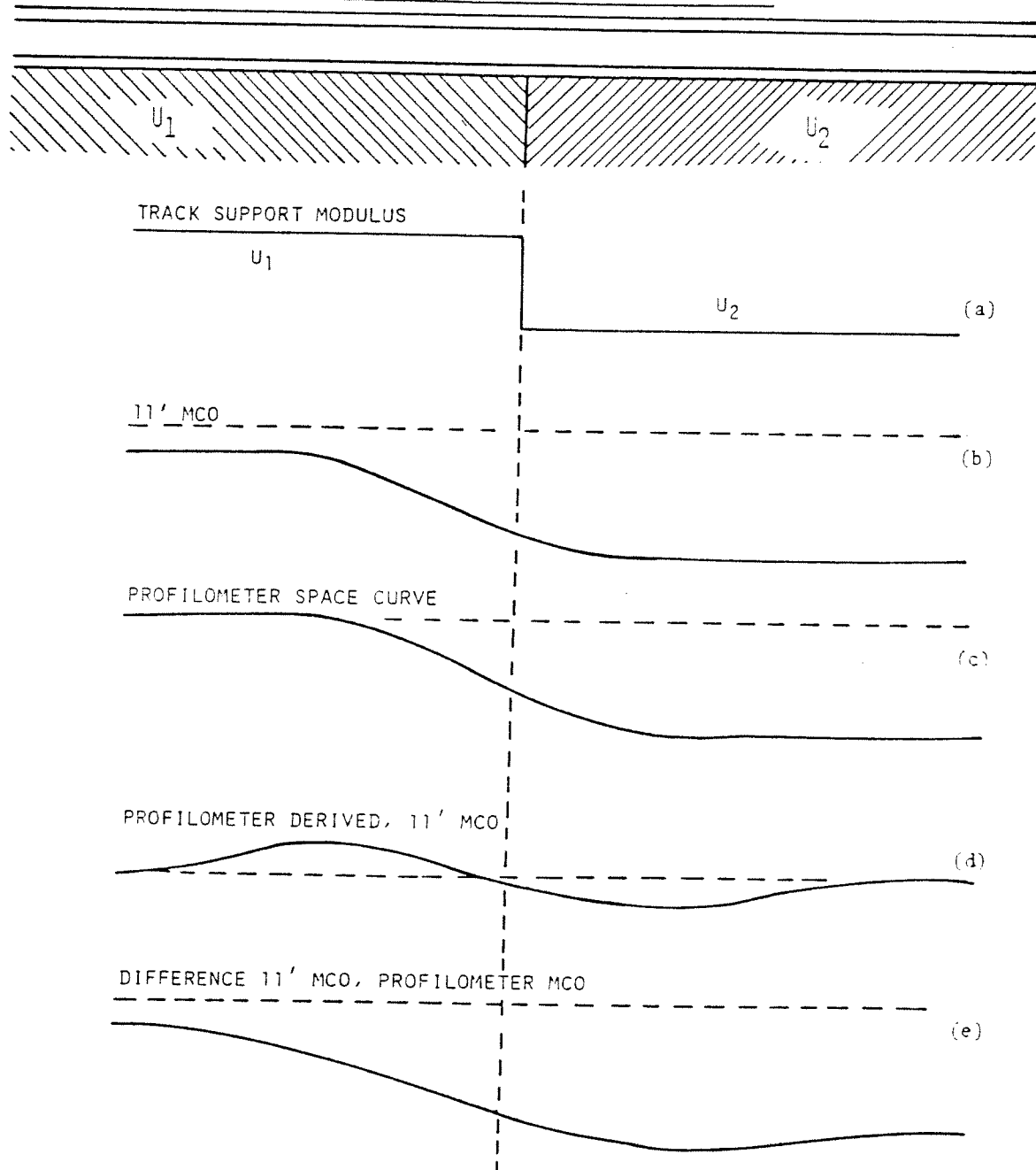


Figure 2-10. Response of Track Stiffness System to a Step Change in Track Support Modulus

values derived some distance before and after the interface with a transition region of about 12 feet duration.

Two important points should be observed from this discussion. First, even an instantaneous change in track support modulus (or the physical makeup of the track) will generate a response in the system of 10 to 20-foot duration. This indicates that the examination of wavelengths shorter than 10 to 20 feet requires detailed analysis, since any physical event along the track produces a longer response in the track stiffness curve. Second, the complicated transition region, qualitatively an indication of a change in track stiffness, is amenable to quantitative analysis. Appendix A describes the approach to the solution of the bridge problem with discrete changes in stiffness at each bent.

3.0 TEST RESULTS

3.1 PHASE I

3.1.1 REASONS FOR THE TEST

The initial phase of this program was concerned with the development of the theory required to prove the viability of the measurement concept. It was also required that several configurations of the measurement technique be considered in order to determine the relationships of their respective results to track stiffness.

This phase was also concerned with the development of time efficient data processing techniques for future use in a real-time system and the application of advanced off-line processing techniques. Studies were also made to compare the results of the system's output to known characteristics of special test track. Detailed discussions of the techniques used to accomplish these objectives are contained in the appendices.

The Phase I report [10] contained the following:

- An explanation of the theory concerning the method to be used for obtaining track stiffness information from track geometry measurements.
- A description of the design of the stiffness measurement system (summarized in Appendix C of this report).
- A description of the data processing techniques (summarized in Appendix D of this report).

3.1.2 TEST ZONE

This test was conducted over sections of Southern Railway track in the vicinity of Manassas, VA and at the Kansas Test Track. Appendix B contains details describing the test zones.

3.1.3 TEST RESULTS

The results of the first test were very promising and led to recommendations for further testing. The most important results were:

- Validation of the measurement concept utilizing the known stiffness characteristics of various segments of the Kansas Test Track.
- Determination of the relative sensitivity of different configurations of the measurement system.
- Establishment of instrumentation criteria.

3.2 PHASE II

3.2.1 REASONS FOR THE TEST

The tests conducted during the second phase were designed to evaluate improvements in the measurement instrumentation and in the data processing procedures.

The test results report [11] contained the following:

- A general explanation of the basic theory involved in the design of the stiffness measurement system.
- A physical description of the measurement system.
- A description of the test.
- A description of the analysis procedures.
- A description of the data processing procedures.

3.2.2 TEST ZONE

The test was conducted over Southern Railway track from Alexandria, VA to Lynchburg, VA. Details describing the test zone are presented in Appendix B.

3.2.3 TEST RESULTS

The test results generally exceeded original expectations. Difficulty was experienced only in the area of determining absolute stiffness. With the beam mid-chord-offset measurement system, the mid-chord-offset measurement must be made with respect to a straight line. However, any beam, used as the reference line, will not be straight because it deflects under its own weight. An attempt was made to measure this deflection using surveying instruments but these measurements did not have the required accuracy.

The most important results were:

- Variations in track stiffness down to 30 feet in wavelength were measurable and could be correlated to track and subgrade features.
- The response of the system at bridge approaches, road crossings, soft joints, switches, old and new construction, and at cuts and fills reflects its ability to examine tie/ballast interface and rail and subgrade conditions.

3.2.4 TEST TO TEST DIFFERENCES

The differences between the Phase I and Phase II tests were as follows:

- The cylindrical wheels on the R-1 vehicle were replaced with newly turned wheels prior to the Phase II test to improve accuracy.

- The T-7 data acquisition vehicle was used in conjunction with Southern's R-1 vehicle. T-7 was used to eliminate software incompatibilities between ENSCO and Southern Railway data systems. It also provided a more rapid transition in setup and teardown as well as advanced coding and programming of off-line data processing.
- Improved data processing procedures were developed.
- A study was conducted on revenue track to establish the ability of the system to detect maintenance-related track stiffness problems. Southern Railway personnel examined the track and responded to questionnaires establishing a strong relationship between changes in stiffness and track structure irregularities. Figure 3-1 and Table 3-1 present an example of the stiffness changes observed and the probable causes. Figure 3-1 shows the locations of the events described in Table 3-1; the stiffness indicated in Figure 3-1 represents the average relative stiffness on a per mile basis.

3.3 PHASE III

3.3.1 REASONS FOR THE TEST

The third and final phase of the Track Stiffness Measurement System Evaluation Program was conducted to demonstrate the usefulness of the system, and to perform a detailed stiffness-related, signature study for track anomalies and for long-and short-span bridges.

This phase ended with the production of the final report summarizing the three-phase program.

3.3.2 TEST ZONE

The test zone for this phase was Southern Railway track from Cincinnati, OH, through Lexington, KY, Chattanooga, TN, and Birmingham, AL to Mobile, AL. Details of the test zone are described in Appendix B.

Date: 20 January 1978

Page: 1 of 1

Tape: D

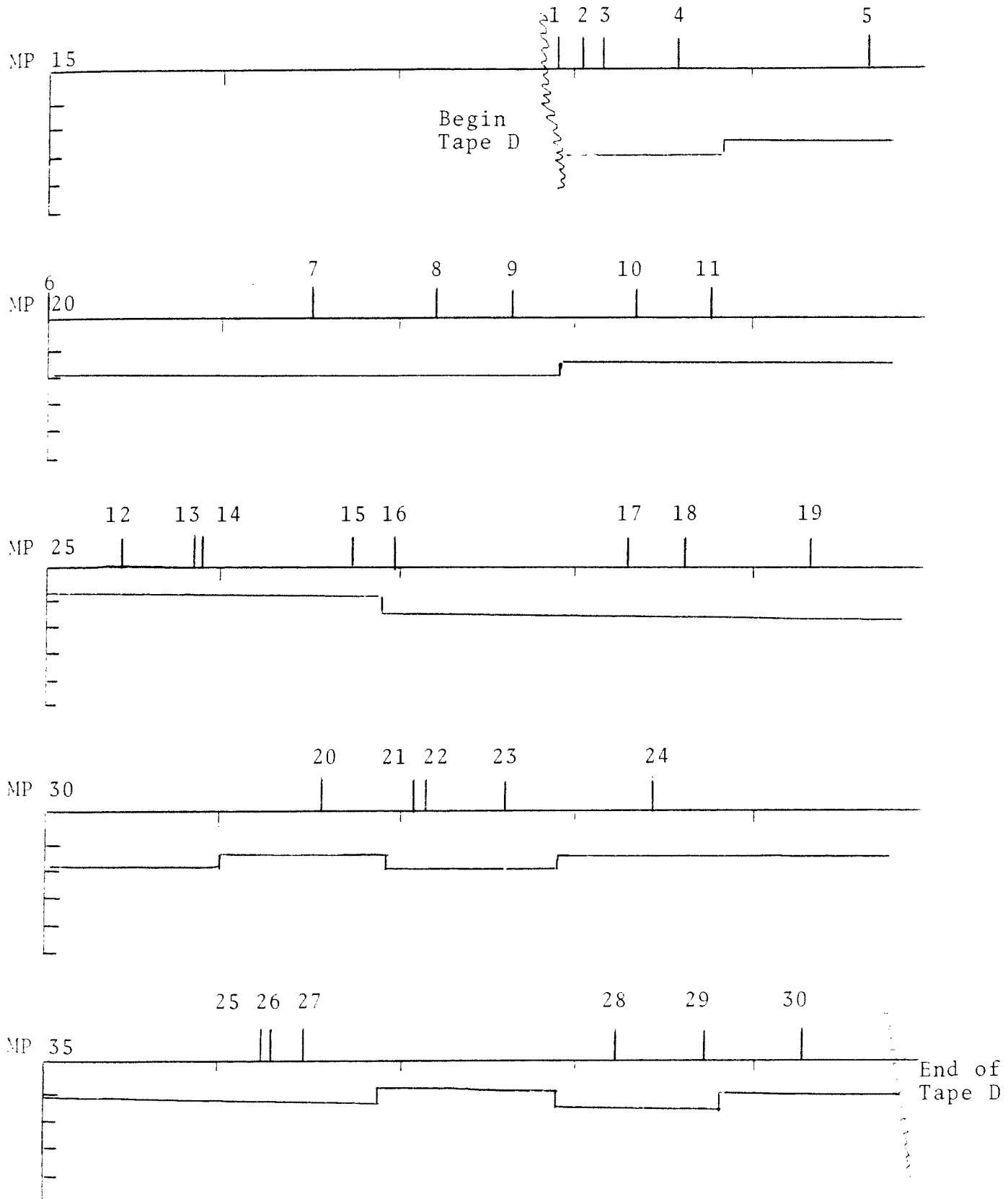


Figure 3-1. Relative Stiffness on a Per Mile Basis

TABLE 3-1
TRACK STIFFNESS SYSTEM EVALUATION

Tape: D

Date: 20 January 1978

Page: 1 of 3

EVENT #	MILEPOST	EXTENT	ENSCO COMMENTS	SOUTHERN RR COMMENTS
1	18.0	Short	Softer.	Cut with slight slope uphill to south. May have poor drainage.
2	18.2	Short	Softer, joints.	Turnout to gas plant.
3	18.3	Short	Softer, joints.	Part of same turnout.
4	18.7	300'	Very soft.	Cut under new Rolling Road bridge. Exact area is under new bridge.
5	19.85	Short	Softer, joints Message #21 - road.	Insulated joints for road and north signal at Burke - generally not well drained.
6	20.0	1/10 mi.	Softer, joints probably interlock.	Burke Interlocking, side hill location, but ballast fouled with clay slurry from derailment in 1976.
7	21.6	50'	Very hard, Message #24 - road.	New Sideburn Road Crossing, paved and only two to three years old.
8	22.4	400'	Softer.	Entering cut at top of Fairfax Hill.
9	22.75	100'	Softer.	Still in cut, approaching overhead bridges.
10	23.45	75'	Two soft spots, joints.	?
11	23.9	150'	Harder.	Fill.
12	25.45	400'	Harder.	Fill.
13	25.85	150'	Softer.	Probably short cut.

TABLE 3-1 (Cont)
TRACK STIFFNESS SYSTEM EVALUATION

Tape: D

Date: 20 January 1978

Page: 2 of 3

EVENT #	MILEPOST	EXTENT	ENSCO COMMENTS	SOUTHERN RR COMMENTS
14	25.9	2/10 mi.	Harder, Message #26, bridge.	Bridge is at 26.05 actually, but a bridge over Popes Run is here.
15	26.8	1/10 mi.	Activity, joints, Message #28 - road.	Clifton Interlocking - has a road through middle. Generally well drained due to slope.
16	27.05	100'	Two soft spots, Message #29 - not recorded.	Probably ends of bridge over small creek.
17	28.4	200'	Harder.	Side hill cut at approximately foot of hill.
18	28.7	300'	Harder, then softer, Message #30 - bridge.	Bull Run bridge, one or two spans approached at ends from side hill cuts.
19	29.6	120'	Harder.	Alternating small cuts and fills ascending toward Manassas.
20	31.7	75'	Softer, joints.	Switch and road crossing together.
21	32.25	100'	Softer.	Road crossing.
22	32.3	150'	Very soft, joints, Message #31 - road.	This should be switch.
23	32.7	150'	Softer, joints (Manassas), Message #35 - road.	Four road crossings close together and two or three switches. Generally soggy area in wet weather.
24	33.65	150'	Softer, joints.	S. Switch Manassas.

TABLE 3-1 (Cont)
TRACK STIFFNESS SYSTEM EVALUATION

Tape: D

Date: 20 January 1978

Page: 3 of 3

EVENT #	MILEPOST	EXTENT	ENSCO COMMENTS	SOUTHERN RR COMMENTS
25	36.35	50'	Softer, joints.	Road crossing, swell country, unpaved type.
Look for short bridge between these two.				
26	36.4	350'	Activity, joints.	Interlocking plant at Bristow.
27	36.6	50'	Softer, joints, Message #39 - road.	S. road crossing at Bristow.
28	38.4	75'	Slightly softer.	Overhead bridge, track in a cut on hillside.
29	38.85	50'	Slightly softer, joints.	Signals - insulated joints.
30	39.5	250'	Harder, Message #40 - road.	Town prep, paved road crossing.

3.3.3 TEST RESULTS

The results of this test were as follows:

- For short span bridges, the spans and supports produce signatures that matched the theoretical model. There was a signature reversal not originally anticipated but a logical result of support flexibility. Appendix C contains the matched signatures and Appendix A contains the mathematical theory that predicts a signature reversal. Figure 3-2 shows the theoretical stiffness signatures for a span with differing levels of relative stiffness of the span with respect to the support. The lower signatures indicate that the spans are less stiff than the supports while the upper signatures indicate the opposite.
- During a field trip, one bridge with distinct signatures was subjected to locomotive loading while deflection measurements were made at the supports and along the spans. The resultant static stiffness matched the signatures and the theoretical model. Figure 3-3 shows a theoretical stiffness signature compared to actual data collected during the test. The theoretical signature was established using the relative stiffness of the span with respect to the supports that were calculated by observing the deflections of the supports along the span with the locomotive positioned in several locations along the bridge. Details are presented in Appendix A.
- A method was developed for the analytical verification of the stiffness signatures for continuous track but was not implemented.
- The usefulness of the system for the detection of maintenance related track problems (not detectable from track geometry measurements) was demonstrated during field trips (pp B-14 through B-21). The effect of poorly supported joints was observed. Areas with poor drainage were distinguishable. Zones with fouled ballast were detected.

3.3.4 TEST TO TEST DIFFERENCES

The differences between the Phase III and the Phase II tests were as follows:

- A detailed bridge-signature study was conducted (Appendix A).
- For bridges, the relationship of differences in mid-chord-offset to absolute stiffness was established (pp A-43 through A-49).
- A method for establishing the relationship of differences in mid-chord-offset to absolute stiffness on continuous track was outlined (pp A-1 through A-8).
- Joint field trips were conducted to Mobile, AL and Lexington, KY including ENSCO, FRA, Southern and AAR personnel to evaluate areas with interesting signatures (pp B-14 through B-21). This allowed a more in-depth and objective investigation of problems with the track structure as indicated by the stiffness signatures.

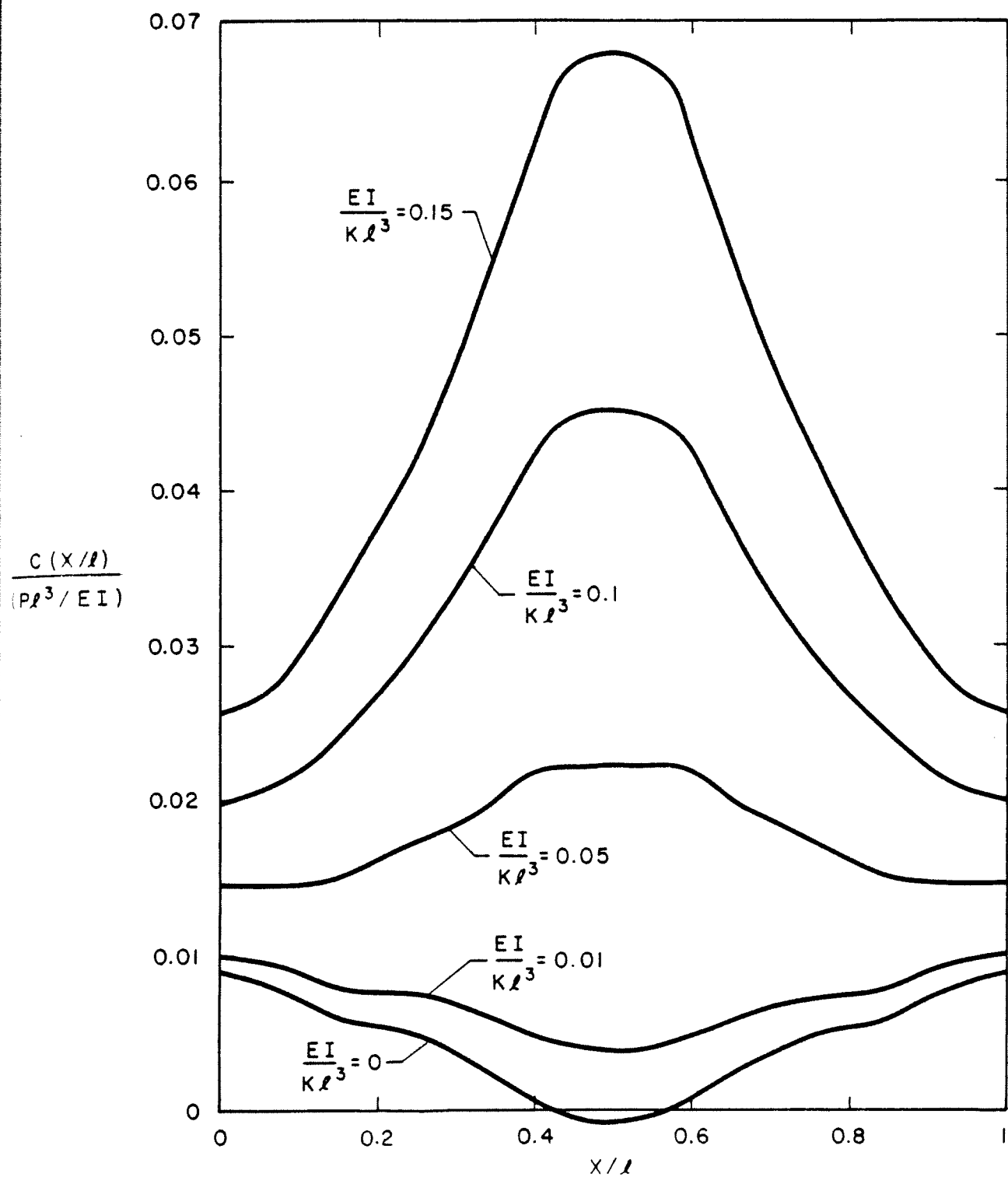


Figure 3-2. Signature of MCO-Difference for Short Spans ($11 \text{ Feet} \leq l \leq 22 \text{ Feet}$) with Flexible Supports. $\Delta/l = 0.423$

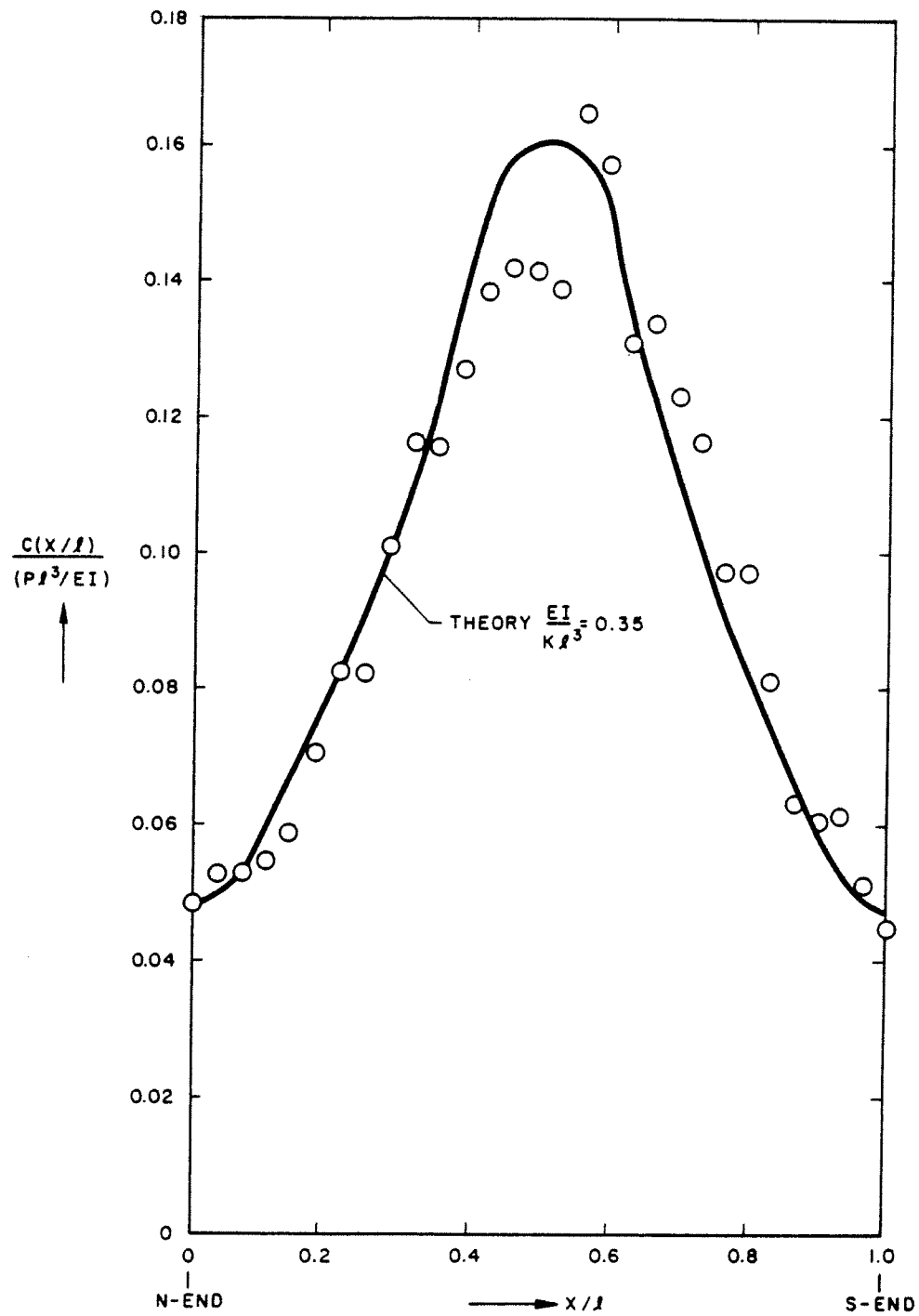


Figure 3-3. Solution for $EI/\kappa l^3 = 0.35$, $EI = 1.7 \times 10^{11}$, $\kappa = 9.01 \times 10^4$ lbf/in. Comparison with Field Data for Bridge at MP 87.50 MB

4.0 CONCLUSIONS AND RECOMMENDATIONS

Interviews conducted with members of the rail-industry (CONRAIL, Canadian National, Bessemer and Lake Erie, Denver and Rio Grand Western and Southern Railway) and articles in railroad periodicals [1] indicate that there is a real rail-industry need for a track-stiffness-measurement system capable of survey operations at track speeds. It has been demonstrated that the system evaluated under this program does have the potential of being that system. No mechanical modifications are required to implement the system on a three-axle truck. It only requires a simple combination of two accepted track-geometry-measurement techniques.

The inertial profilometer and the beam mid-chord-offset provide the measurements that are combined to remove the effect of track geometry from the resulting displacement measurement. This displacement measurement is a function only of the vehicle load and the vertical stiffness of the track support system.

There are many track structure anomalies that can be detected with current track geometry instrumentation. As an example, low joints can be detected with profile measurements. The track stiffness measurement system has demonstrated that it can actually distinguish low joints that are unsupported by ties from low joints that have tie support (pp B-18).

From the bridge signature analysis conducted during the third phase of this program, it is apparent that the basic stiffness theory has been verified. The correspondence studies (correspondence of stiffness signature variations to localized track problems) conducted during the latter phases indicate that the stiffness measurement system can

detect a variety of track structure anomalies and further offers the promise of complementing geometry measurements to distinguish one anomaly from another.

Further testing should be directed at developing more absolute criteria for distinguishing anomalous track in terms of the degree of stiffness variation and classification of the type of anomaly. The reliability and accuracy limitations of the system must be established.

The following is a list of recommendations/questions that should be addressed:

- Is it possible to make this measurement on-board a test car (track geometry car) in real time and in such a manner that interpretation is straightforward?
- Is it possible to measure absolute track stiffness?
- Is there a way to differentiate areas of fouled and muddy ballast from subsoil instability?
- Is it feasible to make bridge stiffness measurements to reflect accurately the condition of supporting structural members? Can a significant weakness be detected?
- Will track stiffness measurements indicate a variation in maintenance practices?

The recommendations listed above must be addressed as to the technical approach required to successfully answer the questions.

Currently track stiffness data is processed off line into several filtered versions. The format for data display has been plots of stiffness traces similar to strip chart plots.

Real time processing has always been an ultimate goal of the program. Consequently, all of the algorithms used in processing have been designed to be time conservative. The filters represent the most time consuming processing. Using the longest filter, a delay of approximately 200 feet is expected before an analog strip chart will display the data. Data processing can be accomplished through commercially available micro processors or minicomputers onboard the test vehicle.

Measuring absolute stiffness has also been a goal of the program. The difficulty here has been that the measurement derived from the difference between profilometer and beam mid-chord-offsets is relatively small, on the order of two one hundredths of an inch. While the accuracy of profilometer measurements is adequate for the required sensitivity, the beam measurement requires special consideration.

The simply supported beam, although as stiff as possible, does deflect statically and dynamically. Ideally a perfectly straight line is required as the baseline for the mid-chord-offset measurement. Filtering can effectively eliminate the effect of dynamic deflection of the beam but not the static deflection. Survey techniques were attempted during the second over-the-road test but did not have the required accuracy. An optical calibration procedure has been proposed that will have the required accuracy. The procedure involves mounting a coherent light source on one outer axle and a position sensing photo detector on the other outer axle. A lens is then mounted at the center of the beam. If the mechanical beam is not deflected, the light beam (one millimeter in diameter) will pass through the center of the lens onto the center of the photo detector. If the mechanical beam is deflected, the light beam will be refracted by the lens through its focal point onto the photo detector yielding a current output proportional to the position of the light beam with respect to the electrical contacts on the photo-detector.

The vehicle load and the corrected mid-chord-difference will be combined to yield the absolute stiffness measurement.

With the realization of real time processing, the differentiation of fouled or muddy ballast from subsoil instability might be possible. Much of the data gathered during the three tests was not usable for evaluations of this type. During the interim period between the tests and the subsequent field investigations, areas with interesting stiffness signatures were repaired making an investigation meaningless.

The work conducted during this program on bridge structures was entirely conclusive; short panel wooden bridges yield a highly resolved stiffness signature that is indicative of the relative stiffness of the panels and bents. Real-time testing must be carried out to determine the effects of any of several types of significant weaknesses on the stiffness signature.

Detection of variations in maintenance practices is an area of quality control that will probably be effectively augmented through stiffness testing. Here again, real-time processing is necessary and extensive testing is required to establish a degree of confidence in this use of the measurement system.

Additionally, it is recommended that research be initiated into development of a measurement system specifically designed for a two-axle truck. All anticipated FRA track inspection vehicles will have two-axle trucks. The earliest tests of the concept have demonstrated the feasibility of the two-axle measurement. It is not expected to have quite the sensitivity of a three-axle measurement. Generation of a corrected-beam, mid-chord-offset is simpler for a two-axle truck. The mechanical beam is hard mounted to the two-axle housings. It is overhung and magnetic proximity sensors are mounted at the two ends just outside the wheel diameter and at the center

of the beam. The coherent light source, photo detector, and lens, as used in calibration of the three-axle system, will be mounted directly to the three magnetic sensors at the ends and in the center of the beam, respectively. This direct mounting allows mechanical isolation of the optical components from the shock and vibration environment of the mechanical beam. This configuration allows for beam MCO corrections statically and dynamically. Elimination of the filtering required for the three-axle system is desirable since filtering always attenuates some of the desired signal.

5.0 REFERENCES

1. Railway Track and Structures, October 1976, Vol. 72, No. 10, Editorial Opinion (excerpts).
2. Ballard, R.F. and Cooper, S.S., "Engineering and Geophysical Studies of the Kansas Test Track," Technical Proceedings of the FRA Track Program Review, February 1976.
3. Winkler, E., "The Theory of Elasticity and Strength," Prague, 1967, pp. 182-184.
4. Talbot, A.N., "Stresses in Railroad Track," American Railway Engineering Association, Chicago, Illinois, Progress Reports 1-7, AREA Proceedings, Vol. 19-21, 24, 26, 31, 35 and 42.
5. Test Specification, Track Geometry Survey in Support of Kansas Test Track Project, Test Request RG-116, September 17, 1974, ENSCO, Inc. (Unpublished)
6. Cooper, S.S., "Nondestructive Testing of Roadbed Soils and Track Support Systems," U.S. Army Engineering Waterways Experiment Station, Vicksburg, Mississippi, August 21-22, 1975.
7. Dietrich, R.J. and Salley, J.R., "Embankment Support for a Railroad Test Track," Rail Technology Division, Federal Railroad Administration and Atchison, Topeka and Santa Fe Railway Co. PB-202 808.
8. Corbin, J.C. and Talapatra, D.C., "A Feasibility Study of a Method for Observing Track Stiffness from Mid-Chord Offset and Profilometer Measurements," ENSCO, Inc., presented at the IEEE Industry Applications Society Tenth Annual Meeting Conference, September 28 - October 2, 1975, pp. 512-526.
9. Kaiser, W.D., Meacham, H.C. and Tuten, J.M., "Design and Analysis of a Track Compliance Measurement System," Battelle Labs Interim Report, PB-285 559/AS.
10. Corbin, J. C. "Development of an Onboard System for Track Stiffness Measurement" ENSCO Interim Report. (Unpublished)
11. Gunn, G. "Test Results Report Track Stiffness Measurement System Evaluation Program" ENSCO Report. (Unpublished)

APPENDIX A

MATHEMATICAL MODELING

A.1 INTRODUCTION

The importance of quantitative information regarding the stiffness of track-subgrade has long been recognized. This data can be utilized in a variety of ways. For example:

- As an aid to the railroads in defining maintenance criteria which will improve operational safety and economy.
- As an input to FRA in determining a new set of safety standards which incorporate subgrade conditions.
- As a parameter in analytical models used to predict allowable loading for given equipment or to design equipment so as to insure a desired level of ride quality.

The present method for measuring track stiffness is based on the concept that mid-chord-offset, measured by a beam on a three-axle truck and by a profilometer, which are two independent measurement systems, respond differently to changes in rail profile. These changes occur due to variations in rail geometry and/or subgrade. The profilometer performs a point-by-point measurement of the profile whereas the beam mid-chord-offset (MCO) is inherently a distributed measurement. When the continuous profilometer output is converted to an equivalent MCO and compared with the beam MCO, it is found that the difference between the two quantities is independent of track geometry, and is only a function of elastic deflections of the rail-subgrade. In principle, these deflections can be related to track stiffness through appropriate equations from bending theory. Therefore, at least in concept, it should be possible to determine absolute track stiffness. A proof for the preceding statements is presented in the following paragraphs.

A.2 BASIC CONCEPTS

Under loaded conditions, the inertial profile at a point \hat{x} on the track (Figure A-1) is the sum of unloaded track profile and an additional contribution due to the three-axle truck located at $\hat{x} = H$. Thus

$$D(\hat{x}, X) = TG(\hat{x}) + S(\hat{x}, X; P_1, P_2, P_3, \Delta) \quad (1)$$

where

$TG(\hat{x})$ = Track geometry profile at \hat{x} with no applied load.

$S(\hat{x}, X; P_1, P_2, P_3, \Delta)$ = Absolute deflection at \hat{x} due to wheel loads P_1, P_2, P_3 with axle spacing Δ and with center axle at $\hat{x} = X$.

$D(\hat{x}, X)$ = Loaded track profile at \hat{x} due to truck located at $\hat{x} = X$. Explicit dependence on P_1, P_2, P_3 , and Δ has been omitted for brevity.

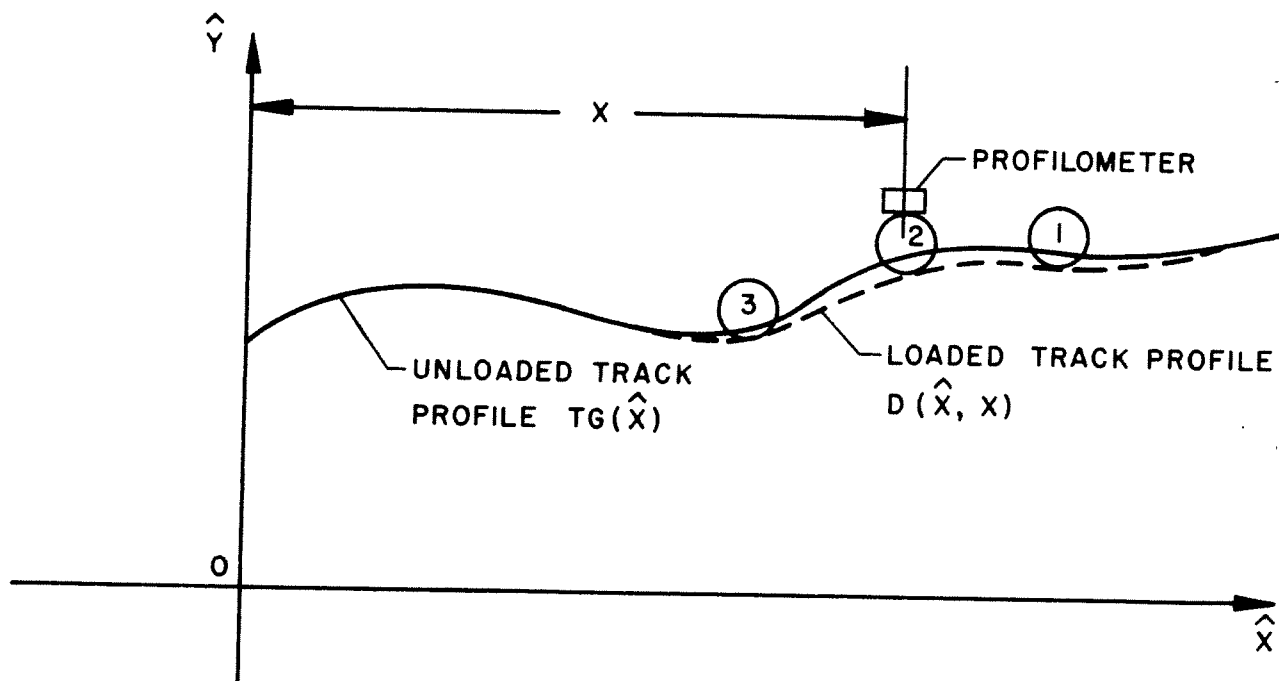


Figure A-1. Inertial Profile of Loaded Track

The MCO measured by the beam system of length 2Δ , as defined in Figure A-2 is

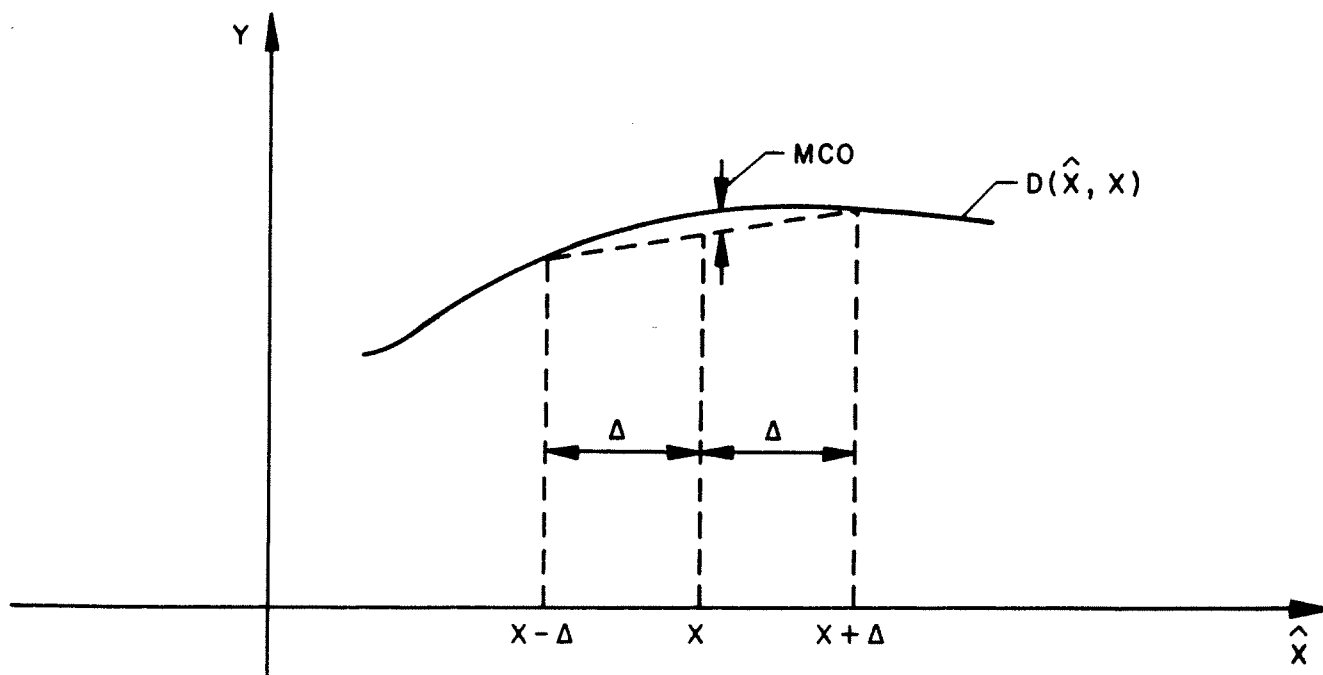
$$\text{MCO}_B(X) = \frac{1}{2}D(X - \Delta, X) - D(X, X) + \frac{1}{2}D(X + \Delta, X) \quad (2)$$

where

$$\text{MCO}_B(X) = \text{Beam MCO measurement at } \hat{x} = X$$

The MCO derived from the point-by-point profile measured by the profilometer is given by

$$\text{MCO}_P(X) = \frac{1}{2}D(X - \Delta, X - \Delta) - D(X, X) + \frac{1}{2}D(X + \Delta, X + \Delta) \quad (3)$$



$$\text{MCO}_B(X) = \frac{1}{2}D(X-\Delta, X) - D(X, X) + \frac{1}{2}D(X+\Delta, X)$$

Figure A-2. MCO Measured by Beam System of Length 2Δ

The profilometer may either be mounted on the center axle or on the leading (or trailing) axle. In the latter case, profilometer output is corrected for $\pm\Delta$ for use in Equation (3).

Subtracting Equation (3) from Equation (2), the MCO difference $C(X)$ is

$$\begin{aligned} C(X) &= MCO_B(X) - MCO_P(X) \\ &= \frac{1}{2}D(X - \Delta, X) + \frac{1}{2}D(X + \Delta, X) - \frac{1}{2}D(X - \Delta, X - \Delta) \\ &\quad - \frac{1}{2}D(X + \Delta, X + \Delta) \end{aligned} \quad (4)$$

Substituting Equation (1) into Equation (4)

$$\begin{aligned} 2C(X) &= \cancel{TG(X - \Delta)} + S(X - \Delta, X) + \cancel{TG(X + \Delta)} + S(X + \Delta, X) \\ &\quad - \cancel{TG(X - \Delta)} - S(X - \Delta, X - \Delta) - \cancel{TG(X + \Delta)} \\ &\quad - S(X + \Delta, X + \Delta) \end{aligned}$$

Notice that the track geometry terms cancel out. In the above expression, the parameters P_1 , P_2 , P_3 and Δ have been omitted from the arguments of S for the sake of brevity. These parameters, however, are understood to be present implicitly.

Then,

$$\begin{aligned} 2C(X) &= S(X - \Delta, X) + S(X + \Delta, X) \\ &\quad - S(X - \Delta, X - \Delta) - S(X + \Delta, X + \Delta) \end{aligned} \quad (5)$$

Recall that the deflection terms in Equation (5) have the following interpretation.

$S(X - \Delta, X)$ = Deflection under trailing axle
when the truck center axle is
located at X .

Other terms in Equation (5) are similarly defined. Referring to Figure A-3, assuming equally loaded wheels, and superimposing deflections at each point

$$S(X - \Delta, X) = \delta(X - \Delta, X - \Delta) + \delta(X - \Delta, X) \\ + \delta(X - \Delta, X + \Delta)$$

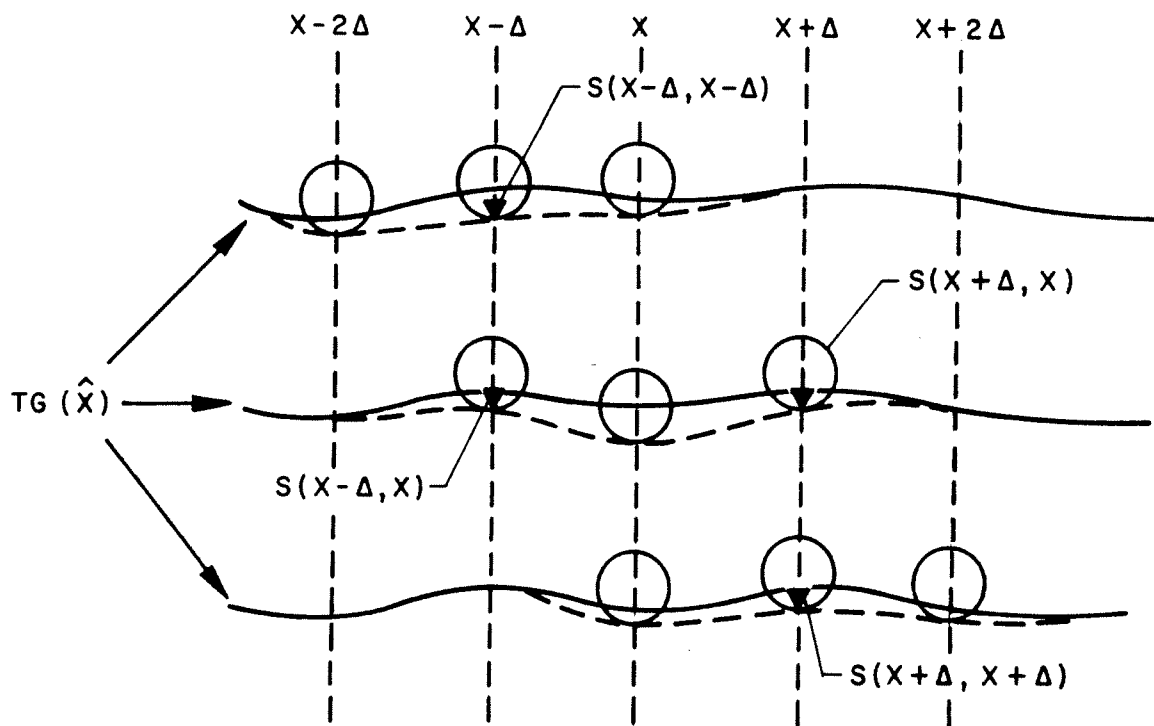


Figure A-3. Deflections Caused by a Three-Axle Truck

$$\begin{aligned}
S(X + \Delta, X) &= \delta(X + \Delta, X - \Delta) + \delta(X + \Delta, X) \\
&\quad + \delta(X + \Delta, X + \Delta) \\
S(X - \Delta, X - \Delta) &= \delta(X - \Delta, X - \Delta) + \delta(X - 2\Delta, X - \Delta) \\
&\quad + \delta(X - \Delta, X) \\
S(X + \Delta, X + \Delta) &= \delta(X + \Delta, X) + \delta(X + \Delta, X + \Delta) \\
&\quad + \delta(X + \Delta, X + 2\Delta)
\end{aligned} \tag{6}$$

where $(X - \Delta, X + \Delta)$ stands for deflection at $(X - \Delta)$ due to a load applied at $(X + \Delta)$, etc.

Substituting Equations (6) into Equation (5)

$$\begin{aligned}
2C(X) &= \delta(X - \Delta, X - \Delta) + \delta(X - \Delta, X) + \delta(X - \Delta, X + \Delta) \\
&\quad + \delta(X + \Delta, X - \Delta) + \delta(X + \Delta, X) + \delta(X + \Delta, X + \Delta) \\
&\quad - \delta(X - \Delta, X - 2\Delta) - \delta(X - \Delta, X - \Delta) \\
&\quad - \delta(X - \Delta, X) - \delta(X + \Delta, X) - \delta(X + \Delta, X + \Delta) \\
&\quad - \delta(X + \Delta, X + 2\Delta)
\end{aligned}$$

or

$$\begin{aligned}
2C(X) &= \delta(X - \Delta, X + \Delta) + \delta(X + \Delta, X - \Delta) \\
&\quad - \delta(X - \Delta, X - 2\Delta) - \delta(X + \Delta, X + 2\Delta)
\end{aligned}$$

(7)

Note that the deflections δ in Equation (7) are measured positive upward in the coordinate system of Figure 2-1. Equation (7) shows that the MCO difference $C(X)$, which is

a measured quantity, is directly related to deflections only. The relationship of $C(X)$ to an appropriately defined "track stiffness" or "track compliance" is an indirect one and it is discussed below.

In order to extract stiffness information from Equation (7) it is necessary to introduce a model for the physical structure underneath the track. For instance, in the case of a bridge, the model will be a beam with given properties and support conditions for each span. The elastic deflection of a beam is governed by the equation

$$EI(X) \frac{d^2 \delta}{dX^2} = M(X) \quad (8)$$

where,

$M(X)$ = Bending moment at X which is a function of the wheel load P and its location.

$EI(X)$ = Flexural rigidity of beam (including rail) at X .

If there is continuous subgrade underneath the rail with a modulus $\mu(X)$ expressed in force per unit vertical deflection per unit length along X , the governing equation for elastic deflection of the rail is

$$EI \frac{d^4 \delta}{dX^4} = - \mu(X) \delta \quad (9)$$

where,

EI = Flexural rigidity of rail, a constant for given rail.

It is now clear how Equation (7) is indirectly related to track stiffness, which is $EI(X)$ in the case of a bridge and $\mu(X)$ for a continuous subgrade. If Equations (7) and (8) or (7) and (9) are combined or solved simultaneously, subject to appropriate boundary conditions, the physical properties $EI(X)$ or $\mu(X)$ can be evaluated, at least in principle. Following the foregoing idea, models were developed for bridges and subgrade, and theoretical signatures $C(X)$ were derived. A comparison between theory and actual test data has been carried out for the special case of short-span bridges. These details are presented in subsequent appendices.

A.3 MODEL FOR LONG SPAN BRIDGES

A.3.1 SIMPLY SUPPORTED SPANS

Since the MCO measurement is made with a beam of finite length, the ratio of bridge span to beam length plays an important role. Consider a simply supported bridge span with length $\ell \geq 4\Delta$, where Δ is half the beam length (i.e., equal to the axle spacing). Bridge spans satisfying this condition will be referred to as long spans. The significance of the limit 4Δ will be clear in the following paragraphs and in the next section. Figure A-4a shows two adjacent simply supported spans of equal length with constant EI . Since the instrumentation response is expected to be symmetric about the center of each span, three distinct-solution regions can be identified as an isolated three-axle truck traverses the span.

$$\text{I.} \quad 2\frac{\Delta}{\ell} \leq \frac{X}{\ell} \leq \left(1 - \frac{2\Delta}{\ell}\right)$$

$$\text{II.} \quad \left(1 - \frac{2\Delta}{\ell}\right) \leq \frac{X}{\ell} \leq \left(1 - \frac{\Delta}{\ell}\right)$$

$$\text{III.} \quad \left(1 - \frac{\Delta}{\ell}\right) \leq \frac{X}{\ell} \leq 1$$

These cases will now be considered in detail.

CASE I: $2\frac{\Delta}{\ell} \leq \frac{X}{\ell} \leq \left(1 - \frac{2\Delta}{\ell}\right)$

All three wheels lie in Region (1) of Figure A-4a (see also Figure A-5).

For the simply supported beam of Figure A-4b, the deflections at a point Z due to a load P applied at point a is given by

$$\begin{aligned}\delta(Z, a) &= -\frac{PbZ}{6EI\ell} \left[\ell^2 - Z^2 - b^2 \right] \quad \text{for } 0 \leq Z \leq a \\ &= -\frac{Pb}{6EI\ell} \left[\frac{\ell}{b} (Z - a)^3 + (\ell^2 - b^2)Z - Z^3 \right] \quad \text{for } a \leq Z \leq \ell\end{aligned}$$

Since $b = \ell - a$, the above expression becomes

$$\delta(Z, a) = \frac{-P(\ell - a)Z}{6EI\ell} \left[\ell^2 - Z^2 - (\ell - a)^2 \right] \quad \text{for } 0 \leq Z \leq a \quad (10a)$$

$$\begin{aligned}&= \frac{-P(\ell - a)}{6EI\ell} \left[\frac{\ell}{(\ell - a)} (Z - a)^3 \right. \\ &\quad \left. - a(a - 2\ell)Z - Z^3 \right] \quad \text{for } a \leq Z \leq \ell \quad (10b)\end{aligned}$$

Notice that a minus sign has been introduced in the above equations because downward deflection is considered negative. It may also be mentioned that Equations 10a and 10b are solutions of the differential Equation (8) subject to simply supported boundary conditions. In order to derive an equation for the MCO-difference, one must use Equation (7) in

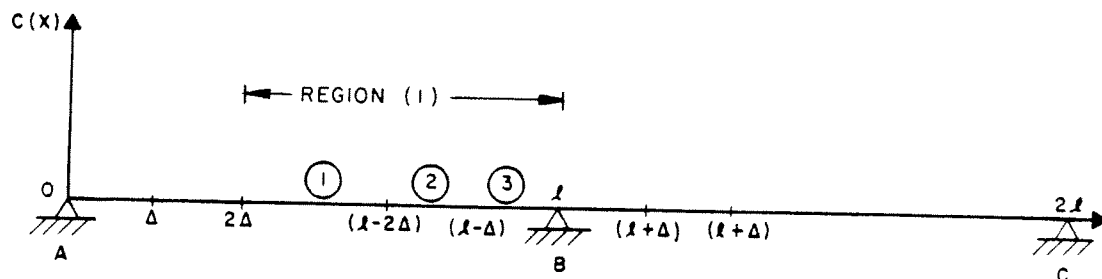


Figure A-4a. Two Adjacent Simply Supported Spans of Equal Length

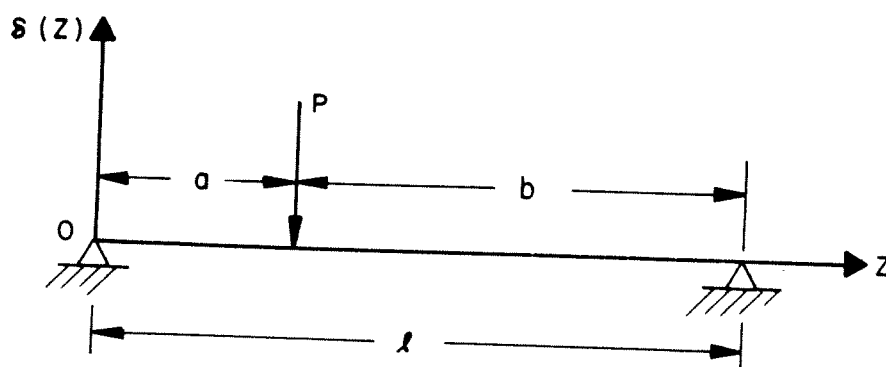


Figure A-4b. Simply Supported Beam

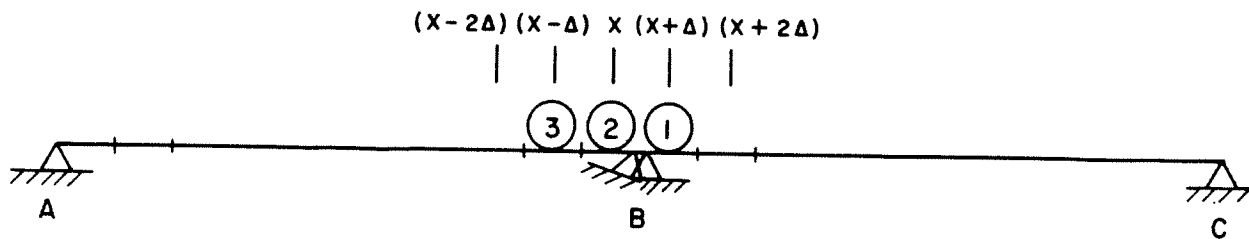
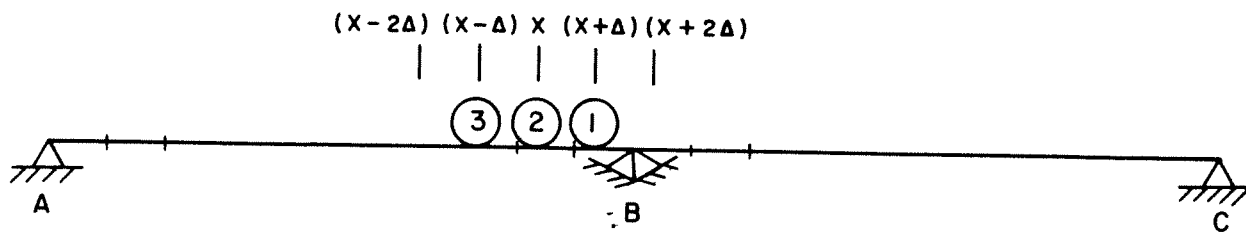
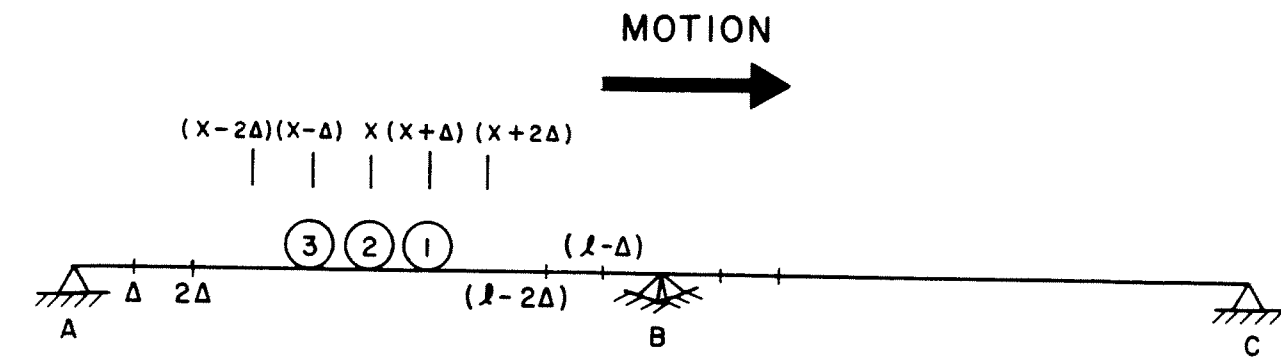


Figure A-5. Wheel Locations for a Long Span Bridge

combination with Equations (10a) and (10b). The term $\delta(X - \Delta, X + \Delta)$ is calculated by substituting $Z = X - \Delta$ and $a = X + \Delta$ in Equation (10a) since the deflection is evaluated between 0 and a . Therefore

$$\delta(X - \Delta, X + \Delta) = \frac{-P(\ell - X - \Delta)(X - \Delta)}{6EI\ell} \cdot \left[\ell^2 - (X - \Delta)^2 - (\ell - X - \Delta)^2 \right] \quad (11a)$$

Similarly

$$\begin{aligned} \delta(X + \Delta, X - \Delta) &= \frac{-P(\ell - X + \Delta)}{6EI\ell} \left[\frac{\ell}{(\ell - X + \Delta)} (2\Delta)^3 \right. \\ &\quad \left. - (X^2 - \Delta^2)(X - \Delta - 2\ell) - (X + \Delta)^3 \right] \\ &= \delta(X - \Delta, X + \Delta) \end{aligned} \quad (11b)$$

$$\begin{aligned} \delta(X - \Delta, X - 2\Delta) &= \frac{-P(\ell - X + 2\Delta)}{6EI\ell} \left[\frac{\ell}{(\ell - X + 2\Delta)} \Delta^3 \right. \\ &\quad \left. - (X - 2\Delta)(X - 2\Delta - 2\ell)(X - \Delta) \right. \\ &\quad \left. - (X - \Delta)^3 \right] \end{aligned} \quad (11c)$$

$$\begin{aligned} \delta(X + \Delta, X + 2\Delta) &= \frac{P(\ell - X - 2\Delta)}{6EI\ell} (X + \Delta) \\ &\quad \left[\ell^2 - (X + \Delta)^2 - (\ell - X - 2\Delta)^2 \right] \end{aligned} \quad (11d)$$

It is found, upon direct expansion and simplification of Equations (11a) and (11b), that $\delta(X - \Delta, X + \Delta) = \delta(X + \Delta, X - \Delta)$. Substituting the expressions (11a), (11b), (11c), and (11d) into Equation (7) and carrying out lengthy algebraic manipulations, the result is

$$C(X) = \frac{P}{12EI\ell} \left[54 X^2 \Delta^2 - 54 X \Delta^2 \ell - 7 \Delta^3 \ell + 12 \ell^2 \Delta^2 + 24 \Delta^4 \right]$$

Simplifying further, the dimensionless signature for the MCO-difference $C(X)$ is,

$$\frac{C(X/\ell)}{(P\ell^3/EI)} = \left(\frac{\Delta}{\ell}\right)^2 \left[\left(1 - 3 \frac{X}{\ell}\right) \left(1 - \frac{3}{2} \frac{X}{\ell}\right) - \frac{7}{12} \left(\frac{\Delta}{\ell}\right) + 2 \left(\frac{\Delta}{\ell}\right)^2 \right] \quad (12)$$

It may be verified that the right-hand side of Equation (12) is symmetric about $X/\ell = 1/2$ and has a minimum at that point.

CASE II: $\left(1 - 2 \frac{\Delta}{\ell}\right) \leq \frac{X}{\ell} \leq \left(1 - \frac{\Delta}{\ell}\right)$

In this case the location $(X + 2\Delta)$ lies on the adjacent beam BC and therefore, assuming independent spans, a load applied at $(X + 2\Delta)$ does not produce a deflection at $(X + \Delta)$. Consequently

$$\delta(X + \Delta, X + 2\Delta) \equiv 0$$

The terms $\delta(X - \Delta, X + \Delta)$, $\delta(X + \Delta, X - \Delta)$, and $\delta(X - \Delta, X - 2\Delta)$ are the same as in Equation (11a), (11b) and (11c). With these substitutions, Equation (7) yields

$$\begin{aligned}
\frac{C(X/\ell)}{(P\ell^3/EI)} = & - 2 \left(\frac{X}{\ell}\right)^4 + 4 \left(1 - 3 \frac{\Delta}{\ell}\right) \left(\frac{X}{\ell}\right)^3 \\
& - \left\{ 2 - 18 \frac{\Delta}{\ell} - 27 \left(\frac{\Delta}{\ell}\right)^2 \right\} \left(\frac{X}{\ell}\right)^2 \\
& - 3 \left(\frac{\Delta}{\ell}\right) \left(1 + 3 \frac{\Delta}{\ell}\right) \left(2 + 3 \frac{\Delta}{\ell}\right) \left(\frac{X}{\ell}\right) \\
& + 2 \left\{ 4 + 3 \left(\frac{\Delta}{\ell}\right) + 7 \left(\frac{\Delta}{\ell}\right)^2 \right\}
\end{aligned} \tag{13}$$

CASE III: $\left(1 - \frac{\Delta}{\ell}\right) \leq \frac{X}{\ell} \leq 1$

For this case the point, $(X + \Delta)$ lies on the beam BC and the point $(X - \Delta)$ lies on the beam AB. Therefore, there is no deflection at $(X - \Delta)$ due to loads at $(X + \Delta)$ and vice versa. Hence, in Equation (7)

$$\delta(X - \Delta, X + \Delta) \equiv 0$$

$$\text{and } \delta(X + \Delta, X - \Delta) \equiv 0$$

The term $\delta(X - \Delta, X - 2\Delta)$ is the same as in Equation (11c). To evaluate the last term $\delta(X + \Delta, X + 2\Delta)$, one must exercise care since both points of load application, $(X + 2\Delta)$, and the point at which deflection is considered, i.e., $(X + \Delta)$, occur on beam BC. Therefore, Equation (10a) must be modified to match the coordinate system of Figure A-4a. This is accomplished by recognizing that

$$a = X + 2\Delta - \ell$$

$$\text{and } Z = X + \Delta - \ell$$

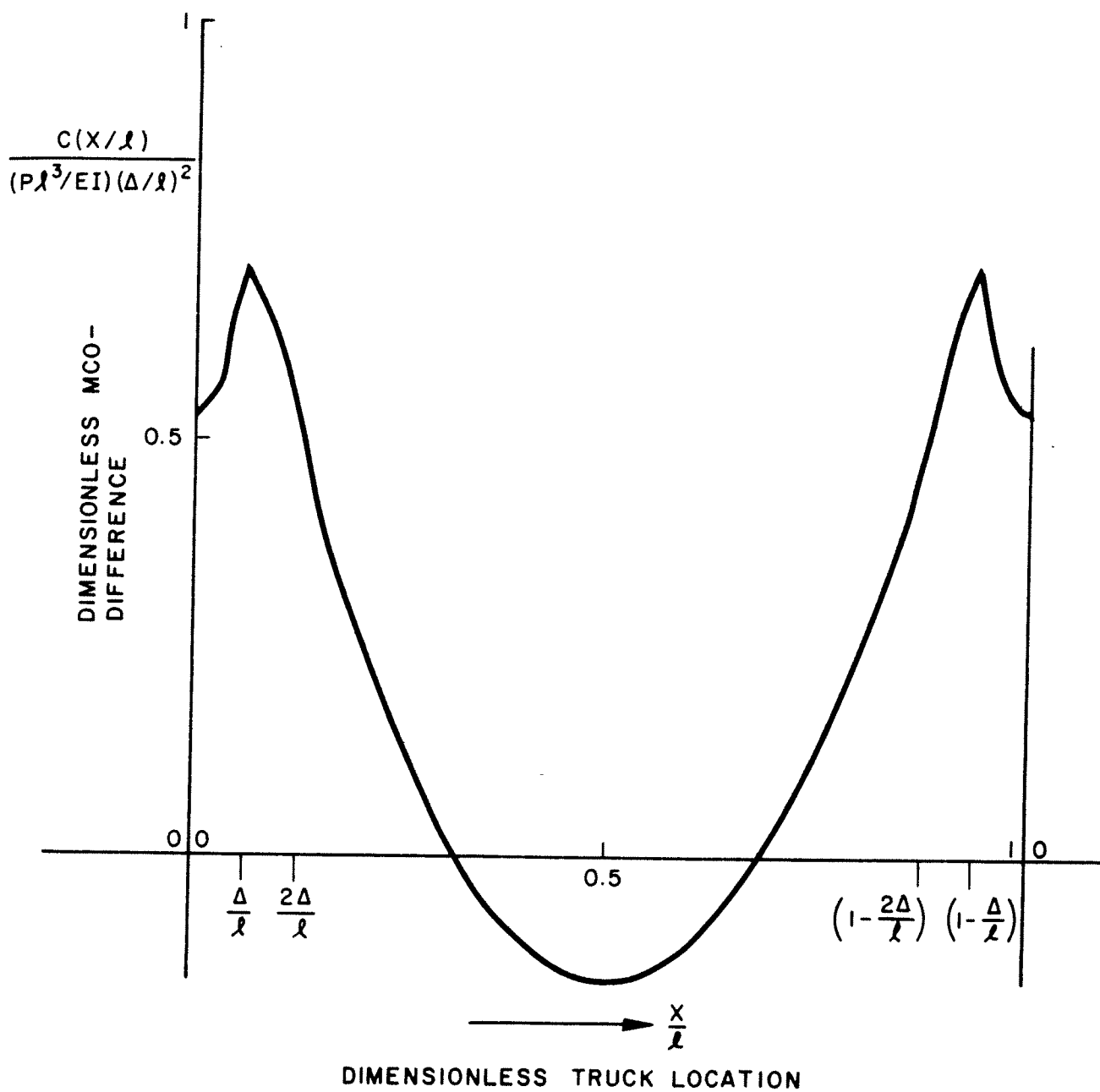


Figure A-6. Signature of MCO-Difference for a Simple Supported Span with Length $l \geq 4\Delta$

in Equation (10a). Thus

$$\delta(X + \Delta - \ell, X + 2\Delta - \ell) = - \frac{P}{6EI\ell} (2\ell - X - 2\Delta)(X + \Delta - \ell).$$

$$\left[\ell^2 - (X + \Delta - \ell)^2 - (2\ell - X - 2\Delta)^2 \right]$$

Incorporating the aforementioned deflection formulas into Equation (7), and performing the necessary algebra, the resulting MCO-difference is given by

$$\begin{aligned} \frac{C(X/\ell)}{(P\ell^3/EI)} = & 4 \left(\frac{X}{\ell} \right)^4 - 16 \left(\frac{X}{\ell} \right)^3 + 2 \left\{ 14 - 18 \left(\frac{\Delta}{\ell} \right) + 27 \left(\frac{\Delta}{\ell} \right)^2 \right\} \left(\frac{X}{\ell} \right)^2 \\ & - 12 \left\{ 2 - 6 \left(\frac{\Delta}{\ell} \right) + 9 \left(\frac{\Delta}{\ell} \right)^2 \right\} \left(\frac{X}{\ell} \right) \\ & + \left\{ 8 - 36 \left(\frac{\Delta}{\ell} \right) + 62 \left(\frac{\Delta}{\ell} \right)^2 - 26 \left(\frac{\Delta}{\ell} \right)^3 + 20 \left(\frac{\Delta}{\ell} \right)^4 \right\} \quad (14) \end{aligned}$$

Equations (12), (13) and (14) represent the complete solution for the MCO-difference. It should be mentioned that the expressions for $C(X)$ in the ranges $0 \leq \frac{X}{\ell} \leq \frac{\Delta}{\ell}$ and $\frac{\Delta}{\ell} \leq \frac{X}{\ell} \leq 2 \frac{\Delta}{\ell}$ are obtained by replacing $\frac{X}{\ell}$ with $(1 - X/\ell)$ in Equations (14) and (13), respectively.

As a numerical example, consider the Accotink bridge with $\frac{\Delta}{\ell} \approx \frac{5.5}{80} \approx \frac{1}{16}$, the signature for the MCO-difference, obtained from Equations (12), (13) and (14) is shown in Figure A-6. Notice the discontinuities in slope at $\frac{X}{\ell} = \frac{\Delta}{\ell}$ and $(1 - \Delta/\ell)$. This signature form, which has been obtained for one span, will repeat itself as the 3-axle truck traverses a bridge having equal spans. Strictly speaking, for a long bridge under consideration, the effect of the second 3-axle truck (as in the case of the R-1 car) should also be investigated.

A.3.2 FIXED END SPANS

The deflection equation for a beam fixed at both supports (i.e. resisting moment at each end) is, in terms of the notation of Figure A-4b.

$$\delta(Z, a) = \frac{-P(\ell - a)^2 Z^2}{6EI\ell^3} \left[3a\ell - 3aZ - (\ell - a)Z \right] \quad (15a)$$

for $0 \leq Z \leq a$

$$\delta(Z, a) = \frac{-Pa^2(\ell - Z)^2}{6EI\ell^3} \left[3\ell(\ell - a) - (\ell - Z)(3\ell - 2a) \right] \quad (15b)$$

for $a \leq Z \leq \ell$

Following the same procedure as in Sec. 3.1, three different cases are treated.

CASE I: $2 \frac{\Delta}{\ell} \leq \frac{X}{\ell} \leq \left(1 - 2 \frac{\Delta}{\ell}\right)$

$$\delta(X - \Delta, X + \Delta) = \frac{-P(\ell - X - \Delta)^2 (X - \Delta)^2}{6EI\ell^3} \left[3\ell(X + \Delta) - 3(X^2 - \Delta^2) - (\ell - X - \Delta)(X - \Delta) \right] \quad (16a)$$

$$\delta(X + \Delta, X - \Delta) = \frac{-P(X - \Delta)^2 (\ell - X - \Delta)^2}{6EI\ell^3} \left[3\ell(\ell - X + \Delta) - (\ell - X - \Delta)(3\ell - 2X + 2\Delta) \right] \quad (16b)$$

$$= \delta(X - \Delta, X + \Delta)$$

$$\delta(X - \Delta, X - 2\Delta) = \frac{-P(X - 2\Delta)^2 (\ell - X + \Delta)^2}{6EI\ell^3} \left[3\ell(\ell - X + 2\Delta) - (\ell - X + \Delta)(3\ell - 2X + 4\Delta) \right] \quad (16c)$$

$$\delta(X + \Delta, X + 2\Delta) = \frac{P(\ell - X - 2\Delta)^2 (X + \Delta)^2}{6EI\ell^3} \left[3\ell(X + 2\Delta) - 3(X + 2\Delta)(X + \Delta) - (\ell - X - 2\Delta)(X + \Delta) \right] \quad (16d)$$

Substituting Equations (16a) through (16d) into the MCO-difference Equation (7), one obtains

$$\begin{aligned} \frac{C(x/\ell)}{(P\ell^3/EI)} = & -\left(\frac{\Delta}{\ell}\right)^2 \left[12\left(\frac{x}{\ell}\right)^4 - 24\left(\frac{x}{\ell}\right)^3 + \left\{ 15 + 21\left(\frac{\Delta}{\ell}\right)^2 \right\} \left(\frac{x}{\ell}\right)^2 \right. \\ & - \left\{ 3 + 21\left(\frac{\Delta}{\ell}\right)^2 \right\} \left(\frac{x}{\ell}\right) + \frac{7}{12}\left(\frac{\Delta}{\ell}\right) + 3\left(\frac{\Delta}{\ell}\right)^2 \\ & \left. + 3\left(\frac{\Delta}{\ell}\right)^4 \right] \end{aligned} \quad (17)$$

Equation (17) should be compared with Equation (12) for the simply supported case. It is evident that Equation (17) is of 4th order, whereas the right-hand side of Equation (12) is a 2nd order expression. Thus, Equation (17) has four real zeros (as will be shown later by a numerical example) as opposed to two for Equation (12), and therefore, the signatures $C(x)$ are expected to be characteristically different. The symmetry of Equation (17) about $\frac{x}{\ell} = \frac{1}{2}$ may be readily verified by introducing a linear transformation $\zeta = \frac{x}{\ell} - \frac{1}{2}$. Also, there is a minimum at $\frac{x}{\ell} = \frac{1}{2}$.

Case II : $(1 - 2 \frac{\Delta}{\ell}) \leq \frac{x}{\ell} \leq (1 - \frac{\Delta}{\ell})$

In this case

$$\delta(x + \Delta, x + 2\Delta) \equiv 0$$

and $\delta(x - \Delta, x + \Delta)$, $\delta(x + \Delta, x - \Delta)$, $\delta(x - \Delta, x - 2\Delta)$ are given by Equations (16a), (16b), and (16c), respectively. Combining these deflections with Equation (7), the MCO-difference is

$$\begin{aligned} \frac{C(x/\ell)}{(P\ell^3/EI)} &= \frac{1}{6} \left(\frac{x}{\ell}\right)^6 - \frac{1}{2} \left(1 - 3 \frac{\Delta}{\ell}\right) \left(\frac{x}{\ell}\right)^5 \\ &+ \frac{1}{4} \left\{ 2 - 15 \left(\frac{\Delta}{\ell}\right) - 26 \left(\frac{\Delta}{\ell}\right)^2 \right\} \left(\frac{x}{\ell}\right)^4 \\ &- \frac{1}{6} \left\{ 1 - 18 \left(\frac{\Delta}{\ell}\right) - 78 \left(\frac{\Delta}{\ell}\right)^2 - 63 \left(\frac{\Delta}{\ell}\right)^3 \right\} \left(\frac{x}{\ell}\right)^3 \\ &- \frac{1}{4} \left\{ 3 \left(\frac{\Delta}{\ell}\right) + 34 \left(\frac{\Delta}{\ell}\right)^2 + 63 \left(\frac{\Delta}{\ell}\right)^3 + 40 \left(\frac{\Delta}{\ell}\right)^4 \right\} \left(\frac{x}{\ell}\right)^2 \\ &+ 2 \left\{ \left(\frac{\Delta}{\ell}\right)^2 + 3 \left(\frac{\Delta}{\ell}\right)^3 + 5 \left(\frac{\Delta}{\ell}\right)^4 + 3 \left(\frac{\Delta}{\ell}\right)^5 \right\} \left(\frac{x}{\ell}\right) \\ &- \frac{1}{3} \left\{ 3 \left(\frac{\Delta}{\ell}\right)^3 + 3 \left(\frac{\Delta}{\ell}\right)^4 + 9 \left(\frac{\Delta}{\ell}\right)^5 + 5 \left(\frac{\Delta}{\ell}\right)^6 \right\} \end{aligned} \quad (18)$$

Case III: $(1 - \frac{\Delta}{\ell}) \leq \frac{x}{\ell} \leq 1$

For this case,

$$(x - \Delta, x + \Delta) \equiv 0$$

$$(x + \Delta, x - \Delta) \equiv 0$$

The term $\delta(x - \Delta, x - 2\Delta)$ is again given by Equation (16c) and the term $\delta(x + \Delta, x + 2\Delta)$ is replaced by

$$\delta(x + \Delta - \ell, x + 2\Delta - \ell) = \frac{-P(2\ell - 2\Delta)^2(x - \ell + \Delta)^2}{6EI\ell^3}$$

$$\begin{aligned} & \left[3\ell (x - \ell + 2\Delta) \right. \\ & - 3(x - \ell + 2\Delta)(x - \ell + \Delta) \\ & \left. - (2\ell - x - 2\Delta)(x - \ell + \Delta) \right] \end{aligned}$$

$C(x)$ is obtained by substituting the above expressions into Equation (7). The result is

$$\frac{C(x/\ell)}{(P\ell^3/EI)} \quad (19)$$

Numerical calculations for $C(x)$ were performed for $\Delta/\ell = 1/16$ and the signature is plotted in Figure A-7. It is evident that the response is characteristically different from the simply supported case (Figure A-6). In particular, there are four zero crossings and the signature amplitude is quite small for the fixed-end spans. Figure A-7 shows the actual MCO-difference signature obtained during a previous field test. This signal has been passed through a 9.5-foot filter to eliminate noise due to wheel asymmetries. Using the left and right space curves, approximate locations of bridge supports are shown by the vertical lines. The resemblance between the theoretical signature of Figure A-7 and test data of Figure A-8 is encouraging. However, conclusive statements regarding the applicability of the theory can be made only after the theoretical curves are replaced by actual computations and the effects of filtering are taken into account.

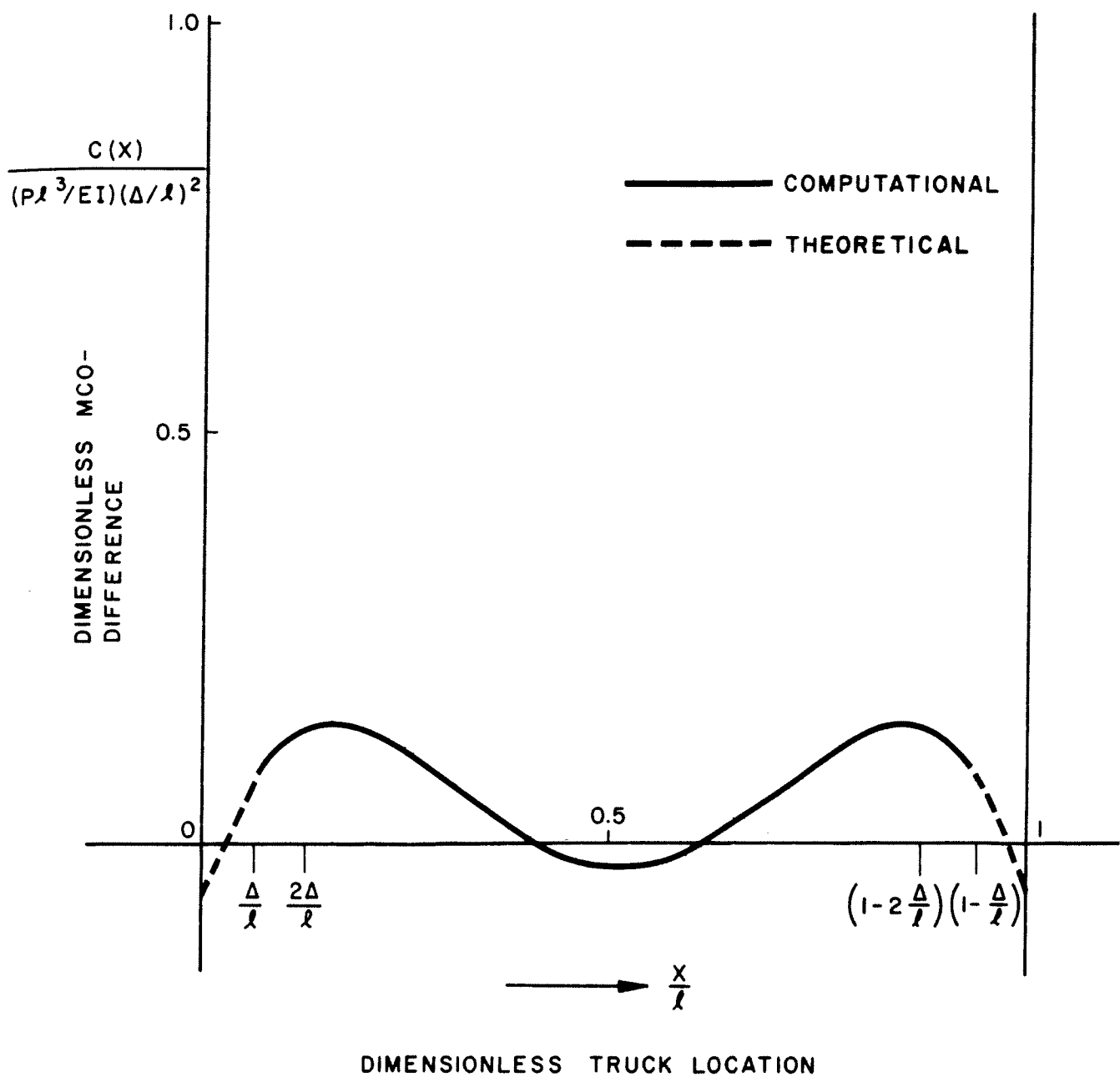


Figure A-7. Signature of MCO-Difference for a Fixed End Span with Length $l \geq 4\Delta$

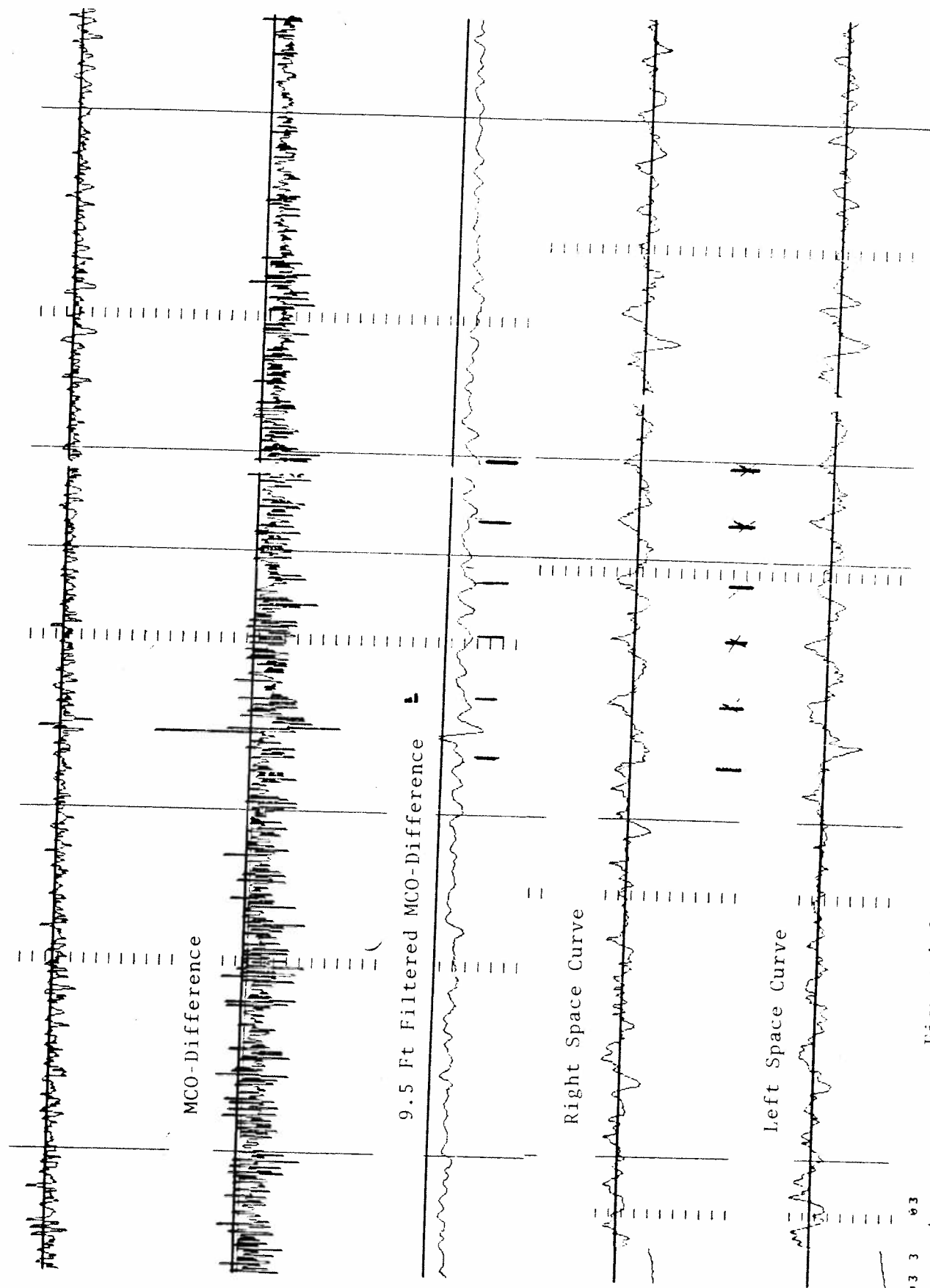


Figure A-8. MCO-Difference Signature for Accotink Bridge

A.4 MODEL FOR SHORT-SPAN BRIDGES

A.4.1 GENERAL

During the Selma-Mobile run, several timber bridges with supports in wet and muddy ground were encountered. These bridges were constructed by laying wooden beams on timber pile supports and leveling the spans with shims. These shims, and sometimes the caps on the support piles, crush under the weight of a train. Also, the piles themselves can pump in muddy ground. Consequently, timber bridge supports behave like springs. Another feature of these bridges is their short spans (13 - 15 feet). This length requires investigation of a set of solutions different from that of the previous section. In the following sections, this analysis is developed for short bridges ($l/4 \leq \Delta \leq l/2$ or $2\Delta \leq l \leq 4\Delta$, $\Delta = 5.5'$) with both rigid and flexible supports.

A.4.2 BRIDGES WITH RIGID SUPPORTS

The MCO-difference signature for a bridge with all spans of identical length and flexural rigidity is expected to be symmetric. Therefore, it is sufficient to consider the following cases:

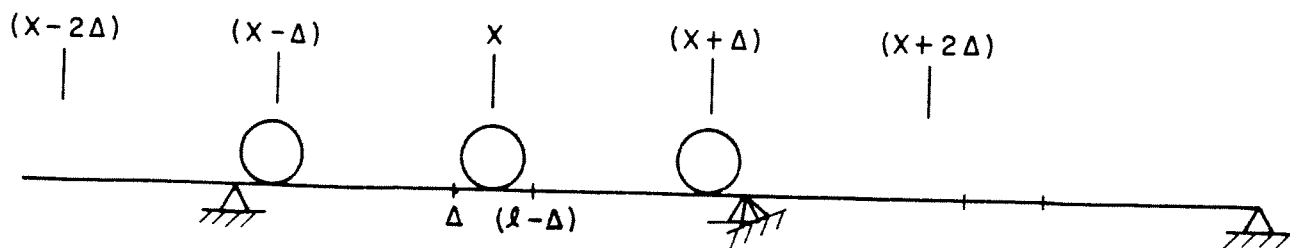
$$\text{I.} \quad \frac{\Delta}{l} \leq \frac{X}{l} \leq (1 - \frac{\Delta}{l})$$

$$\text{II.} \quad (1 - \frac{\Delta}{l}) \leq \frac{X}{l} \leq 2 \frac{\Delta}{l}$$

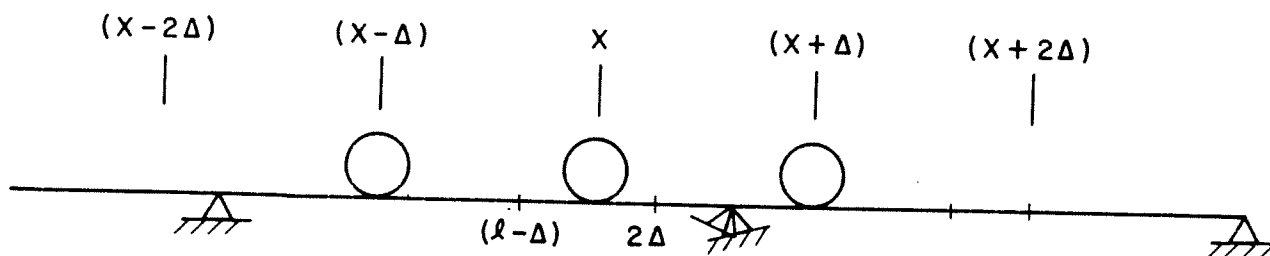
$$\text{III.} \quad 2 \frac{\Delta}{l} \leq \frac{X}{l} \leq 1$$

Figure A-9 depicts the above three regimes of solution for three adjacent spans.

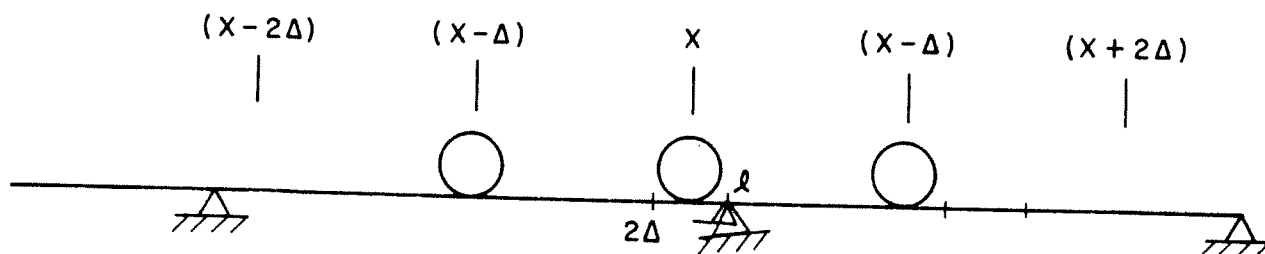
$$\text{Case I:} \quad \frac{\Delta}{l} \leq \frac{X}{l} \leq (1 - \frac{\Delta}{l})$$



CASE I



CASE II



CASE III

Figure A-9. Wheel Locations for a Short Span Bridge

From Figure A-9

$$\delta(X - \Delta, X - 2\Delta) \equiv 0$$

$$\delta(X + \Delta, X + 2\Delta) \equiv 0$$

And from Equations (10a) and (10b) for a simply supported beam

$$\delta(X - \Delta, X + \Delta) = \delta(X + \Delta, X - \Delta)$$

$$= \frac{-P(\ell - X - \Delta)(X - \Delta)}{6EI\ell} \left[\ell^2 - (X - \Delta)^2 - (\ell - X - \Delta)^2 \right]$$

Substituting these deflections into the MCO-difference Equation (7), one obtains

$$\frac{C(X/\ell)}{(P\ell^3/EI)} = \frac{1}{6} \left[-X^2 \left(\frac{X}{\ell}\right)^4 + 4\left(\frac{X}{\ell}\right)^3 - 2\left(\frac{X}{\ell}\right)^2 + 2\left(\frac{\Delta}{\ell}\right)^2 - 4\left(\frac{\Delta}{\ell}\right)^3 + 2\left(\frac{\Delta}{\ell}\right)^4 \right] \quad (20)$$

$$\text{Case II: } (1 - \frac{\Delta}{\ell}) \leq \frac{X}{\ell} \leq 2 \frac{\Delta}{\ell}$$

In this case,

$$(X - \Delta, X - 2\Delta) \equiv 0$$

$$(X + \Delta, X + \Delta) \equiv 0$$

$$(X + \Delta, X - \Delta) \equiv 0$$

and,

$$\begin{aligned} \delta(X + \Delta, X + 2\Delta) &\equiv \delta(X + \Delta - \ell, X + 2\Delta - \ell) \\ &= \frac{-P}{6EI\ell} (2\ell - X - 2\Delta)(X + \Delta - \ell) \\ &\quad \left[\ell^2 - (X + \Delta - \ell)^2 - (2\ell - X - 2\Delta)^2 \right] \end{aligned}$$

Incorporating these deflections into Equation (7), the MCO-difference is

$$\begin{aligned} \frac{C(X/\ell)}{(P\ell^3/EI)} = \frac{1}{12} & \left[2\left(\frac{X}{\ell}\right)^4 - 12 \left\{ 1 - \frac{\Delta}{\ell} \right\} \left(\frac{X}{\ell}\right)^3 \right. \\ & + \left\{ 26 - 54\left(\frac{\Delta}{\ell}\right) + 27\left(\frac{\Delta}{\ell}\right)^2 \right\} \left(\frac{X}{\ell}\right)^2 \\ & + \left\{ -24 + 78\left(\frac{\Delta}{\ell}\right) - 81\left(\frac{\Delta}{\ell}\right)^2 + 27\left(\frac{\Delta}{\ell}\right)^3 \right\} \left(\frac{X}{\ell}\right) \\ & \left. + \left\{ 8 - 36\left(\frac{\Delta}{\ell}\right) + 58\left(\frac{\Delta}{\ell}\right)^2 - 40\left(\frac{\Delta}{\ell}\right)^3 + 10\left(\frac{X}{\ell}\right)^4 \right\} \right] \end{aligned} \quad (21)$$

CASE III: $2\frac{\Delta}{\ell} \leq \frac{X}{\ell} \leq 1$

The deflections in this case (Figure A-9) are given by

$$\delta(X - \Delta, X + \Delta) \equiv 0$$

$$\delta(X + \Delta, X - \Delta) \equiv 0$$

$$\begin{aligned} \delta(X - \Delta, X - 2\Delta) = \frac{-P(\ell - X + 2\Delta)}{6EI\ell} & \left[\frac{\ell}{(\ell - X + 2\Delta)} \Delta^3 \right. \\ & - (X - 2\Delta)(X - 2\Delta - 2\ell)(X - \Delta) \\ & \left. - (X - \Delta)^3 \right] \end{aligned}$$

$$\delta(X + \Delta, X + 2\Delta) = \delta(X + \Delta - \ell, X + 2\Delta - \ell)$$

$$= \frac{-P}{6EI\ell} (2\ell - X - 2\Delta)(X + \Delta - \ell)$$

$$\left[\ell^2 - (X + \Delta - \ell)^2 - (2\ell - X - 2\Delta)^2 \right]$$

The MCO-difference obtained from Equation (7) for the above deflections is,

$$\begin{aligned} \frac{C(X/\ell)}{(P\ell^3/EI)} = \frac{1}{12} \left[4\left(\frac{X}{\ell}\right)^4 - 16\left(\frac{X}{\ell}\right)^3 + 2 \left\{ 14 - 18\left(\frac{\Delta}{\ell}\right) + 27\left(\frac{\Delta}{\ell}\right)^2 \right\} \left(\frac{X}{\ell}\right)^2 \right. \\ \left. - 12 \left\{ 2 - 6\left(\frac{\Delta}{\ell}\right) + 9\left(\frac{\Delta}{\ell}\right)^2 \right\} \left(\frac{X}{\ell}\right) \right. \\ \left. + \left\{ 8 - 36\left(\frac{\Delta}{\ell}\right) + 62\left(\frac{\Delta}{\ell}\right)^2 - 26\left(\frac{\Delta}{\ell}\right)^3 + 20\left(\frac{\Delta}{\ell}\right)^4 \right\} \right] \quad (22) \end{aligned}$$

Similar analysis for a fixed-end, short span leads to the following results:

$$\begin{aligned} \frac{C(X/\ell)}{(P\ell^3/EI)} = \frac{1}{6} \left(1 - \frac{X}{\ell} - \frac{\Delta}{\ell} \right)^2 \left(\frac{X}{\ell} - \frac{\Delta}{\ell} \right)^2 \left[2\left(\frac{X}{\ell}\right)^2 - 2\left(\frac{X}{\ell}\right) - 4\left(\frac{\Delta}{\ell}\right) \right] \\ \text{for } \frac{\Delta}{\ell} \leq \frac{X}{\ell} \leq \left(1 - \frac{\Delta}{\ell} \right) \quad (23a) \end{aligned}$$

$$\begin{aligned} = \frac{1}{12} \left(2 - \frac{X}{\ell} - 2\frac{\Delta}{\ell} \right)^2 \left(\frac{X}{\ell} - 1 + \frac{\Delta}{\ell} \right)^2 \\ \left[3\left(\frac{X}{\ell} - 1 + 2\frac{\Delta}{\ell}\right) \left(\frac{X}{\ell} - 1 + \frac{\Delta}{\ell} \right) \right. \\ \left. + \left(2 - \frac{X}{\ell} - 2\frac{\Delta}{\ell} \right) \left(\frac{X}{\ell} - 1 + \frac{\Delta}{\ell} \right) \right. \\ \left. - 3 \left(\frac{X}{\ell} - 1 + \frac{\Delta}{\ell} \right) \right] \\ \text{for } \left(1 - \frac{\Delta}{\ell} \right) \leq \frac{X}{\ell} \leq \frac{2\Delta}{\ell} \quad (23b) \end{aligned}$$

and

$$\begin{aligned} \frac{C(X/\ell)}{(P\ell^3/EI)} = \\ \text{for } \frac{2\Delta}{\ell} \leq \frac{X}{\ell} \leq 1 \quad (23c) \end{aligned}$$

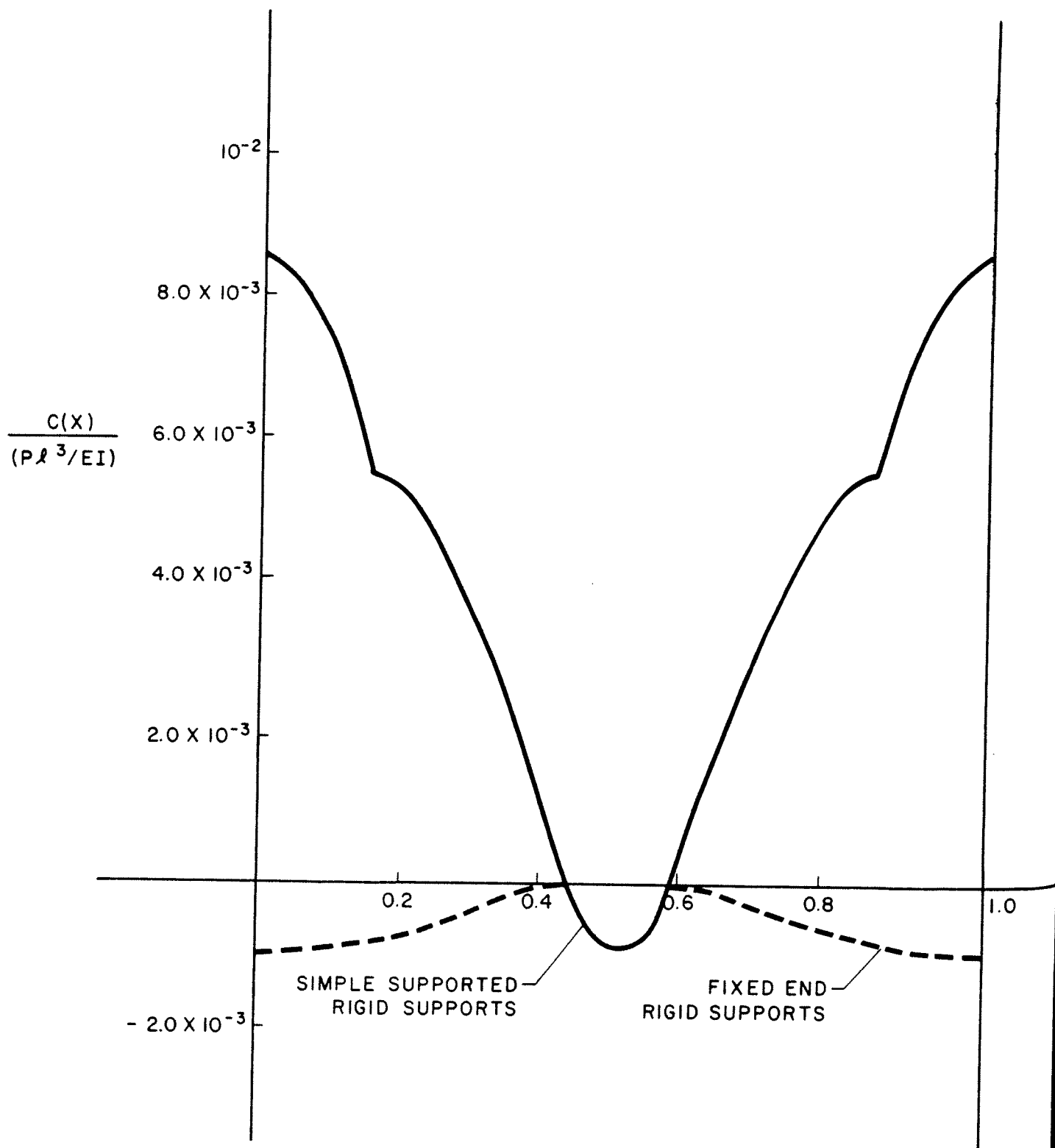


Figure A-10. Signature of MCO-Difference for Short Spans with 11-Feet $\leq l \leq$ 22 Feet

The MCO-difference responses given by Equations (20), (21), (22) and (23) are plotted in Figure A-10. It is of interest to compare Figure A-10 with Figure A-6 and A-7 in order to see the effect of the ratio of beam length to bridge span.

A.4.3 BRIDGE WITH FLEXIBLE SUPPORTS

The preceeding analysis can be extended to a bridge with flexible supports by the application of the principle of superposition. In other words, deflection of an elastic beam on flexible supports is the sum of the deflections of an elastic beam on rigid supports and an inelastic beam on flexible supports (Figure A-11).

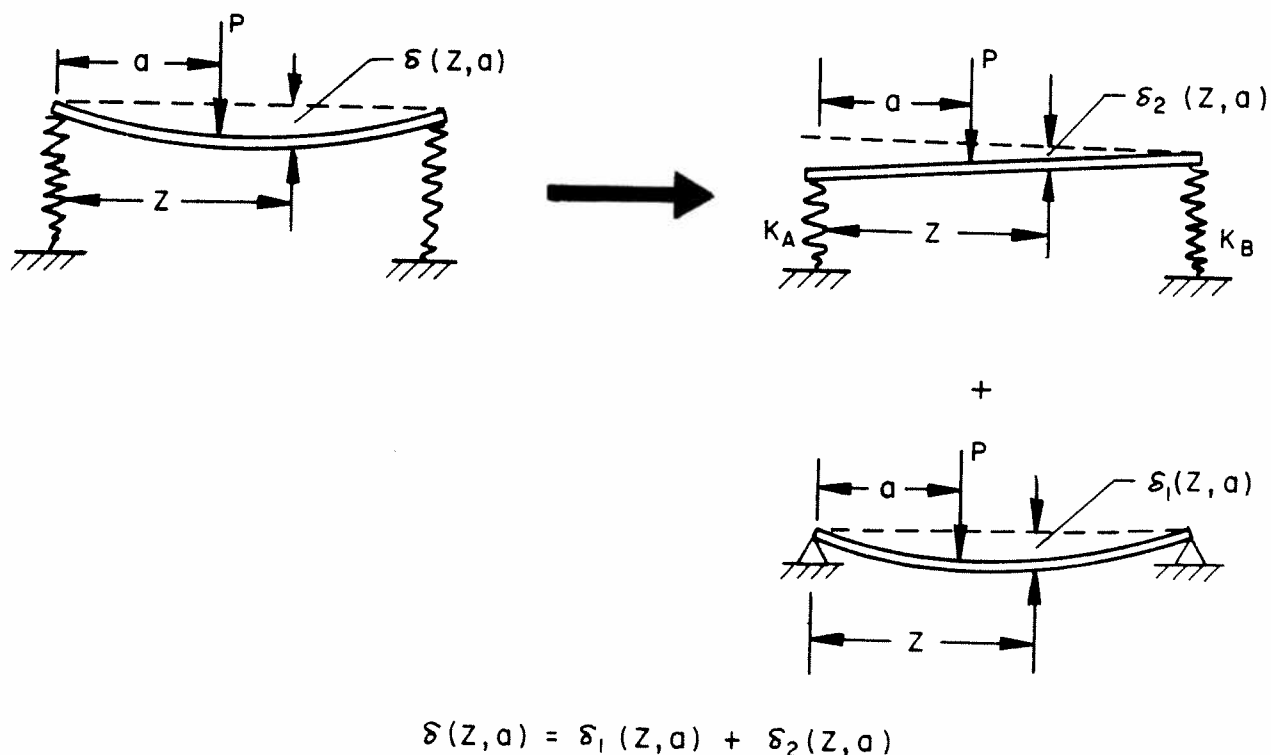


Figure A-11. Superposition of Deflections for an Elastic Beam on Flexible Supports.

It can be readily verified that the deflection function δ_2 is given by the linear relation

$$\delta_2(z, a) = \frac{Pa z}{K_B \ell^2} + \frac{P(\ell - a)(\ell - z)}{K_A \ell^2} \quad (24)$$

where K_A and K_B are spring components (in force per unit deflection) for the flexible supports. For supports with equal flexibility, $K_A = K_B = K$ and Equation (24) becomes

$$\delta_2(z, a) = \frac{P(\ell - a)}{K\ell} + \frac{Pz}{K\ell^2} (2a - \ell) \quad (25)$$

As an example, consider application of the above approach to Case I of Section A.4.2. Figure A-12 shows the various deflections which are required to evaluate the MCO-difference. Note that the spans are assumed to be pin-jointed and can therefore rotate relative to each other. By applying Equation (25) to Figure A-12(a), it is evident that

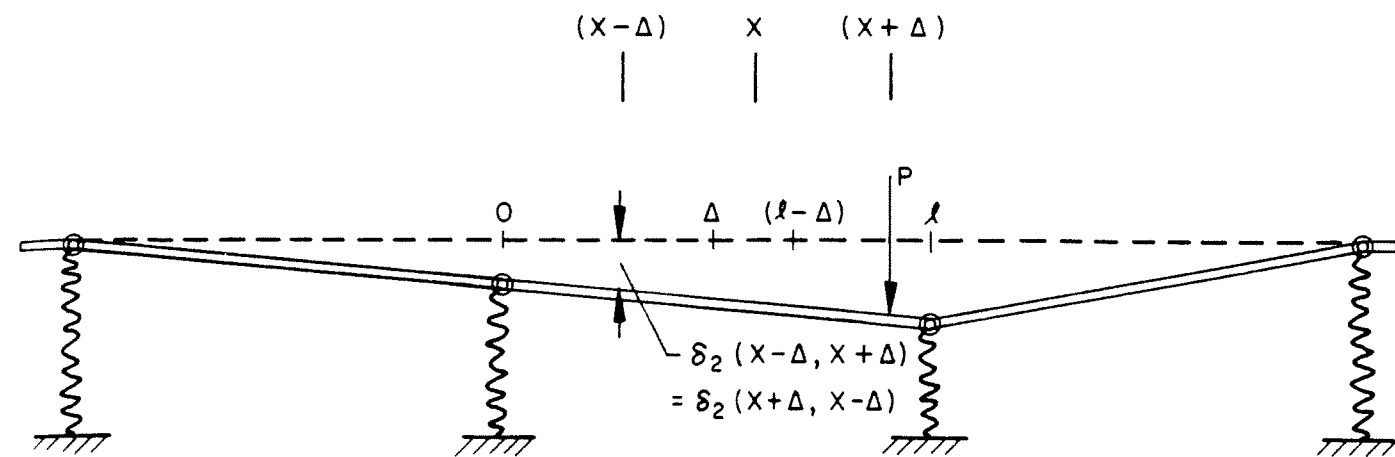
$$\delta_2(X - \Delta, X + \Delta) = \frac{P(\ell - X - \Delta)}{K\ell} + \frac{P(X - \Delta)}{K\ell^2} [2(X + \Delta) - \ell] \quad (26a)$$

$$\delta_2(X + \Delta, X - \Delta) = \delta_2(X - \Delta, X + \Delta) \quad (26b)$$

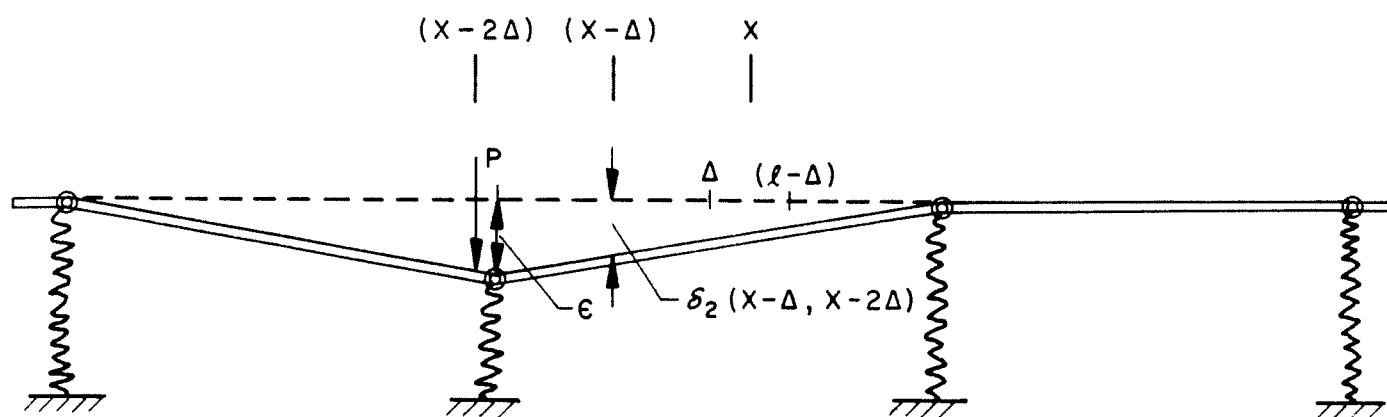
From Figure A-12(b)

$$\delta_2(X - \Delta, X - 2\Delta) = \frac{\varepsilon}{\ell} (\ell - X + \Delta)$$

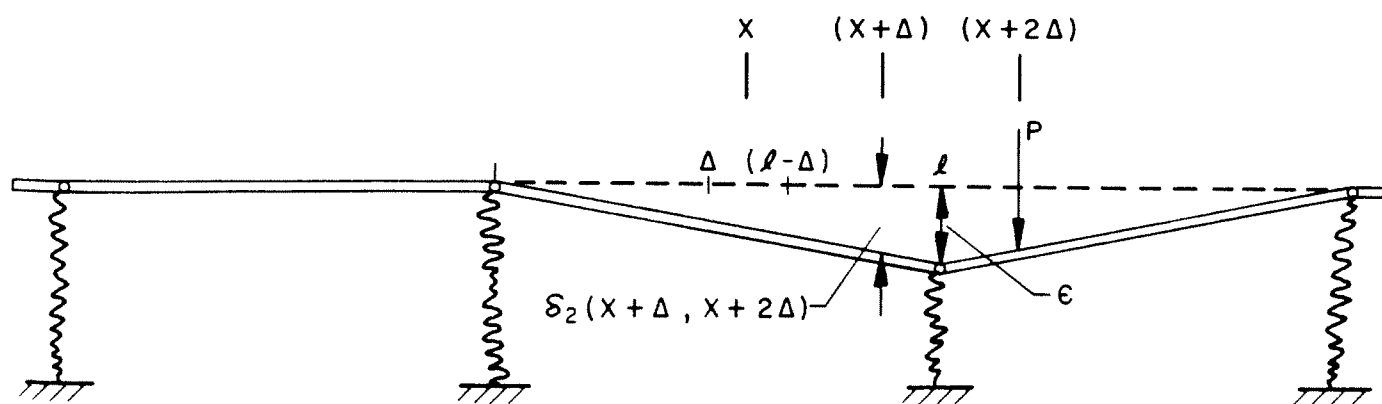
Since $\varepsilon = \delta(0, X - 2\Delta) = \delta(\ell, X - 2\Delta + \ell)$



(a)



(b)



(c)

Figure A-12. Case I for Flexible Supports

$$\text{we have, } \delta_2(X - \Delta, X - 2\Delta) = \frac{(\ell - X + \Delta)}{\ell} \left[\frac{P(\ell - X + 2\Delta - \ell)}{K\ell} + \frac{P\ell}{K\ell^2} (2X - 4\Delta + 2\ell - \ell) \right] \quad (26c)$$

Similarly, it may be verified from Figure A-12(c) that

$$\begin{aligned} \delta_2(X + \Delta, X + 2\Delta) &= \frac{\varepsilon}{\ell} (X + \Delta) \\ &= \frac{(X + \Delta)}{\ell} \delta(\ell, X + 2\Delta) \\ &= \frac{(X + \Delta)}{\ell} \delta(0, X + 2\Delta - \ell) \\ &= \frac{(X + \Delta)}{\ell} \left[\frac{P(2\ell - 2\Delta - X)}{K\ell} \right] \end{aligned} \quad (26d)$$

Substitution of the deflections in Equation (26) into Equation (7) yields the MCO-difference due to a rigid span on flexible supports. Adding to this the contribution of an elastic beam on rigid supports, i.e., Equation (20), the result is

$$\begin{aligned} \frac{C(X/\ell)}{(P\ell^3/EI)} &= \frac{1}{6} \left[-2\left(\frac{X}{\ell}\right)^4 + 4\left(\frac{X}{\ell}\right)^3 - 2\left(\frac{X}{\ell}\right)^2 + 2\left(\frac{\Delta}{\ell}\right)^2 - 4\left(\frac{\Delta}{\ell}\right)^3 \right. \\ &\quad \left. + 2\left(\frac{\Delta}{\ell}\right)^4 \right] + \frac{EI}{2K\ell^3} \left[-6\left(\frac{X}{\ell}\right)^2 + 6\left(\frac{X}{\ell}\right) - 1 + \left(\frac{\Delta}{\ell}\right) \right] \\ &\quad \text{for } \frac{\Delta}{\ell} \leq \frac{X}{\ell} \leq (1 - \frac{\Delta}{\ell}) \end{aligned} \quad (27)$$

Notice in Equation (27) the appearance of the non-dimensional $EI/K\ell^3$, which characterizes the relative importance of flexural rigidity of the beam span and the flexibility of the supports. If the supports are extremely rigid (K very large), $EI/K\ell^3$ is

very small and the first bracketed term in Equation (27) dominates the MCO-difference. On the other hand, for sufficiently soft supports, $EI/K\ell^3$ can have moderate value, and the second bracketed term in Equation (27) becomes significant.

One can carry out the analysis for the remaining two cases and complete MCO-difference response for the entire span.

Thus,

$$\begin{aligned} \frac{C(X/\ell)}{(P\ell^3/EI)} = & \frac{1}{12} \left[2\left(\frac{X}{\ell}\right)^4 - 12 \left\{ 1 - \left(\frac{\Delta}{\ell}\right) \right\} \left(\frac{X}{\ell}\right)^3 \right. \\ & + \left\{ 26 - 54\left(\frac{\Delta}{\ell}\right) + 27\left(\frac{\Delta}{\ell}\right)^2 \right\} \left(\frac{X}{\ell}\right)^2 \\ & + \left\{ -24 + 78\left(\frac{\Delta}{\ell}\right) - 81\left(\frac{\Delta}{\ell}\right)^2 + 27\left(\frac{\Delta}{\ell}\right)^3 \right\} \left(\frac{X}{\ell}\right) \\ & + \left. \left\{ 8 - 36\left(\frac{\Delta}{\ell}\right) + 58\left(\frac{\Delta}{\ell}\right)^2 - 40\left(\frac{\Delta}{\ell}\right)^3 + 10\left(\frac{\Delta}{\ell}\right)^4 \right\} \right] \\ & + \frac{EI}{2K\ell^3} \left[3\left(\frac{X}{\ell}\right)^2 - \left\{ 10 - 9\left(\frac{\Delta}{\ell}\right) \right\} \left(\frac{X}{\ell}\right) + 6 - 6\left(\frac{\Delta}{\ell}\right) \right] \end{aligned} \quad (28)$$

$$\text{for } \left(1 - \frac{\Delta}{\ell}\right) \leq \frac{X}{\ell} \leq 2\frac{\Delta}{\ell}$$

and

$$\begin{aligned} \frac{C(X/\ell)}{(P\ell^3/EI)} = & \frac{1}{12} \left[4\left(\frac{X}{\ell}\right)^4 - 16\left(\frac{X}{\ell}\right)^3 + \right. \\ & + 2 \left\{ 14 - 18\left(\frac{\Delta}{\ell}\right) + 27\left(\frac{\Delta}{\ell}\right)^2 \right\} \left(\frac{X}{\ell}\right)^2 \\ & - 12 \left\{ 2 - 6\left(\frac{\Delta}{\ell}\right) + 9\left(\frac{\Delta}{\ell}\right)^2 \right\} \left(\frac{X}{\ell}\right) \\ & + \left. 6 - 6\left(\frac{\Delta}{\ell}\right) + 3\left(\frac{\Delta}{\ell}\right)^2 \right] \end{aligned} \quad (29)$$

$$+ \left\{ 8 - 36\left(\frac{\Delta}{\ell}\right) + 62\left(\frac{\Delta}{\ell}\right)^2 - 26\left(\frac{\Delta}{\ell}\right)^3 + 20\left(\frac{\Delta}{\ell}\right)^4 \right\}$$

$$+ \frac{EI}{2K\ell^3} \left[6\left(\frac{X}{\ell}\right)^2 - 12\left(\frac{X}{\ell}\right) + 6 - 2\left(\frac{\Delta}{\ell}\right) + 6\left(\frac{\Delta}{\ell}\right)^2 \right]$$

$$\text{for } 2\frac{\Delta}{\ell} \leq \frac{X}{\ell} \leq 1$$

The effect of introducing support flexibility into the MCO-difference signature is shown in Figure A-13. The influence of soft support is quite dramatic in that the signature reverses itself beyond a certain value of $EI/K\ell^3$. The calculations in Figure A-13 apply to typical 13-foot spans of timber bridges, hence $\Delta/\ell = 5.5/13.0 = 0.423$.

A.4.4 ESTABLISHMENT OF ABSOLUTE ZERO OF $C(X)$ USING SYMMETRICAL SIGNATURES

One of the difficulties associated with all stiffness-related measurements has been the calibration of beam MCO. Consequently, the knowledge of a zero reference for the MCO-difference signature does not exist. The symmetrical signatures for infinitely rigid supports (Figure A-10) or in equally flexible supports (Figure A-13) can be used to establish such a reference. This is accomplished as follows. For rigid supports, Equations (20) and (22) yield,

$$\bar{b} = \left[\frac{C(X/\ell)}{(P\ell^3/EI)} \right]_{\max} = \left[\frac{C(X/\ell)}{(P\ell^3/EI)} \right]_{\frac{X}{\ell} = \frac{1}{2}}$$

$$= \frac{1}{6} \left[-\frac{1}{8} + 2\left(\frac{\Delta}{\ell}\right)^2 + 4\left(\frac{\Delta}{\ell}\right)^3 + 2\left(\frac{\Delta}{\ell}\right)^4 \right]$$

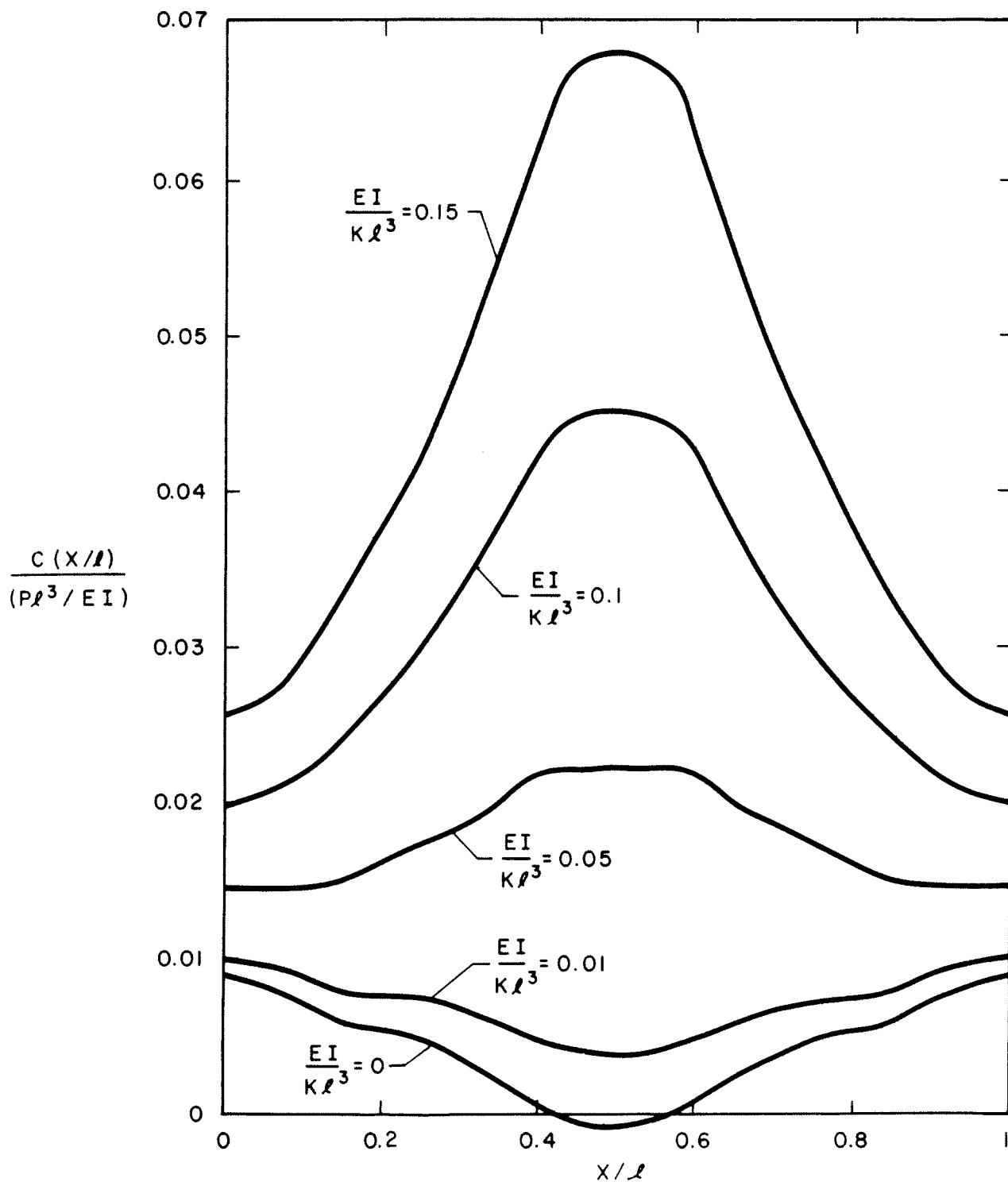


Figure A-13. Signature of MCO-Difference for Short Spans ($11 \text{ Feet} \leq l \leq 22 \text{ Feet}$) with Flexible Supports. $\Delta/l = 0.423$

and

$$\begin{aligned}\bar{a} &= \left[\frac{C(X/\ell)}{(P\ell^3/EI)} \right]_{\min} = \left[\frac{C(X/\ell)}{(P\ell^3/EI)} \right]_{\frac{X}{\ell} = 1} \\ &= \frac{1}{6} \left(\frac{\Delta}{\ell} \right)^2 \left[5 - 13 \left(\frac{\Delta}{\ell} \right) + 10 \left(\frac{\Delta}{\ell} \right)^2 \right]\end{aligned}$$

The ratio \bar{b}/\bar{a} is

$$\frac{\bar{b}}{\bar{a}} = \left(\frac{\bar{b}}{\bar{a}} \right)_{\dim} = \frac{\left[-\frac{1}{8} + 2 \left(\frac{\Delta}{\ell} \right)^2 + 4 \left(\frac{\Delta}{\ell} \right)^3 + 2 \left(\frac{\Delta}{\ell} \right)^4 \right]}{\left(\frac{\Delta}{\ell} \right)^2 \left[5 - 13 \left(\frac{\Delta}{\ell} \right) + 10 \left(\frac{\Delta}{\ell} \right)^2 \right]} = f \left(\frac{\Delta}{\ell} \right) \quad (30)$$

and it is a constant for a bridge of given span since Δ/ℓ is fixed. Now, the dimensional peak-to-peak amplitude $(\bar{b} - \bar{a})$ is measured directly from the MCO-difference data collected in the field (Figure A-14). Assuming the absence of any noise, the absolute zero location \bar{a} is given by

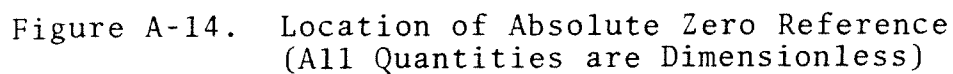
$$(\bar{a})_{\dim} = \frac{(\bar{b} - \bar{a})_{\text{measured}}}{f \left(\frac{\Delta}{\ell} \right) - 1} \quad (31)$$

When the supports are sufficiently flexible ($EI/K\ell^3 > 0.25$), the second terms of Equations (27), (28) and (29) are dominant as pointed out earlier. Therefore

$$b = \left[\frac{C(X/\ell)}{P\ell^3/EI} \right]_{\max} \approx \frac{EI}{2K\ell^3} \left[\frac{1}{2} + \frac{\Delta}{\ell} \right]$$

and

$$a = \left[\frac{C(X/\ell)}{P\ell^3/EI} \right]_{\min} \approx \frac{EI}{K\ell^3} \left(\frac{\Delta}{\ell} \right) \left[3 \frac{\Delta}{\ell} - 1 \right]$$


$$\frac{b}{a} = \left(\frac{b}{a}\right)_{\text{dim}} = \frac{1 + 2\left(\frac{\Delta}{\ell}\right)}{4\left(\frac{\Delta}{\ell}\right)\left(3\frac{\Delta}{\ell} - 1\right)} = g\left(\frac{\Delta}{\ell}\right) \quad (32)$$
$$(a)_{\text{dim}} = \frac{(b - a)_{\text{measured}}}{g\left(\frac{\Delta}{\ell}\right) - 1} \quad (33)$$

A-37

Finally, the case of slightly flexible supports ($0 < EI/K\ell^3 < 0.25$) can be treated as follows. In contrast to the previous extreme cases, the knowledge of EI and P is required in addition to the bridge span ℓ . Evaluating Equation (27) at $X/\ell = 1/2$ and Equation (29) at $X/\ell = 1$, one obtains

$$b = \frac{1}{6} \left[-\frac{1}{8} + 2\left(\frac{\Delta}{\ell}\right)^2 - 4\left(\frac{\Delta}{\ell}\right)^3 + 2\left(\frac{\Delta}{\ell}\right)^4 \right] + \frac{EI}{2K\ell^3} \left(\frac{1}{2} + \frac{\Delta}{\ell} \right) \quad (34a)$$

and

$$a = \frac{1}{6}\left(\frac{\Delta}{\ell}\right)^2 \left[4 - 13\left(\frac{\Delta}{\ell}\right) + 10\left(\frac{\Delta}{\ell}\right)^2 \right] - \frac{EI}{K\ell^3} \left(\frac{\Delta}{\ell}\right) \left(3\frac{\Delta}{\ell} - 1 \right) \quad (34b)$$

Subtracting Equation (34b) from Equation (34a),

$$(b - a) = \frac{(b - a)_{\text{measured}}}{(P\ell^3/EI)} = -\frac{1}{48} - \frac{1}{3}\left(\frac{\Delta}{\ell}\right)^2 + \frac{3}{2}\left(\frac{\Delta}{\ell}\right)^3 - \frac{4}{3}\left(\frac{\Delta}{\ell}\right)^4 + \frac{EI}{K\ell^3} \left[\frac{1}{4} + \frac{3}{2}\left(\frac{\Delta}{\ell}\right) - 3\left(\frac{\Delta}{\ell}\right)^2 \right] \quad (35)$$

where the dimensional difference $(b - a)$ is measured from the MCO-difference data. Given EI , ℓ and P (wheel or axle load), Equation (34) can be solved for $EI/K\ell^3$ (and K if necessary). Once $EI/K\ell^3$ is known, a and b can be determined from Equations (34a) and (34b) and multiplied by $P\ell^3/EI$ to obtain their dimensional values.

A.4.5 SUPPORTS WITH UNEQUAL FLEXIBILITY

The condition of supports with equal stiffness, which has been employed in the analysis so far, is unlikely to exist in reality. Consider a bridge with supports of different flexibility (Figure A-15). To derive the theoretical MCO-

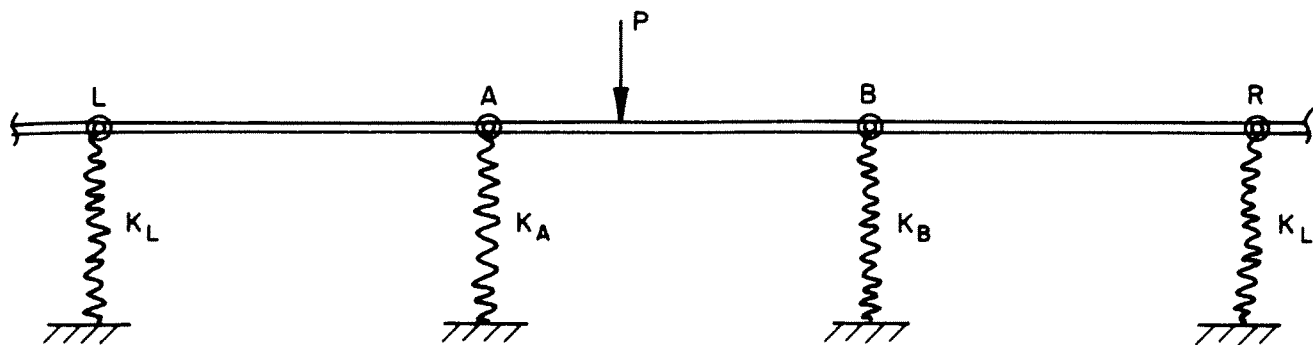


Figure A-15. Supports with Unequal Flexibility

difference signature due to Span AB, the analysis follows the development which in Section A.4.5 except that Equation (24) is used instead of Equation (25).

The results are, after superimposing the solutions for elastic spans over rigid supports,

$$\begin{aligned}
 \frac{C(X/\ell)}{(P\ell^3/EI)} &= \frac{1}{6} \left[-2\left(\frac{X}{\ell}\right)^4 + 4\left(\frac{X}{\ell}\right)^3 - 2\left(\frac{X}{\ell}\right)^2 + 2\left(\frac{\Delta}{\ell}\right)^2 - 4\left(\frac{\Delta}{\ell}\right)^3 \right. \\
 &\quad \left. + 2\left(\frac{\Delta}{\ell}\right)^4 \right] + \frac{EI}{2K_B\ell^3} \left(\frac{X}{\ell} + \frac{\Delta}{\ell} \right) \left(2 - 3\frac{X}{\ell} \right) \\
 &\quad + \frac{EI}{2K_A\ell^3} \left(3\frac{X}{\ell} - 1 \right) \left(1 - \frac{X}{\ell} + \frac{\Delta}{\ell} \right) \\
 &\text{for } \frac{\Delta}{\ell} \leq \frac{X}{\ell} \leq \left(1 - \frac{\Delta}{\ell} \right)
 \end{aligned} \quad (36)$$

$$\frac{C(X/\ell)}{(P\ell^3/EI)} = \frac{1}{12} \left[2\left(\frac{X}{\ell}\right)^4 - 12\left(1 - \frac{\Delta}{\ell}\right)\left(\frac{X}{\ell}\right)^3 \right. \quad (37)$$

$$+ \left\{ 26 - 54\left(\frac{\Delta}{\ell}\right) = 27\left(\frac{\Delta}{\ell}\right)^2 \right\} \left(\frac{X}{\ell}\right)^2$$

$$+ \left\{ -24 + 78\left(\frac{\Delta}{\ell}\right) - 81\left(\frac{\Delta}{\ell}\right)^2 + 27\left(\frac{\Delta}{\ell}\right)^3 \right\} \left(\frac{X}{\ell}\right)$$

$$+ \left\{ 8 - 36\left(\frac{\Delta}{\ell}\right) + 58\left(\frac{\Delta}{\ell}\right)^2 - 40\left(\frac{\Delta}{\ell}\right)^3 + 10\left(\frac{\Delta}{\ell}\right)^4 \right\}$$

$$+ \frac{EI}{2K_A \ell^3} \left(1 - \frac{X}{\ell} + \frac{\Delta}{\ell} \right) \left(\frac{X}{\ell} - 2\frac{\Delta}{\ell} + 1 \right)$$

$$+ \frac{EI}{2K_B \ell^3} \left(2 - \frac{X}{\ell} - \frac{\Delta}{\ell} \right) \left(2 - 3\frac{X}{\ell} \right)$$

$$+ \frac{EI}{2K_R \ell^3} \left(\frac{X}{\ell} + \frac{\Delta}{\ell} - 1 \right) \left(\frac{X}{\ell} + 2\frac{\Delta}{\ell} - 1 \right) \Big]$$

$$\text{for } \left(1 - \frac{\Delta}{\ell} \right) \leq \frac{X}{\ell} \leq 2\frac{\Delta}{\ell}$$

$$\frac{C(X/\ell)}{(P\ell^3/EI)} = \frac{1}{12} \left[4\left(\frac{X}{\ell}\right)^4 - 16\left(\frac{X}{\ell}\right)^3 + 2 \left\{ 14 - 18\left(\frac{\Delta}{\ell}\right) + 27\left(\frac{\Delta}{\ell}\right)^2 \right\} \left(\frac{X}{\ell}\right)^2 \right. \quad (33)$$

$$- 12 \left\{ 2 - 6\frac{\Delta}{\ell} + 9\left(\frac{\Delta}{\ell}\right)^2 \right\} \left(\frac{X}{\ell}\right)$$

$$+ \left\{ 8 - 36\left(\frac{\Delta}{\ell}\right) + 62\left(\frac{\Delta}{\ell}\right)^2 - 26\left(\frac{\Delta}{\ell}\right)^3 + 20\left(\frac{\Delta}{\ell}\right)^4 \right\} \Big]$$

$$+ \frac{EI}{2K_A \ell^3} \left(1 - \frac{X}{\ell} + 2\frac{\Delta}{\ell} \right) \left(1 - \frac{X}{\ell} + \frac{\Delta}{\ell} \right)$$

$$+ \frac{EI}{K_B \ell^3} 2 \left(1 - \frac{X}{\ell}\right)^2 - \left(\frac{\Delta}{\ell}\right) \left(1 - \frac{\Delta}{\ell}\right)$$

$$+ \frac{EI}{2K_R \ell^3} \left(\frac{X}{\ell} + 2 \frac{\Delta}{\ell} - 1\right) \left(\frac{X}{\ell} + \frac{\Delta}{\ell} - 1\right)$$

$$\text{for } 2 \frac{\Delta}{\ell} \leq \frac{X}{\ell} \leq 1$$

Since all K's are different, the MCO-difference signature is not expected to be symmetric about the mid-span. In order to derive the response for $X/\ell \leq \Delta/\ell$, the following interchanges are necessary,

Replace $\frac{X}{\ell}$ by $\left\{ 1 - \frac{X}{\ell} \right\}$

K_R by K_L

K_B by K_A

K_A by K_B

K_L by K_R

in Equations (36), (37) and (38). Equation (36) will remain unchanged. Therefore,

$$\frac{C(x/\ell)}{P\ell^3/EI} = \frac{1}{12} \left[2 \left(1 - \frac{X}{\ell}\right)^4 - 12 \left(1 - \frac{\Delta}{\ell}\right) \left(1 - \frac{X}{\ell}\right)^3 \right. \quad (39)$$

$$+ \left\{ 26 - 54 \left(\frac{\Delta}{\ell}\right) + 27 \left(\frac{\Delta}{\ell}\right)^2 \right\} \left(1 - \frac{X}{\ell}\right)^2$$

$$+ \left\{ -24 + 78 \left(\frac{\Delta}{\ell}\right) - 81 \left(\frac{\Delta}{\ell}\right)^2 + 27 \left(\frac{\Delta}{\ell}\right)^3 \right\} \left(1 - \frac{X}{\ell}\right)$$

$$+ \left\{ 8 - 36 \left(\frac{\Delta}{\ell}\right) + 58 \left(\frac{\Delta}{\ell}\right)^2 - 40 \left(\frac{\Delta}{\ell}\right)^3 + 10 \left(\frac{\Delta}{\ell}\right)^4 \right\} \left. \right]$$

$$\begin{aligned}
& + \frac{EI}{2K_B \ell^3} \left(\frac{x}{\ell} + \frac{\Delta}{\ell} \right) \left(2 - \frac{x}{\ell} - 2 \frac{\Delta}{\ell} \right) \\
& + \frac{EI}{2K_A \ell^3} \left(1 + \frac{x}{\ell} - \frac{\Delta}{\ell} \right) \left(3 \frac{x}{\ell} - 1 \right) \\
& + \frac{EI}{2K_L \ell^3} \left(\frac{\Delta}{\ell} - \frac{x}{\ell} \right) \left(2 \frac{\Delta}{\ell} - \frac{x}{\ell} \right) \\
& \text{for } \left(1 - 2 \frac{\Delta}{\ell} \right) \leq x \leq \frac{\Delta}{\ell}
\end{aligned}$$

and finally,

$$\frac{C(x/\ell)}{(P\ell^3/EI)} = \frac{1}{12} \left[4 \left(1 - \frac{x}{\ell} \right)^4 - 16 \left(1 - \frac{x}{\ell} \right)^3 \right. \quad (40)$$

$$\begin{aligned}
& + 2 \left\{ 14 - 18 \left(\frac{\Delta}{\ell} \right) + 27 \left(\frac{\Delta}{\ell} \right)^2 \right\} \left(1 - \frac{x}{\ell} \right)^2 \\
& - 12 \left\{ 2 - 6 \left(\frac{\Delta}{\ell} \right) + 9 \left(\frac{\Delta}{\ell} \right)^2 \right\} \left(1 - \frac{x}{\ell} \right) \\
& + \left\{ 8 - 36 \left(\frac{\Delta}{\ell} \right) + 62 \left(\frac{\Delta}{\ell} \right)^2 - 26 \left(\frac{\Delta}{\ell} \right)^3 + 20 \left(\frac{\Delta}{\ell} \right)^4 \right\} \\
& + \frac{EI}{2K_B \ell^3} \left(\frac{x}{\ell} + 2 \frac{\Delta}{\ell} \right) \left(\frac{x}{\ell} + \frac{\Delta}{\ell} \right)
\end{aligned}$$

$$+ \frac{EI}{K_A \ell^3} \left[2 \left(\frac{x}{\ell} \right)^2 - \left(\frac{\Delta}{\ell} \right) \left(1 - \frac{\Delta}{\ell} \right) \right]$$

$$+ \frac{EI}{2K_L \ell^3} \left(2 \frac{\Delta}{\ell} - \frac{x}{\ell} \right) \left(\frac{\Delta}{\ell} - \frac{x}{\ell} \right)$$

for

$$0 \leq \frac{x}{\ell} \leq \left(1 - 2 \frac{\Delta}{\ell} \right)$$

It is evident from Equations (36) through (40) that, except for a small portion around the mid-span ($\Delta/\ell \leq x/\ell \leq 1 - \Delta/\ell$), the MCO-difference for a given span depends not only on the flexibility of its own supports (K_A and K_B), but also on the flexibilities of the two adjacent supports on either side (K_L and K_R).

As shown in Figure A-13 for supports with equal flexibility, theoretical signatures were produced for supports having unequal flexibility. Two cases have been investigated, one where one soft support (B) exists among infinitely rigid supports and the other in which the support B is significantly softer than other supports of equal flexibility. The results of these computations are shown in Figures A-16a and A-16b. It is evident that the one soft support causes a dip in the MCO-signature. Thus, from the trace of the field data, supports which have deteriorated and become unusually soft can be readily singled out. It is also noticed that the maximum of the signature shifts away from the support. In fact, it can be shown that beyond a certain relative flexibility ratio K_B/K , the maximum occurs at the same point (i.e., x/ℓ) along the span. In Figure A-16b, with $\Delta/\ell = 0.423$, this value is $K_B/K = 0.66$. Furthermore, if the present theory is verified by experiment, a possibility exists that the difference between the values of MCO-difference at two supports can be directly calibrated to reflect relative softness of the supports. It is also possible, through a somewhat involved procedure, to locate a zero reference for $C(x/\ell)$ using asymmetrical MCO-difference signatures for three consecutive spans.

A.4.6 COMPARISON OF THEORY WITH TEST DATA

During the recent Track Stiffness System Evaluation Test, several timber bridges in marshy terrain were encountered. One such bridge at MP 87.50, on the Selma-Mobile line, produced a symmetrical MCO-difference signature without any

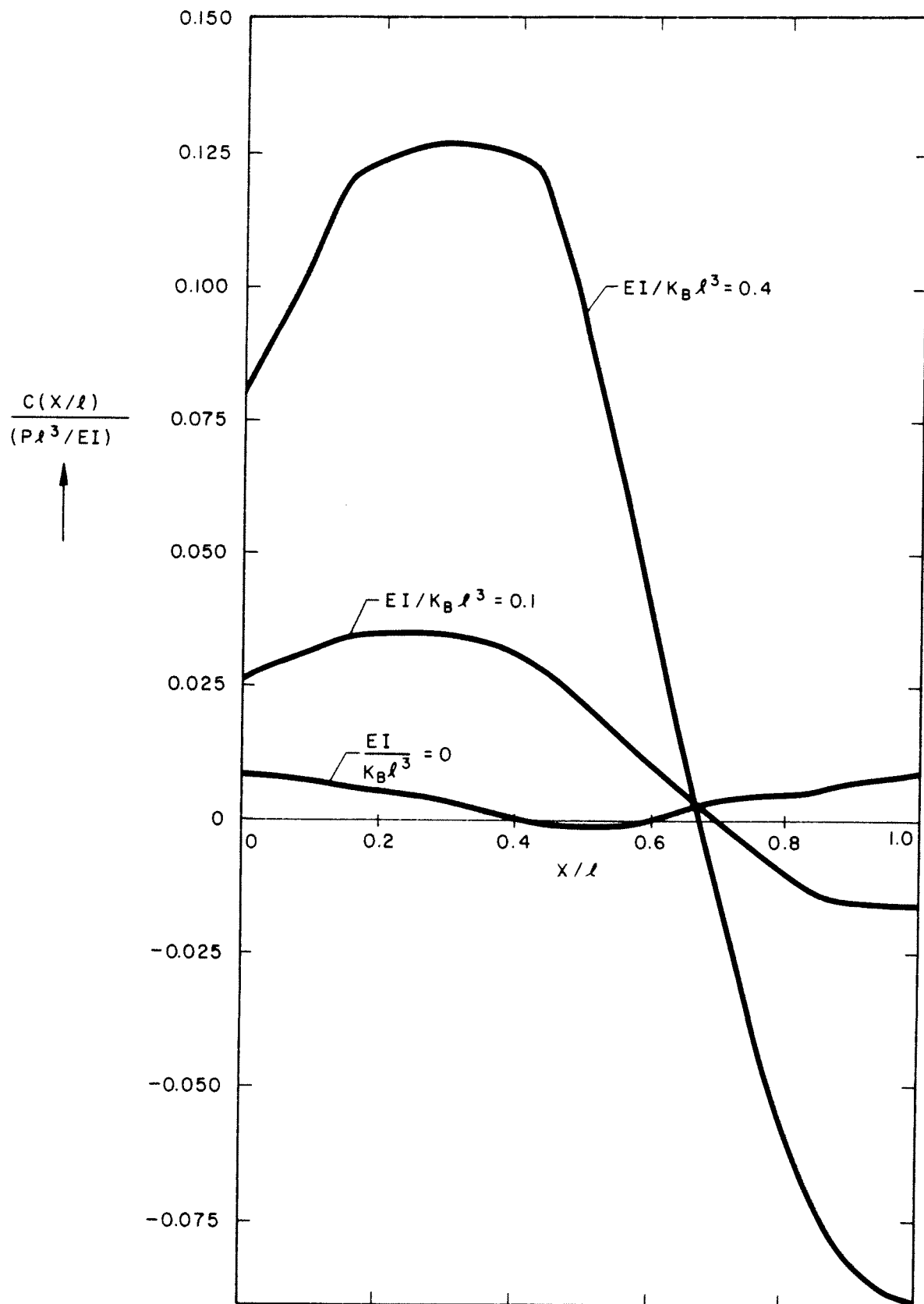


Figure A-16a. MCO-Difference for One Soft Support
Among Infinitely Rigid Supports
A-44

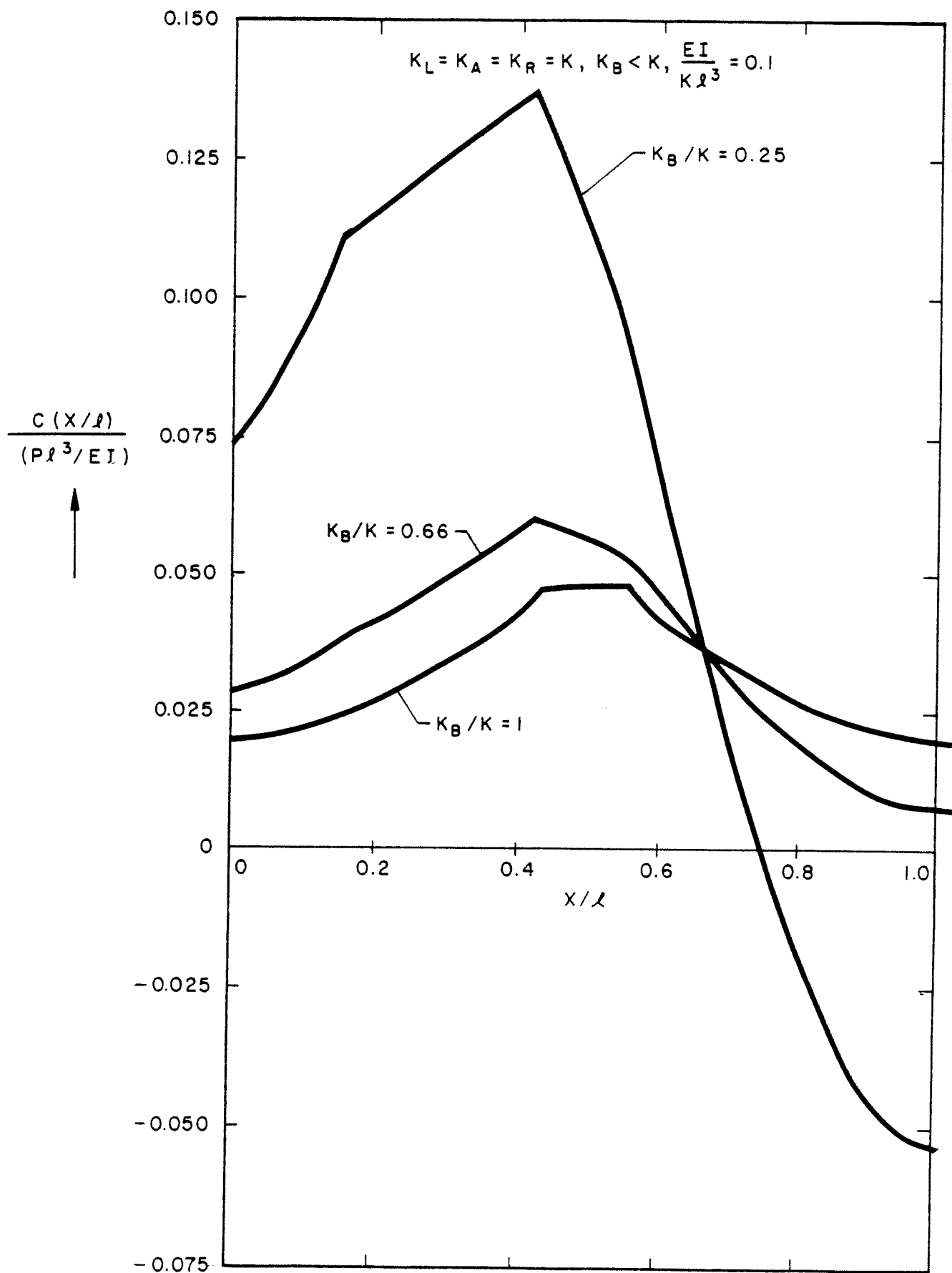


Figure A-16b. MCO-Difference for One Support Significantly Softer Than Other Supports of Equal Flexibility

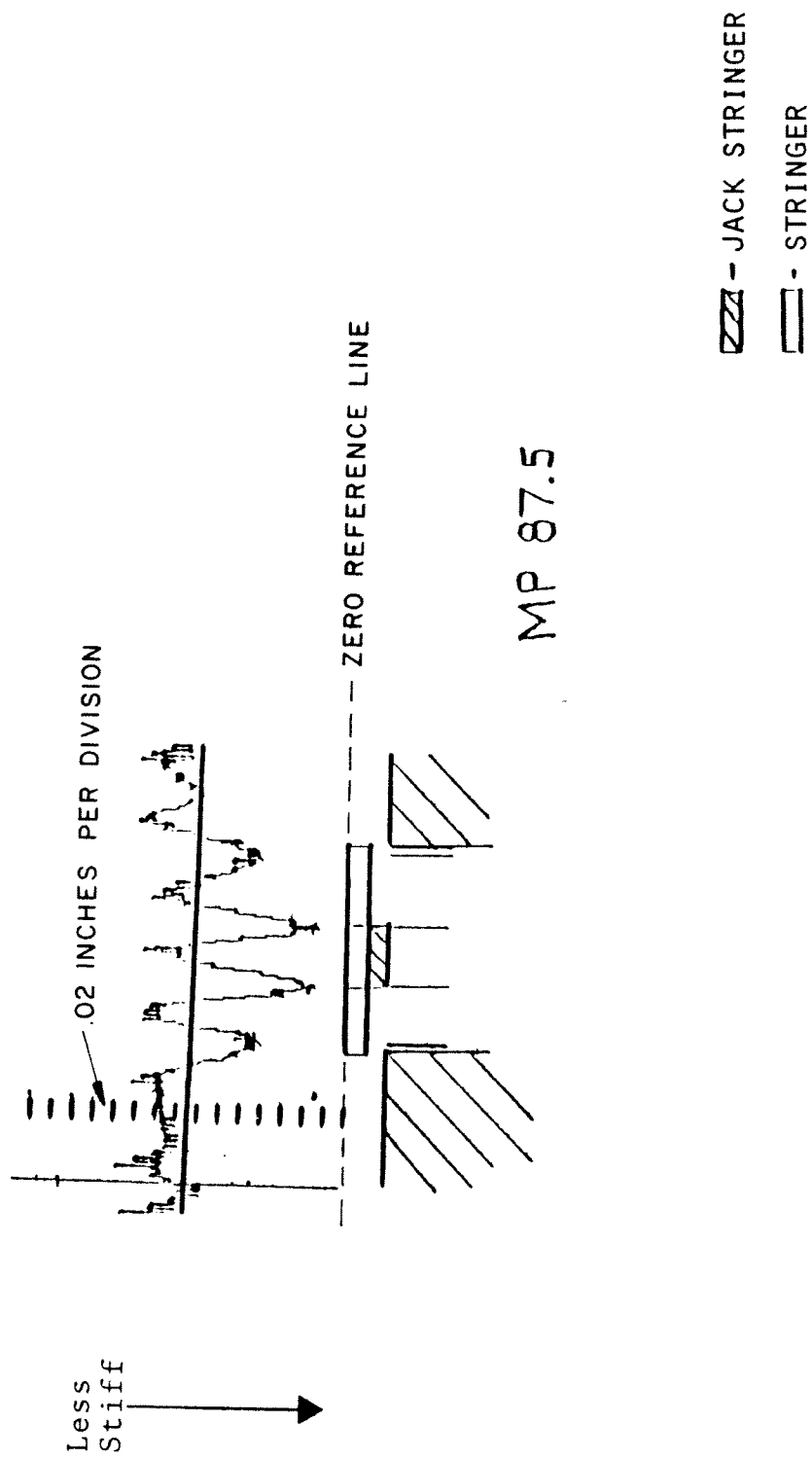


Figure A-16 (c). MCO Difference Trace (Bridge at MP 87.5 on Southern Railway)

unusual characteristics. The schematic of this bridge and the corresponding signature are shown in Figure A-16c. First, it is necessary to examine the signature visually and locate the supports. If one thinks of a bridge with rigid supports, Figure A-16c shows two embankments with three supports in between. In actuality, however, the bridge has two supports between embankments. Then, if the signature is interpreted as due to a bridge with flexible supports, the two middle supports and the embankment supports are readily located. This fact also agrees with a later field observation that the supports are indeed flexible. Therefore, the flexible support theory is appropriate for application to this bridge. The next step was to match the amplitude of the signature of the center span to the theoretical model in Figure A-18. This agreement in amplitude occurred for an $EI/K\lambda^3$ of approximately 0.35. Subsequent calculations showed that the EI product for a span with six 9 x 16-inch stringers is 1.8×10^6 , pound feet/inch, with $\lambda = 14.7$ feet measured from the trace, K has roughly the value 9×10^4 pound feet/inch. It must be pointed out that an axle load of 45,000 pound feet was used as P in the theoretical formulas, since comparisons had been made with the average MCO-difference of the two rails. This also produces reasonably good agreement between theory and experiment. However, a sounder justification for using the axle load rather than the wheel load is necessary. Proceeding with this value of P, the measured MCO-difference data samples were made dimensionless with respect to $P\lambda^3/EI$ and plotted in Figure A-18. The solid line is the theoretical curve calculated using Equations (27), (28) and (29). The agreement between theory and field data is quite good provided $K = 90,000$ pound feet/inch as mentioned earlier. A verification of this value was obtained in the field by positioning a locomotive on the bridge and measuring the deflections at the supports. Knowing the approximate axle loads of the locomotive and using the three moment method, the reactions at the supports and hence the stiffness in

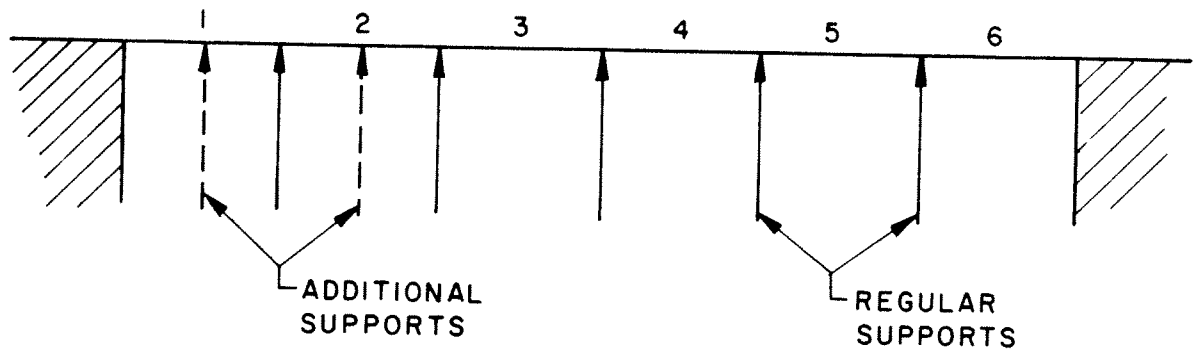


Figure A-17a. Example of Timber Bridge at MP 87.20 MB

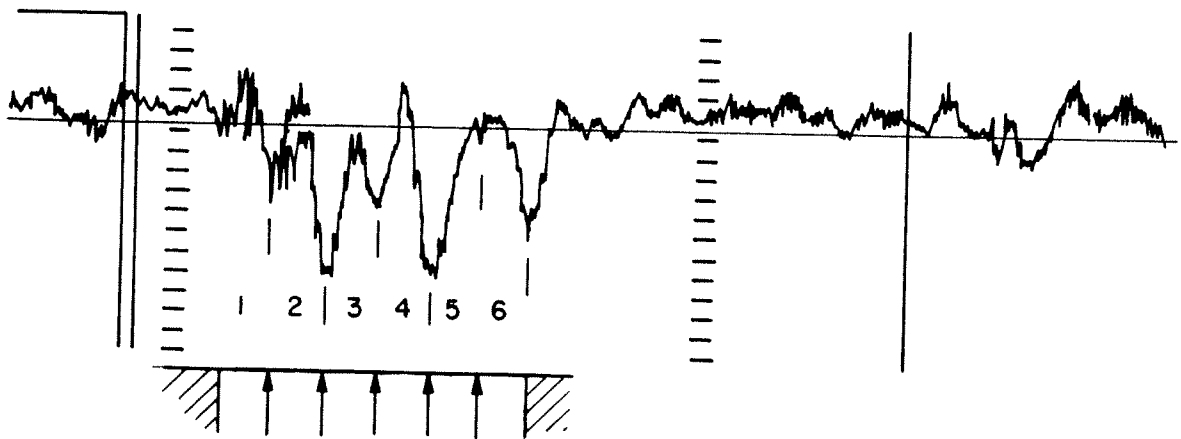


Figure A-17b. MCO-Difference Signature Averaged For Two Rails.

pounds per inch were calculated. The stiffness values were roughly 10^5 pound feet/inch for one support and 4.2×10^5 pound feet per inch for the other. Considering the inexact nature of the deflection measurement, the lack of knowledge of the exact weight of the locomotive, and the changes in bridge condition since the stiffness test, the agreement with the prediction of 9×10^4 pound feet/inch is reasonable. Therefore, the usefulness of the flexible support model is promising. Absolute zero reference for the track in Figure A-16c was determined as follows: For $\Delta/\ell = 5.5/14.7 = 0.423$, Equation (32) gives $b/a = 4.06$. From Figure A-14 $(b - a) = 0.16$ -inch. Therefore, $(a)_{\text{dim}} = 0.16/3.06 = 0.05$ from Equation (33). The preceding calculations should be repeated with more exact values of span length (which appeared to be 14.7 feet on the trace but was actually found to be 13.1 feet), axle load, etc.

An example of a typical asymmetrical signature for a bridge with unequal support flexibilities is shown in Figure A-17a and A-17b. This bridge, at MP 87.20 MB, is also constructed of timber and has supports in muddy ground. The dips in the MCO-difference correspond to softer supports. Notice also the shifting of the peaks on the trace away from softer supports as predicted by theory. No detailed calculations were made for this bridge.

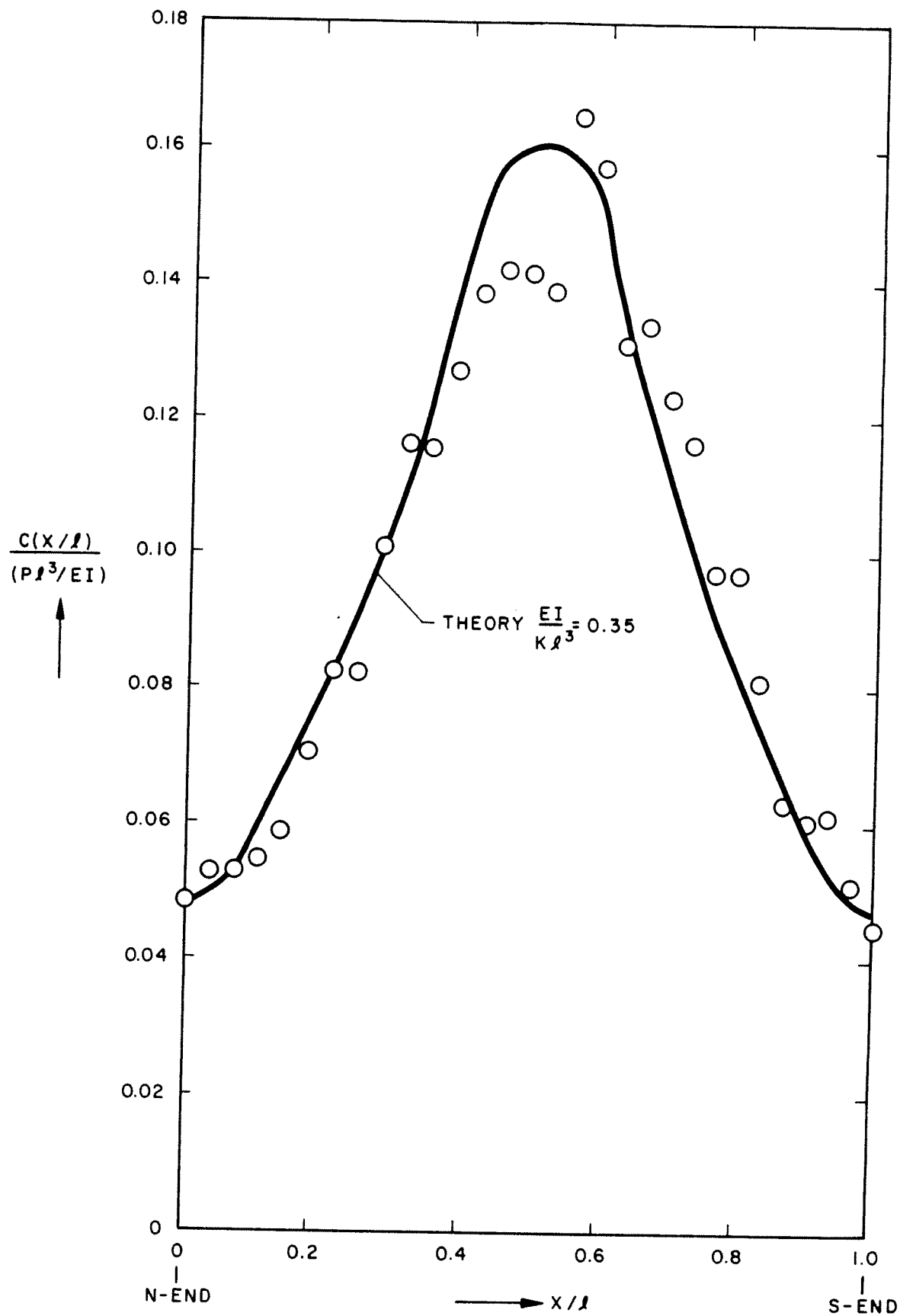


Figure A-18. Solution for $EI/k l^3 = 0.35$. $EI = 1.7 \times 10^{11}$,
 $k = 9.01 \times 10^4$ lbf/in
 Comparison with Field Data for Bridge
 at MP 37.50 MB. A-49

APPENDIX B
TEST ZONE DESCRIPTIONS

B.1 PHASE I

B.1.1 TEST ZONES AND TEST OPERATIONS

The test zone for obtaining compliance data on RM-176.1 was the Southern mainline from Manassas to Bristow, VA. The consist was arranged as shown in Figure B-1a. Back-and-forth runs were performed at Bristow and at the Brickyard according to the following schedule:

- A north and south run at 60 mph.
- A north and south run at 30 mph.
- A north and south run at 15 mph.

Following this testing, the consist moved to Manassas, VA and west-bound measurements were made on the Harrisonburg Branch from MP 0 to MP 8 at Gainesville, VA using the consist shown in Figure B-1a. At Gainesville, the locomotive changed ends and the eastbound return trip to Manassas used the consist shown in Figure B-1b. Speed on the Harrisonburg Branch ranged from 10 to 25 mph.

At Manassas, the consist moved onto the mainline and the consist was configured as shown in Figure B-1c (R-1 was effectively turned end for end). Back-and-forth runs were repeated at Bristow and at the Brickyard locations. Details of the test zone are shown in Figure B-2.

Test operations for RM-176.2 were similar to the above, except that:

- MP 34 through MP 37 was treated as one test zone rather than as two separate zones.
- The Harrisonburg Branch was not surveyed.
- R-1 was not turned on the wye.

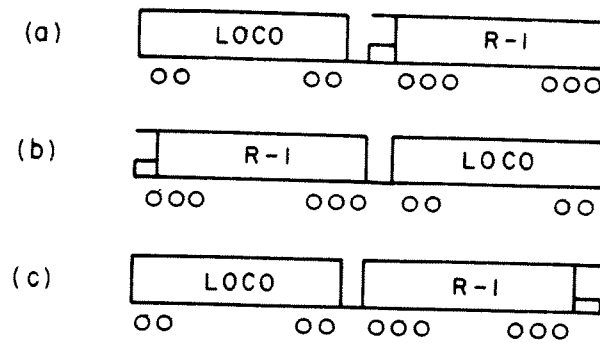


Figure B-1. Test Consist Configurations

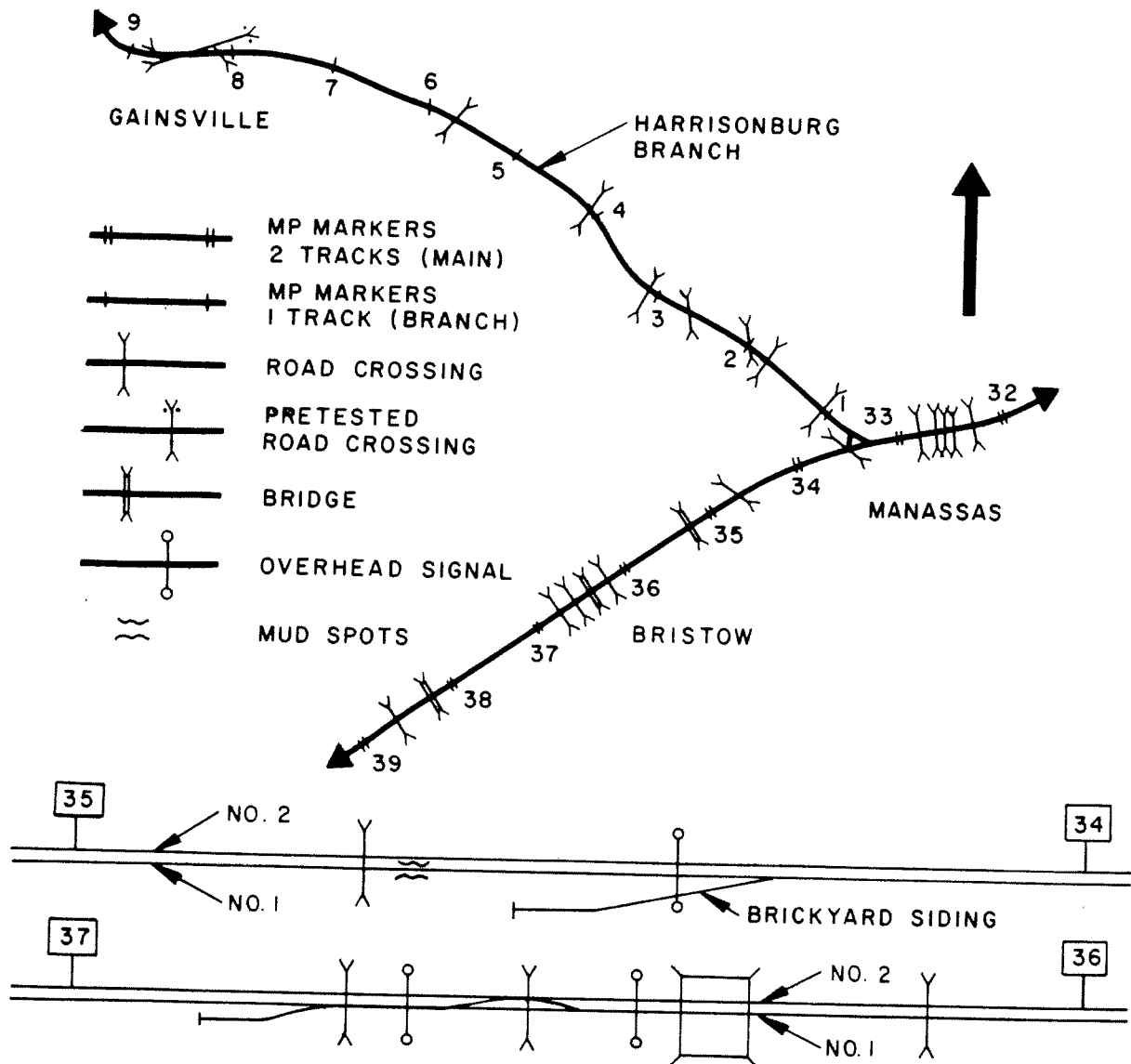


Figure B-2. Test Zone Details of SRS for Manassas, Bristow, and Gainesville Areas.

TABLE B-1
SUMMARY OF DATA PROCESSING DETAILS

Test #1	• RM-176.1	• RM-176.2	• RM-176.3	• RM-176.4
Test Title:	• First Test on Southern	• Second Test on Southern	• Kansas Test Track Re-processing	• Test on B&E
Software Development:	• TL76P1: Tri-modal processing program (see text).	• TL76D2: Program to dump 6 channels of R-1 data to RQPLOT.	• TMGP3: Program to reformat raw data tape for processing program. • TL76P3: Tri-modal processing program. • RCSR2: Regression analysis program--selects channel pairs over specific tones.	• TMGP4: Program to reformat raw data tape for processing program.
Difficulties Encountered:	• Digitizing yielded false scans of data. Program TL76P1 was modified to delete false scans. • Spring-mass interactions produce a ringing response in the 11' MCD data from R-1. Impact of this noise contamination needs to be evaluated.	• No processing to date.	• Existence of gradual capacitive sensor output variations within 0.02 inches of calibrated value. • .04" resolution for profilometer limits system performance to long wavelength or severe local stiffness features.	• No processing to date.
Unresolved Problems:	• High gain of profilometer combined with flutter and wow of tape recorder produces bias drift in data.	• Noise contamination cited in Table 1.	• None, except above noted limitations.	• None encountered to date.
Accomplishments:	• Real-time phase shiftless processing of profilometer data demonstrated using North and South runs at various speeds. Results include: a) Good correlation of profilometer vs. R-1 11' MCD. No phase distortion of profilometer data evident; b) Excellent repeatability of profilometer generated 50' MCD. c) Excellent repeatability of new "pseudo-track" reconstruction technique.	• None to date.	• An improved, single function linearization scheme was developed for the capacitive sensors. • Regression analysis used to fine-tune sensor gains. • Individual sensor data was examined as opposed to a 14.4' MCD.	• None to date.
Major Highlights:	• Real-time processing techniques described above and developed under this program is being implemented in profile and alignment systems on FRA T-6.	• None to date.	• A repeatable track compliance processing developed that is reliable to KIT tones and to cut-fill transactions and to other track structure and sub-grade features on the KIT.	• None to date.
Recommended Actions:	• Reprocess for track compliance using phase shiftless high-pass filter on profilometer to eliminate long wavelength variations that are below profilometer noise floor and that contain bias drift. Such a filter was successfully incorporated in TL76P3.	• Explore possibility of using an envelope detector algorithm to eliminate noise problem.	• Some additional fine-tuning possible. Determine if shorter wavelength defects are more reliably detected.	• Process data using fine-tuned software from RM-176.3.

Test operations for RM-176.3 and RM-176.4 are described to some extent in Table B-1. Greater detail is provided in the appropriate Test Events Reports. Details relative to data collected, difficulties encountered in testing and a general assessment of data quality are also given in Table B-1.

B.2 PHASE II

A brief description of the actual test performed to evaluate the track-stiffness-measurement system is given in the following paragraphs.

Tests were conducted on Southern Railway mainline track (Figure B-3) between Alexandria, VA (MP 9) and Monroe, VA (MP 165). The track segment between MP 34 and MP 37 was used for controlled testing to evaluate system repeatability. A track chart for this segment is shown in Figure B-4.

The test consist (Figure B-5) included a locomotive, the Southern Railway System Research Car R-1 and the Federal Railroad Administration Data Acquisition Car T-7. The R-1 car was instrumented to measure vertical track stiffness and the T-7 car provided the data acquisition system. On the first test day the consist was arranged with the R-1 car between the locomotive and the T-7 car as shown in Figure B-5a. On the second test day the locomotive was moved to the T-7 end of the consist so that the R-1 car was trailing as illustrated in Figure B-5b. The instrumented truck was adjacent to the T-7 car on both test days. A Forward Observer was assigned to the locomotive to assist in the control of train movements and to identify road crossings, bridges and mileposts for entry into the data acquisition system.

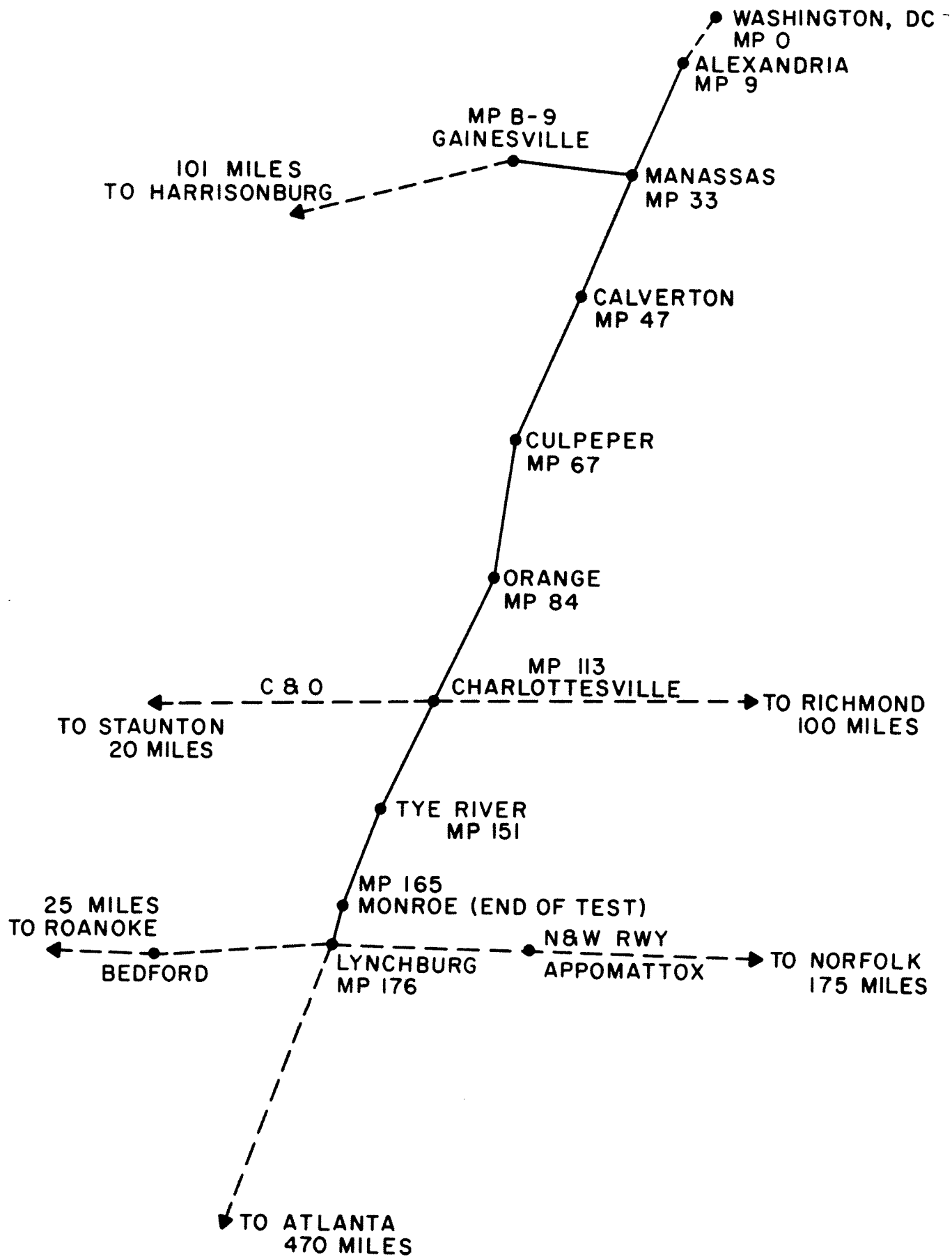


Figure B-3. Map of Test Zone on Southern Railway

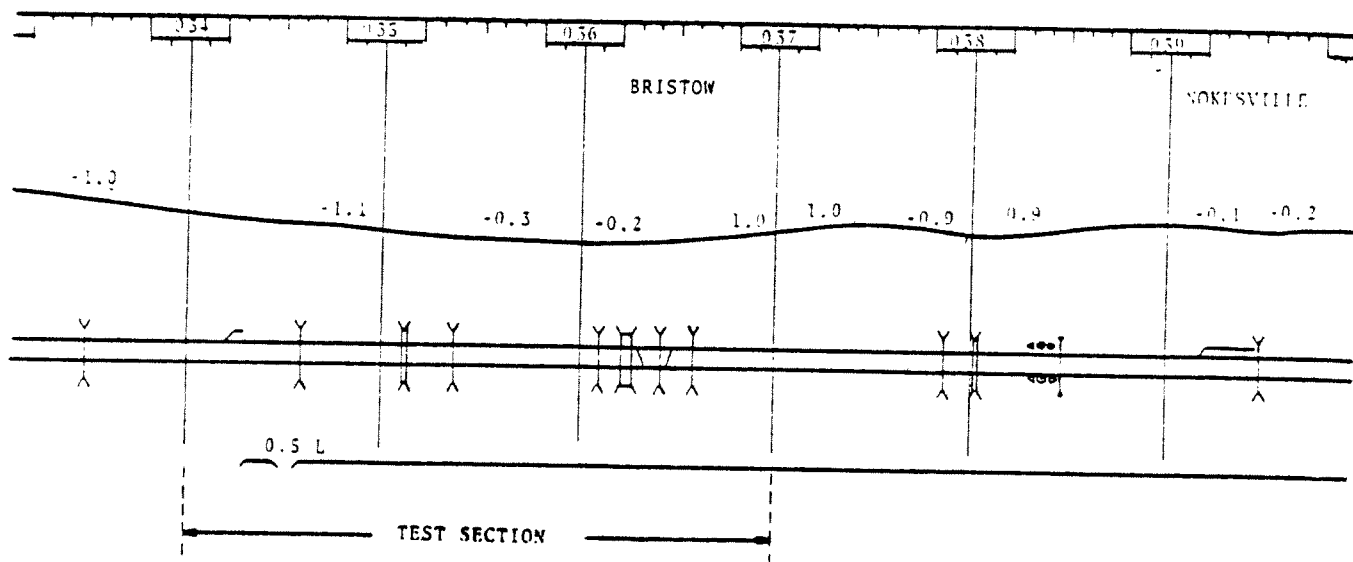


Figure B-4. Track Chart-Repeatability Test Segment

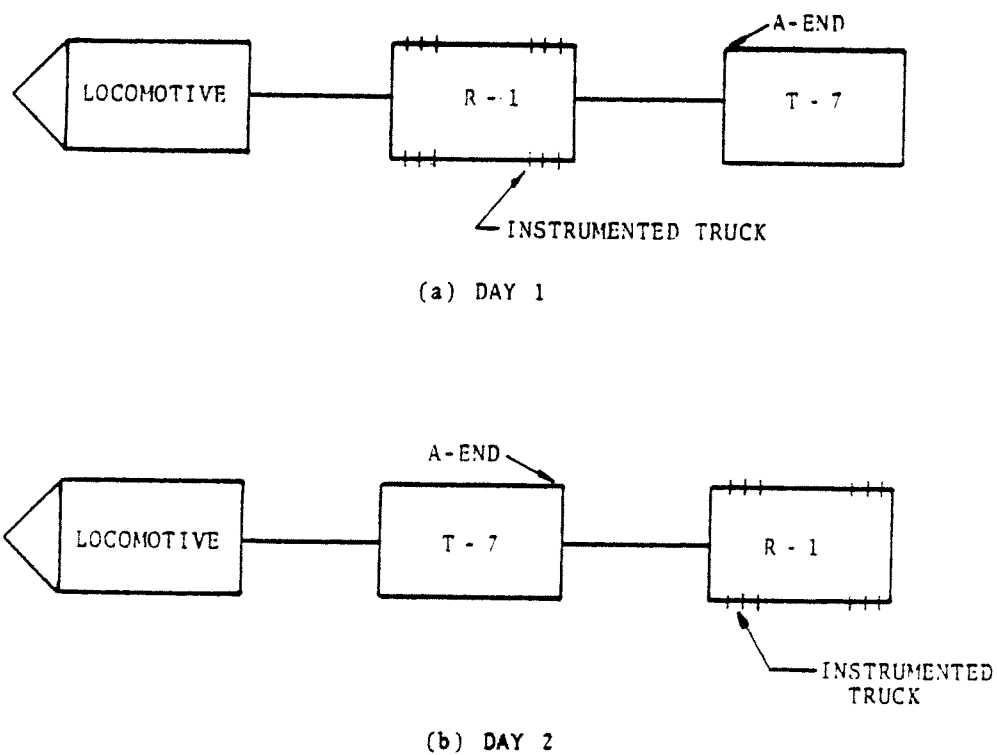


Figure B-5. Test Consist

At the beginning of the first test day a wayside measurement was made at MP 10.4 to determine the baseline for the 11-foot mid-chord offset transducers. All instrumentation was field calibrated at the same time. A data run was made to the controlled testing segment at MP 34-37. The actual run through the segment was made at 60 mph. Repeatability runs were then made at 30 and 15 mph in the southbound direction.

A field calibration and a second wayside measurement were made after the consist had been turned through a wye; then repeatability runs were made in the northbound direction at 30 and 60 mph. Data were collected on the return run to the Southern Yard at Alexandria, VA.

On the second test day, a long data run was made from Alexandria, VA to Monroe, VA at MP 165. An improved method was used to take the wayside measurement and the equipment was field calibrated prior to the data run. There were several instrumentation problems during the second day of testing. At Monroe, VA the test consist was turned through a wye, and the return data run was made. At Monroe, VA and again at Alexandria, VA the equipment was field calibrated.

A more detailed look at three specific track segments shows the correlation of track conditions with measurements of track stiffness. The three examples which follow are typical of the results obtained by comparing measured stiffness data to the physical track. Figure B-6 shows a topographic map of the track from MP64 to MP67 (Culpeper). An analog strip of the 28.5-foot-filtered stiffness data at scale is superimposed on the map. On this strip, softer track is represented by an upward excursion of the trace and harder track by a downward excursion. The baseline of the trace is arbitrarily set to emphasize the variations in the trace. The track lies near

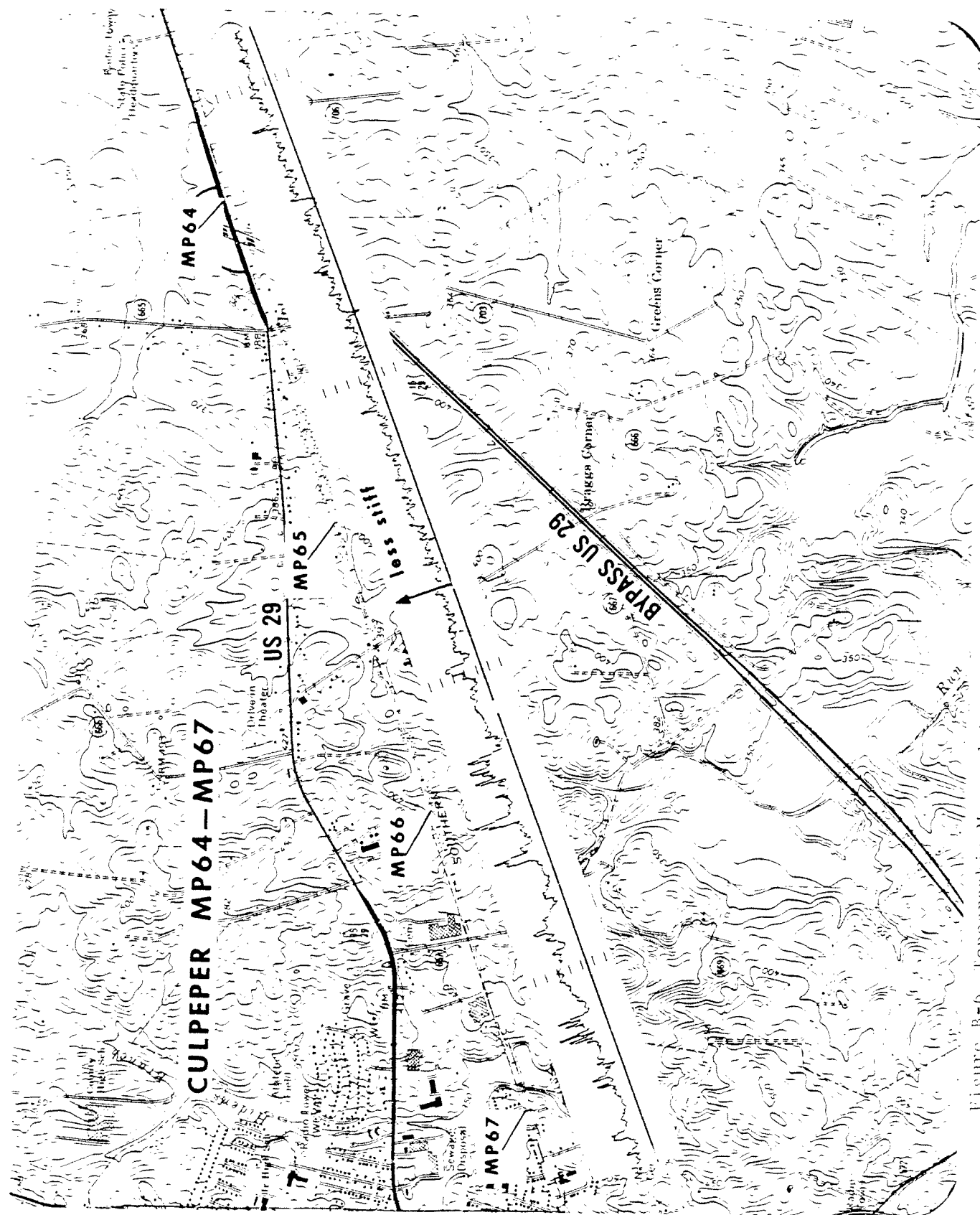


Figure B-6. Topographic Map and Analog Stiffness Trace (MP 64 to 67) - Southern Railway

the trace. Starting from the right-hand edge of the map (corresponding roughly to MP63.7), one can scan the trace and find the physical features on the map corresponding to the excursions. The first less stiff event at MP63.8 corresponds to a culvert as noted by Southern Railway on the stiffness events charts prepared after the test. A corresponding event occurs at MP 64.8. At MP 64.2, a more stiff response results from the existing bridge across the highway. A turnout at MP 65.6 resulted in a softer response as did the interlock at MP 66.0 and the turnouts at MP 66.1, 66.2, 66.4 and 66.7. At MP 66.9, the bridge showed a less stiff response at each of its ends.

Figure B-7 is a similar illustration for the area from MP 115 to MP 116 (Charlottesville). The turnout at MP 115 clearly stands out and correlations with individual rail structures can again be made. However, an additional feature, not present in Figure B-8, is the long-term change from MP 114.6 to MP 118.0. Here the track exhibits softness for the entire 1.4-mile zone corresponding to the presence of a stream which runs closely parallel to the track and at nearly the same elevation, and some recent highway construction. Interstate 64 was built across the tracks just north of MP 115 and US 29 which runs adjacent to the track was widened to four lanes in 1971/1972.

Figure B-8 is a further example for the area from MP 149 to MP 151 (Tye River). The expansion joint just off the end of the bridge at the Tye River (MP 150.25) is clearly visible in the track stiffness trace. Near the center of the bridge, there is an anomalous area of softness that may be associated with a known problem that exists with one of the bridge piers. Another feature is the relatively rapid change in the stiffness trace at MP 150.5 to a more stiff level. This can be related to continuing maintenance effort south of the Tye River. The Tye River Bridge was destroyed in the hurricane of August 1969. The footings under one pier have become soft creating a continuing problem.

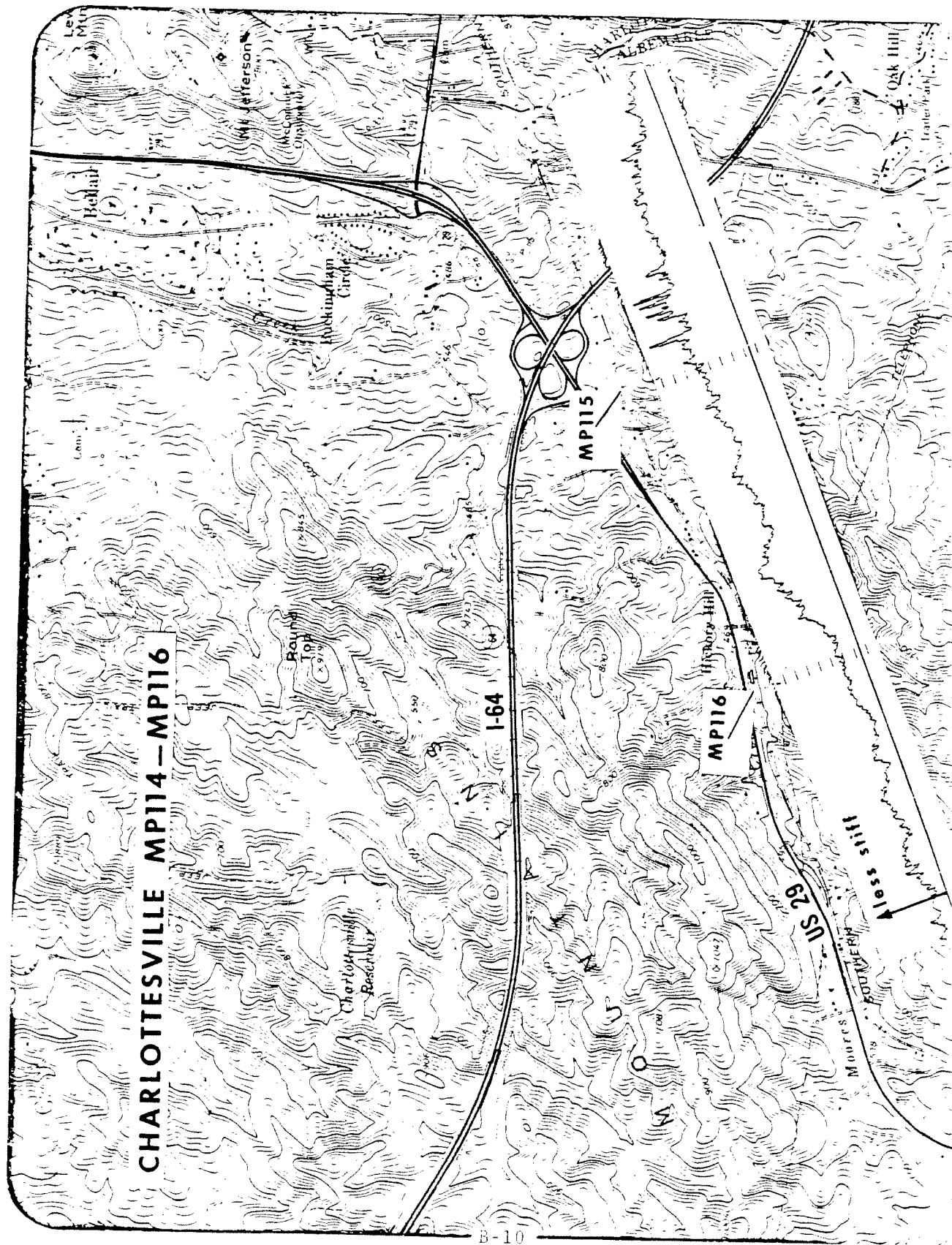


Figure B-7. Topographic Map and Analog Stiffness Trace (MP 114 to 116) - Southern Railway

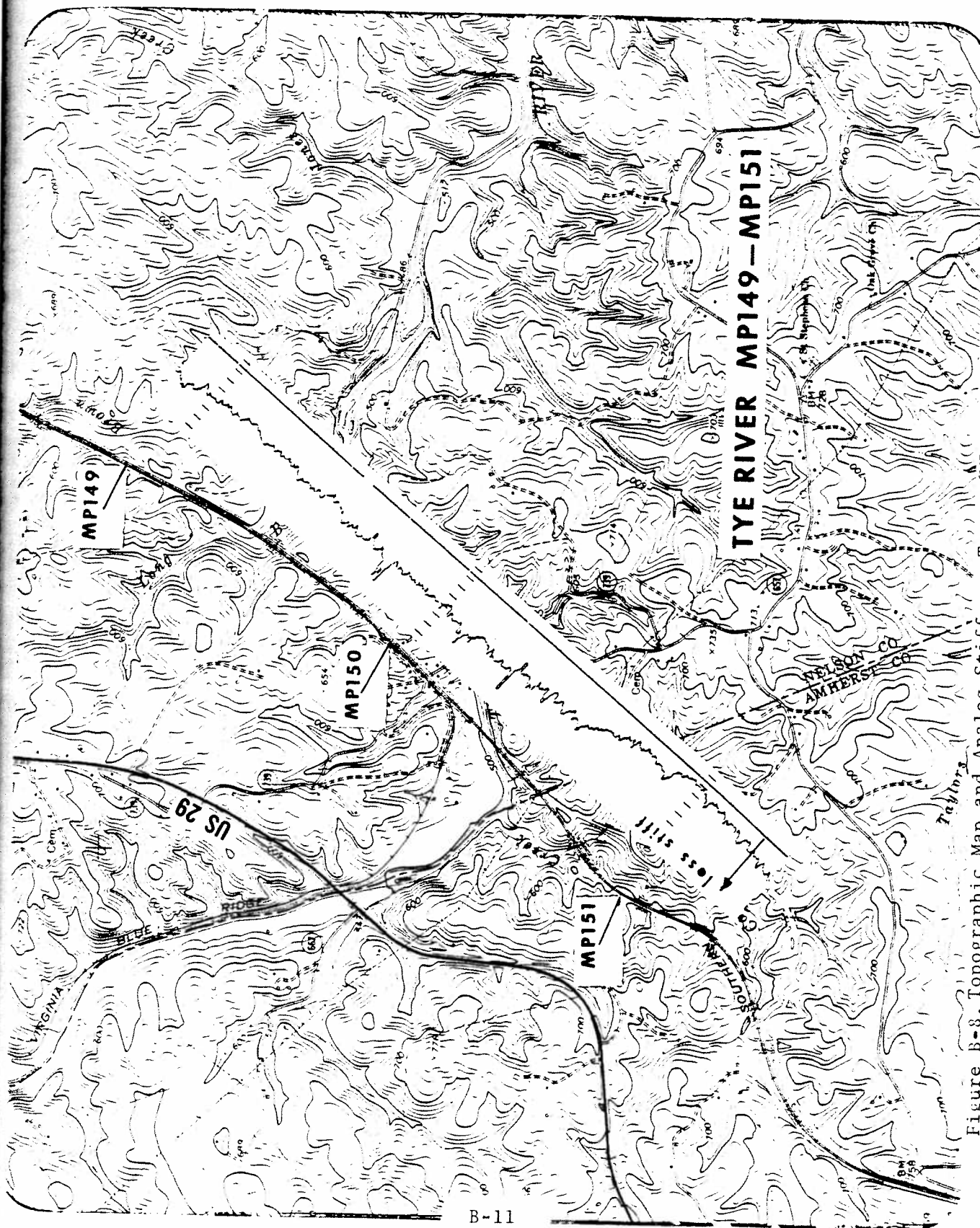


Figure B-8. Topographic Map and Analog Stiffness Trace (MP 149 to 151) - Southern Railway

B.3 PHASE III

B.3.1 TEST ZONE

This test was conducted over two different mainline sections of track (see Figure B-10). The first test zone was on Southern Railway track southeast of Alexandria, VA between MP 9 and MP 40, and was used for system and instrumentation validation. The second test zone was divided into three sections; each section required one day of testing. Section 1 was from Cincinnati, OH to Chattanooga, TN. Section 2 was from Chattanooga, TN to Selma, AL. The third section was from Selma, AL to Mobile, AL. Sections 1 and 3 were of primary interest. Section 1 was tested mainly for roadbed characteristics. Section 3 was tested for characteristics of bridge structures. The consist (see Figure B-9) operated at track speed through the test zones.

Following preliminary data analysis, selected areas of interest were inspected with emphasis on areas of stiffness variation in which no unusual track geometry had been observed.

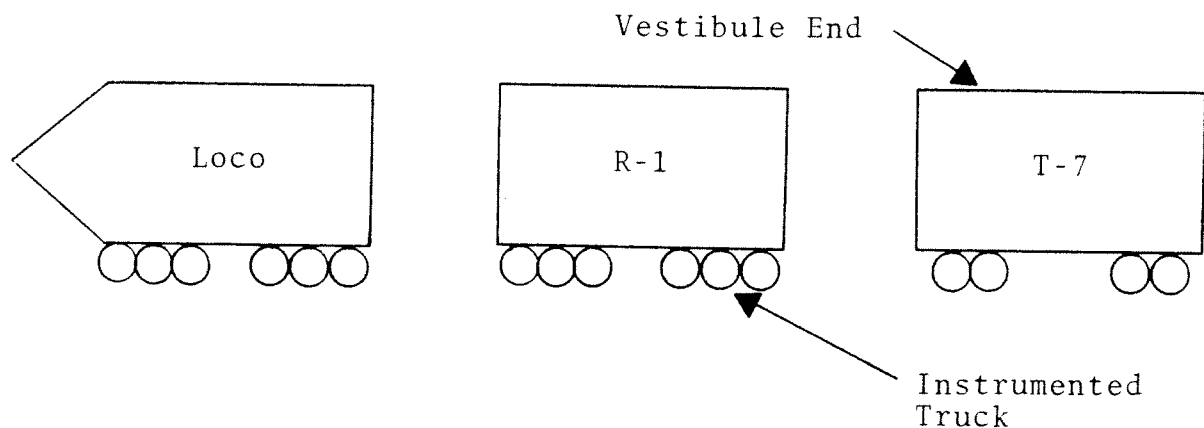


Figure B-9. Configuration of Test Consist

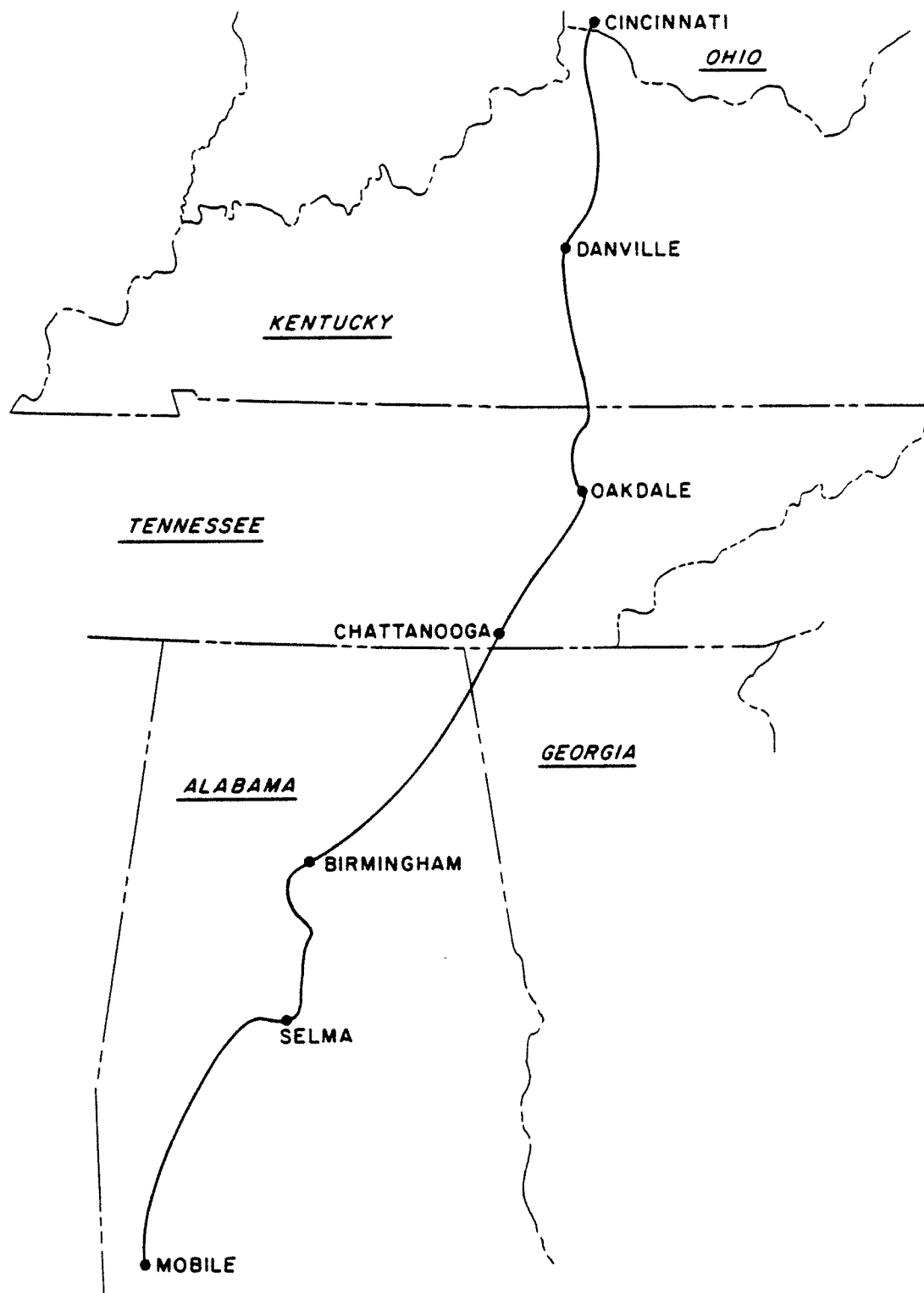


Figure B-10. Test Zones

B.3.2 OBSERVATIONS IN TEST SECTION 1

The areas selected for field examination in Section 1 were in the vicinity of Lexington. The observations obtained are detailed below. Figures B-11 through B-13 show the locations of the areas selected.

MP 103.1: The High Bridge in this area was examined to study physical characteristics of a Conley joint which appears distinctly in bridge signatures.

MP 94.8: This spot was of major interest because a very abrupt change in stiffness-related signature was observed during the test. The area in the vicinity of MP 95.0 was the site of a derailment, and consequently, there are a number of split and loose ties. Initially, it was believed that one particular spot on the track with an almost nonexistent tie might have been the cause of the abrupt change in stiffness. This observation was based on the fact that two out of the five joint-like indications on the stiffness-related signature turned out to be bolted joints north of the spot at roughly the expected distance. The remaining three were thought to be rather low welded joints. This interpretation, however, did not predict correctly the location of a switch south of the abrupt soft spot. It was finally concluded that the soft spot was due to a low bolted joint in the right rail (going from north to south). This joint existed at the time of the test and had been welded recently. A later examination of the test data revealed that the right profilometer saturated in this area and led to erroneous stiffness-related signatures.

MP 92.4: The stiffness-related trace indicated the presence of a switch which was not shown on the track charts. During the inspection, the track supervisor mentioned that the switch existed at the time of the test.

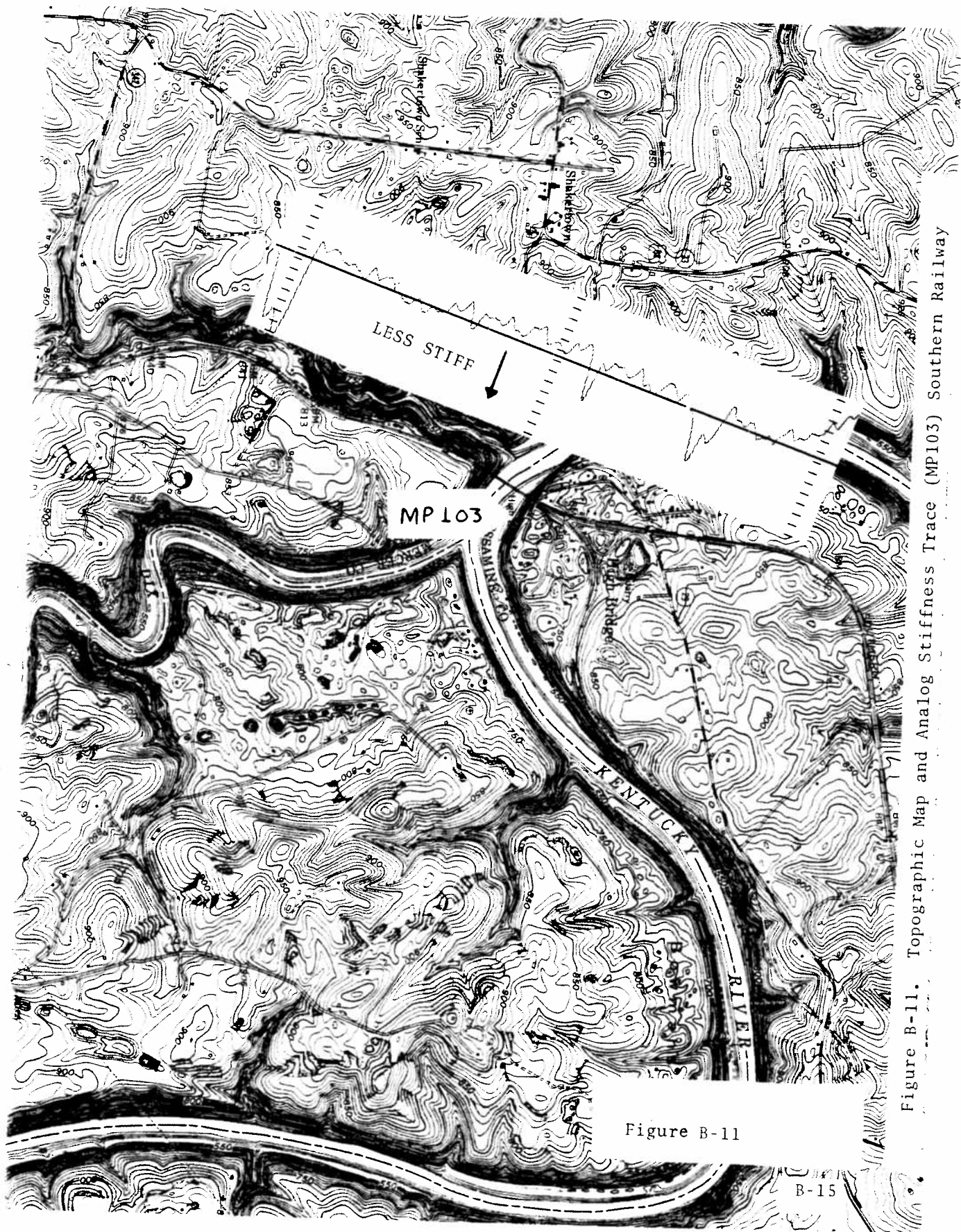


Figure B-11. Topographic Map and Analog Stiffness Trace (MP103) Southern Railway

Figure B-11

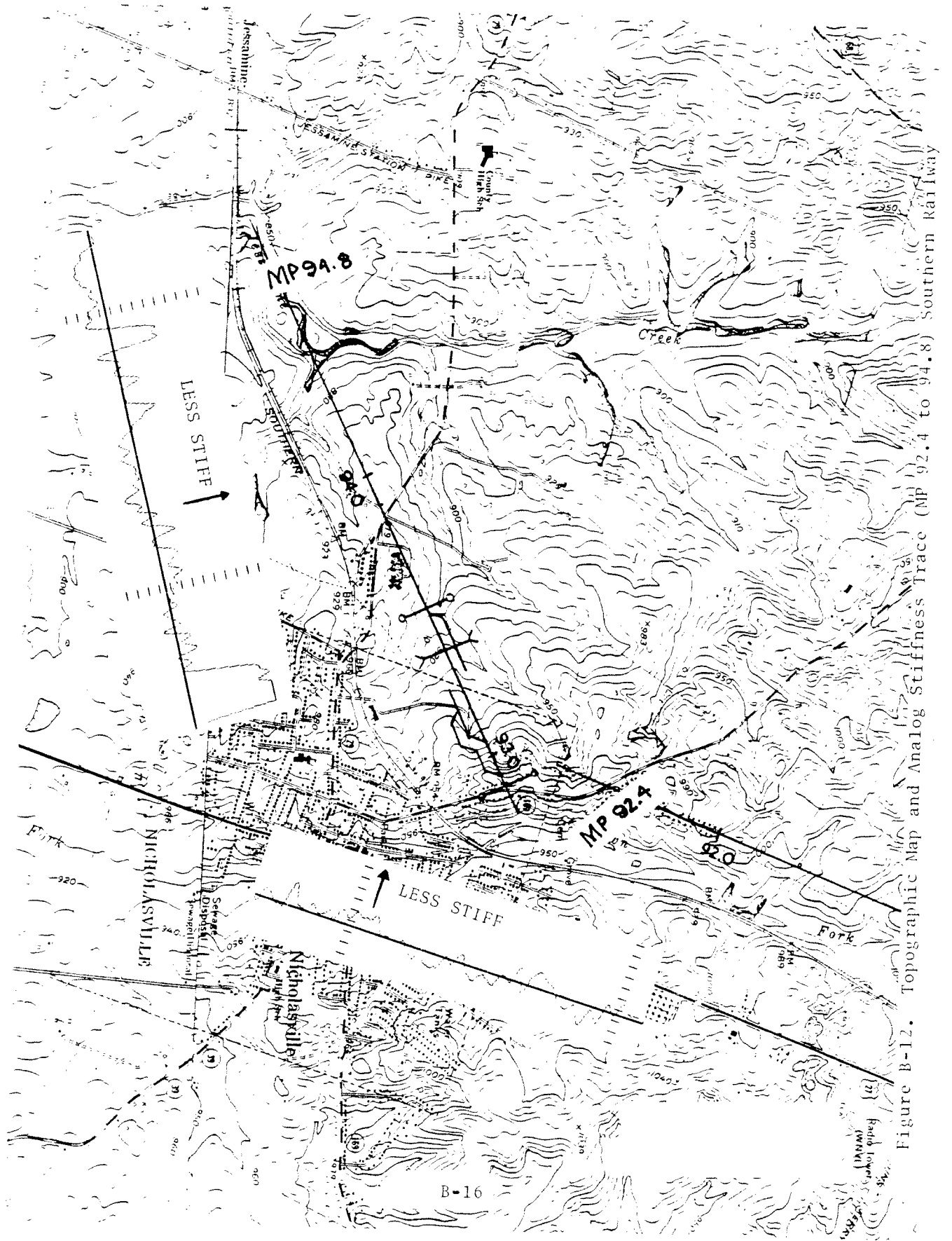


Figure B-12. Topographic Map and Analog Stiffness Trace (MP 92.4 to 94.8) Southern Railway

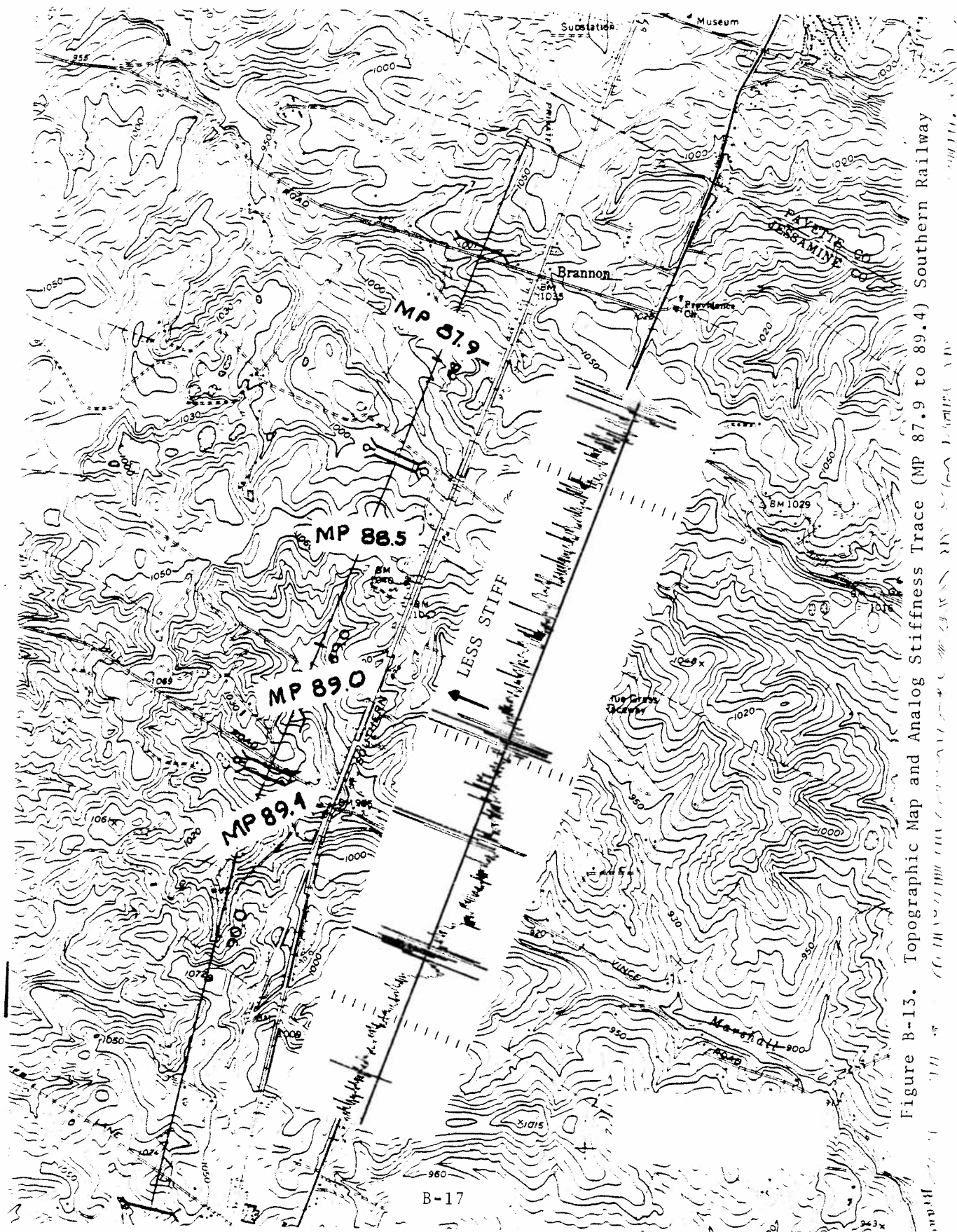


Figure B-13. Topographic Map and Analog Stiffness Trace (MP 87.9 to 89.4) Southern Railway

MP 89.4: The stiffness-related signature indicated three low joints on the right rail and one on the left rail. It was found that there was a signal between Joints 2 and 4 which were insulated. Joint 1 showed significantly more batter and wear compared to other joints. It was also noted that there was mud and that there were three or four loose tie plates around this joint. The beam MCO response did not show the joint to be unusually different from others but the stiffness trace indicated that it was much softer than the others. Also, it was observed that this joint pumped more than the others under the passage of a train. In this case, therefore, the MCO-difference, which is related to stiffness, yields considerably more information than the beam-MCO measurement alone.

MP 89.0: The stiffness-related signature indicated a large (about 400 feet) soft area around this milepost followed by a hard zone. The transition was more pronounced here than in any other zone tested. Field inspection revealed the presence of a number of crushed ties, a stretch of pumping mud, and the track was laid in parallel with a small flowing stream. The stream was blocked off where the muddy area terminated. It apparently went under the track at that point but no culvert was visually evident. The soil in the fill was soft and moist adjacent to the stream but after the stream it was hard and dry.

MP 87.9: The stiffness-related signature indicated transition from a soft to a hard zone. This area was found to be very muddy with water visible around the ties and in cribs. This zone, in general, was muddier than MP 89.0. This fact is reflected in the stiffness-related signature also. The beam-MCO signature did not reveal any characteristic changes in this soft zone.

MP 88.5: There was a section of very muddy track around this milepost. The stiffness-related trace, however, did not show significant reduction in its value. This observation could possibly indicate that the water had not penetrated significantly in the subgrade which appeared to be hard.

The bridges from Section 3 selected for examination and the results obtained from inspection are included in the following section. Figure B-13 shows stiffness-related signatures for selected bridges and their physical correspondence.

B.3.3 OBSERVATIONS IN SECTION 3

The field inspection here was concerned with the characteristics of the five bridges in the vicinity of Selma and Jackson, AL (refer to Figures B-14, B-15 and B-16). The MCO-difference traces are oriented with less stiff being downward. As discussed in Appendix A, the signature reverses itself. This is due to the bridge panel length being close to the spacing of the outer axles of an R-1 truck. As the R-1 vehicle passes a bent and the measurement truck is centered over it, the bent carries practically the full load and there is a corresponding deflection. When the truck is centered on the span the two bents split the load and consequently the deflection of the bents is less, the center span consequently appears stiffer than the supports. This was indeed verified physically utilizing the wooden panel bridge at MP 87.5 (Figure B-16) when deflection measurements were carried out in conjunction with locomotive loading at several discrete points on the bridge. This effect tends to emphasize the relative stiffness of each bent of a short-span bridge.

Physically, most of the bent-associated deflection occurs at the bent caps. These are normally shimmed with plywood to accomodate uneven settling among the bents. The plywood shims tend to crush after some service time. The stiffness trace can be used to determine where new shimming is necessary or where helper bents are required.

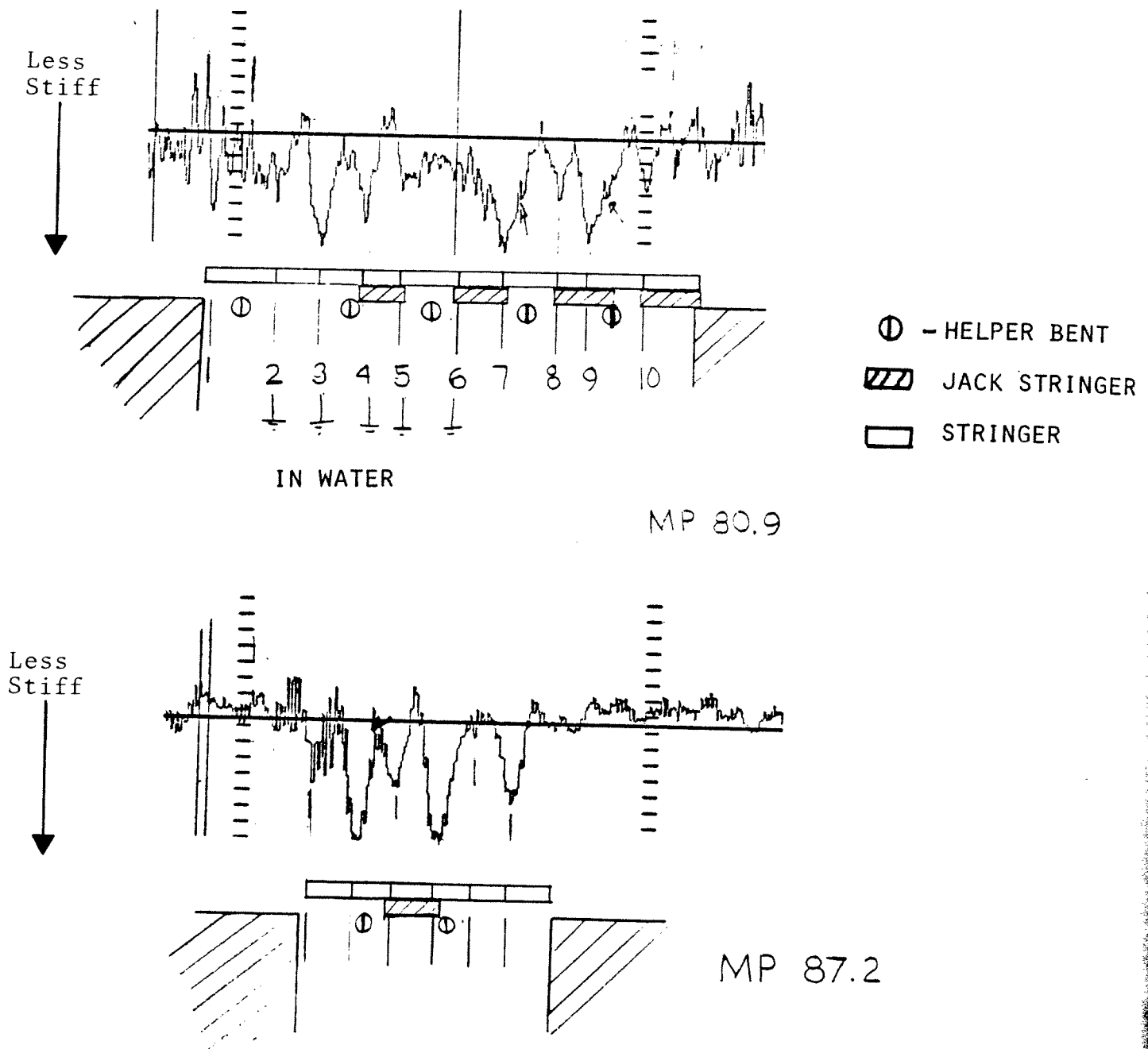


Figure B-14. MCO Difference Traces (Bridges at MP 80.9 and 87.2 on Southern Railway)

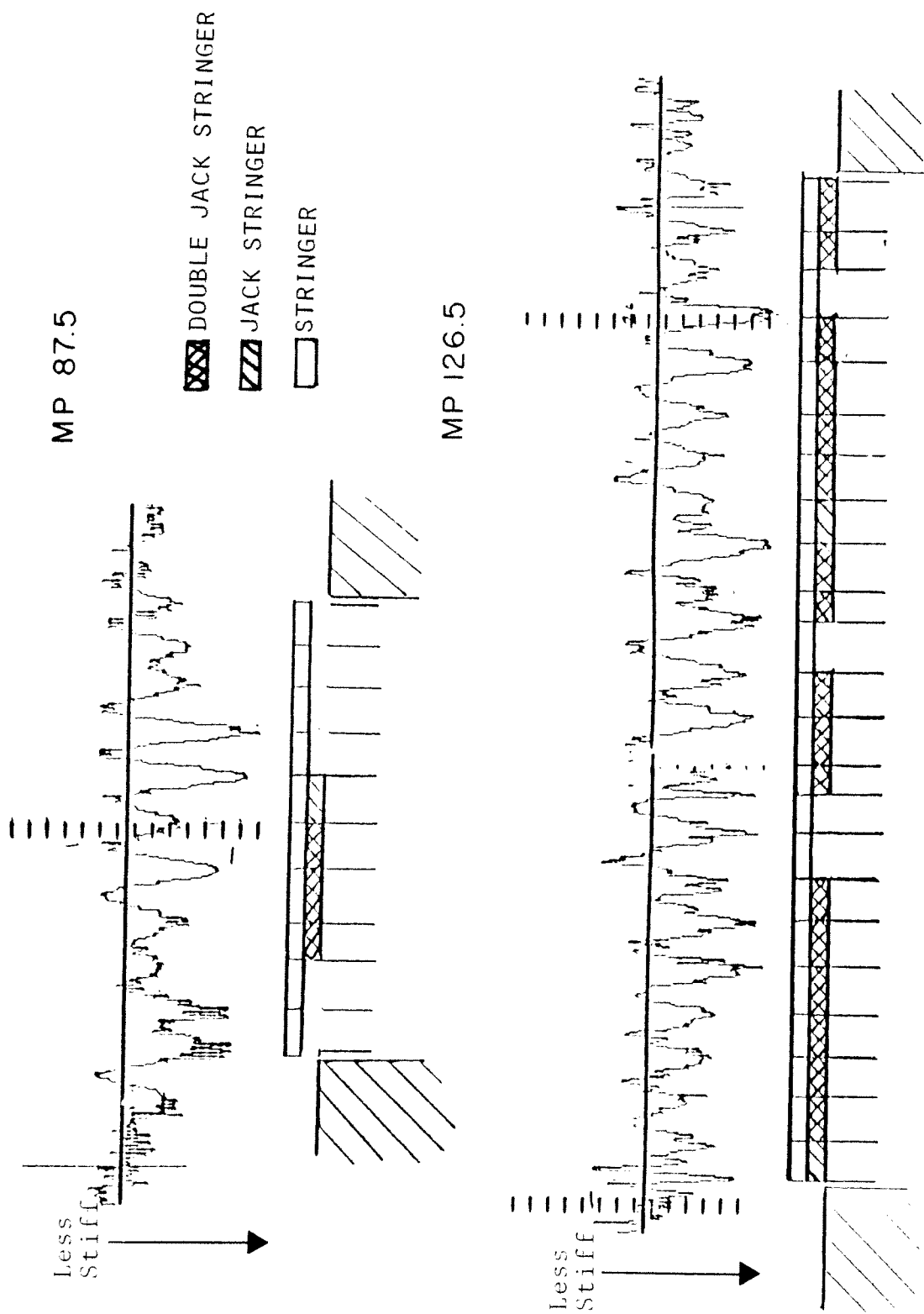
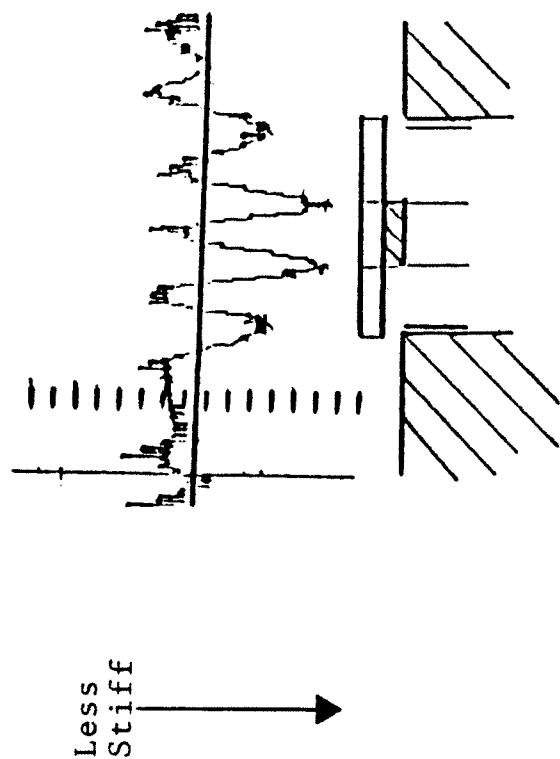



Figure B-15. MCO Difference Traces (Bridges at MP 134.3, 126.5 and 134.3 on Southern Railway)



MP 87.5

 DOUBLE JACK STRINGER

 JACK STRINGER


 STRINGER

Figure B-16 • MCO Difference Trace (Bridge at MP 87.5 on Southern Railway)

APPENDIX C

DATA PROCESSING

C.1 PHASE I

C.1.1 DEVELOPMENT OF REFINED DATA PROCESSING TECHNIQUES

The results of the initial analysis of Test RG-116 data indicated the feasibility of measuring stiffness by comparing two differently obtained profile measurements. However, the processing scheme used to achieve the above results was complex and was limited to down-stream data processing methods. The next stage of the program was to devise data processing techniques that could compute track stiffness information in real-time, onboard a track geometry car, in a manner similar to that presently used to compute track geometry parameters.

To accomplish this, a series of analysis tasks and field test runs, designated RM-176.1 through RM-176.4 were carried out. Altogether, three field test runs were performed in addition to the original tests on the Kansas Test Track (KTT); two on the Southern Railway System and one on the Bessemer & Lake Erie Railroad.

Attention was first directed toward the original KTT data because more details are known about the KTT track and sub-grade structure than any of the other track systems that were tested. As progress was made in the analysis of the KTT data, it became apparent that the objectives of generating reliable stiffness or compliance data, of relating the data to physical track conditions, and of devising real-time processing procedures would be accomplished most efficiently by focussing on the KTT data. Consequently, this phase of the program was concentrated primarily on the KTT data. It was planned that the track stiffness measurement technique would be demonstrated on the other railroad track that was tested, when the necessary data processing procedures had been perfected.

C.1.2 DATA PROCESSING TECHNIQUES FOR GENERATION OF EQUIVALENT MCO FROM PROFILOMETER DATA

It is necessary to convert the profilometer data to an equivalent MCO in order to extract the stiffness information. Little difficulty is encountered when producing MCO data from profilometer data for the purpose of Track Safety Standards, since the profile exception thresholds are large fractions of an inch (e.g., 0.5-inch MCO for a 62-foot chord on Class 6 track). However, when generating equivalent MCO data in the present application, displacements of a few hundredths of an inch are critical. To obtain this accuracy, special data processing techniques had to be developed.

The profilometer itself is an electromechanical device in which accelerometer and displacement transducer signals are passed through analog electronic processing circuits (e.g., integrators and other filters) to obtain the track geometry profile data. Inherent in this process is the introduction of time delays or phase shifts, which result in distortions of the data. It is, therefore, necessary to devise data processing techniques for creating MCO data from profilometer data that are sufficiently free of phase shift to allow proper extraction of stiffness data. This set of computer programs was designated Mode 1 processing.

In Figure C-1, the results of Mode 1 processing are shown for some data acquired on the Southern Railway (Test RM-176.1). By comparing Graph (a) with Graph (b) and Graph (c) with Graph (d), it is clear that the timing of simultaneous events is well correlated. Graphs (a) and (c) were obtained from the Southern Railway, R-1, 11-foot chord system, while Graphs (b) and (d) were generated by processing profilometer data. The high frequency ringing effect in the chord data is believed to be instrument induced (i.e., some vibration of the mechanical parts of the sensor system). The beam

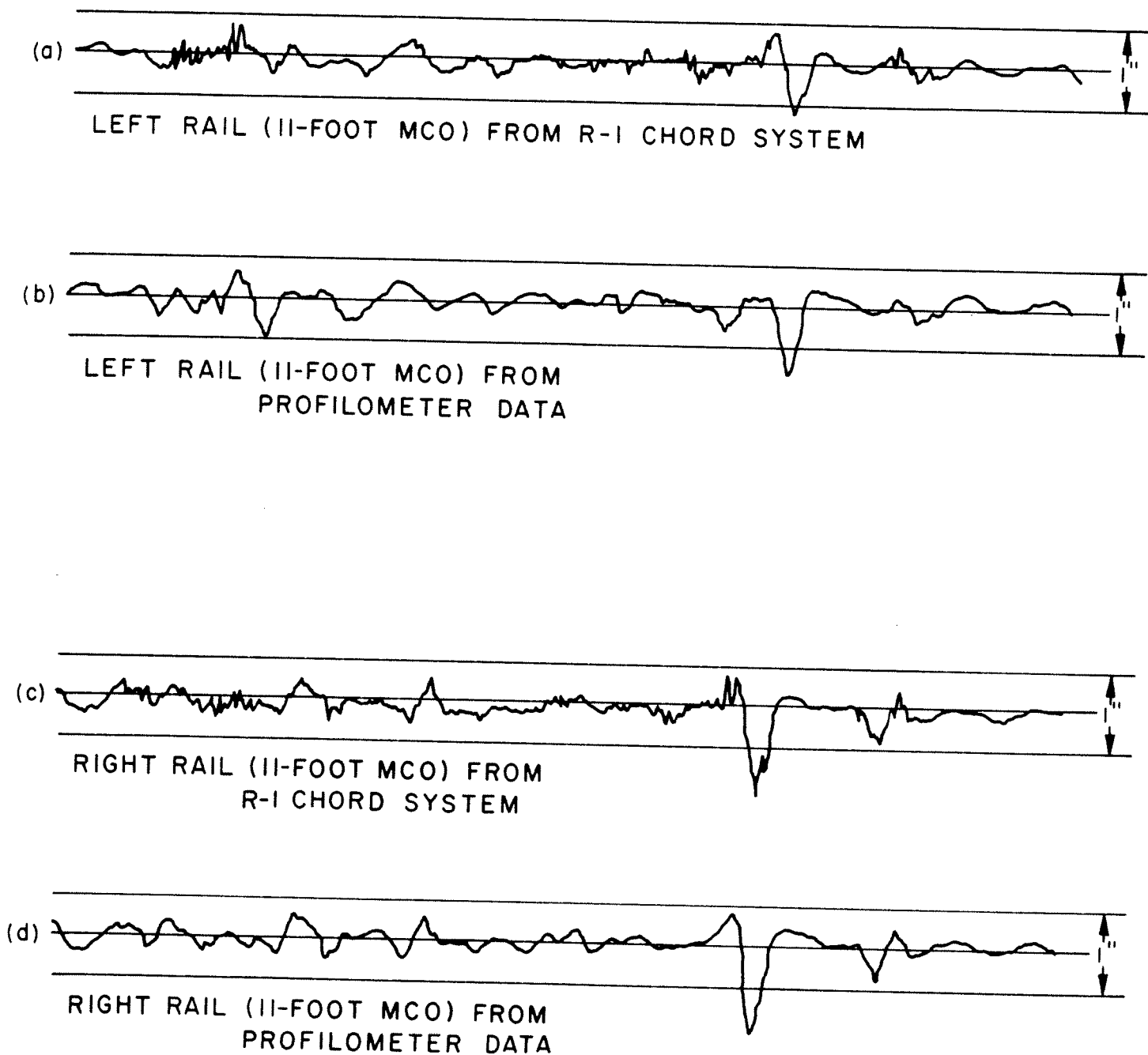


Figure C-1. Mode 1 Processing at Turnout

system installed on R-1 was eleven years old at the time of the test and was scheduled for replacement in November 1978. Considerable play had developed in the bearings at each frame corner and the frame was also subject to occasional flutter. Therefore, high-frequency ringing was injected into the MCO measured by R-1 (this ringing was not part of the track data). In the normal use of R-1, the ringing was not a problem since the actual error was approximately ± 0.031 inch. However, an error of this magnitude becomes quite critical in stiffness measurements.

To further demonstrate the elimination of the undesirable phase shifts, data taken traveling in two different directions on the same section of track were processed using Mode 1 techniques. Once again, if there are significant phase shifts or time delays in the analog processing of the profilometer data, the distortions in the data will cause differences to appear when comparing northbound versus southbound runs on the same section of track. In Figure C-2, the high quality of the Mode 1 data processing is again demonstrated. The patterns seen from left to right (southbound) are repeated very well when seen from right to left (northbound). The profilometer-derived, 11-foot MCO's also agree well with the chord values measured by the R-1 test car.

Curves (c) and (f) of Figure C-2 are profilometer derived MCO's for a 50-foot chord length. The long chord involves profile data that are more sensitive to long wavelength deviations than short chord. Again the results show that the Mode 1 processing is effective in eliminating phase shifts.

SOUTHBOUND

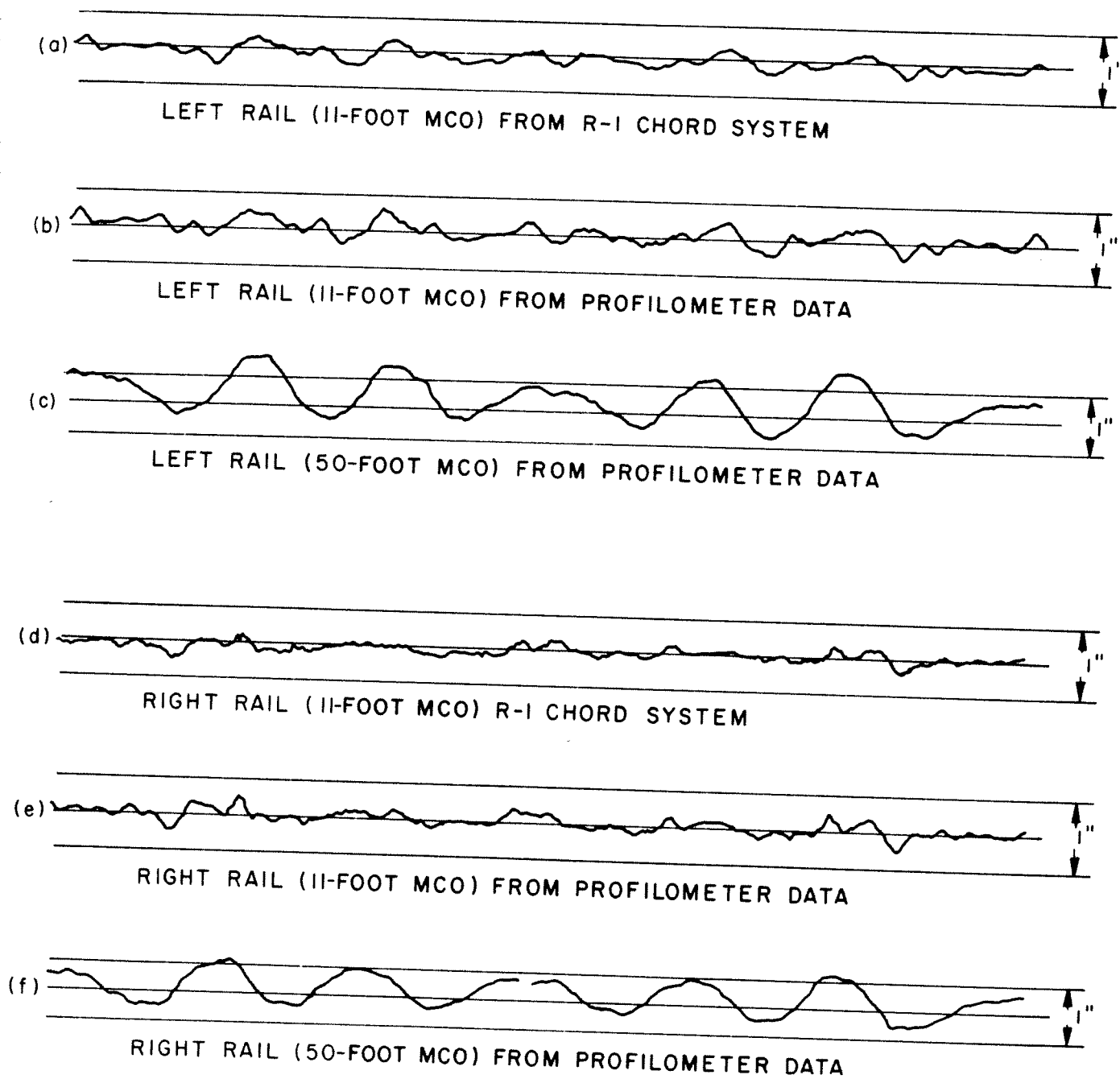


Figure C-2. Mode 1 Processing Comparing Northbound versus Southbound Runs.

C.1.5 AVERAGING TECHNIQUES FOR OPTIMUM EXTRACTION OF STIFFNESS DATA

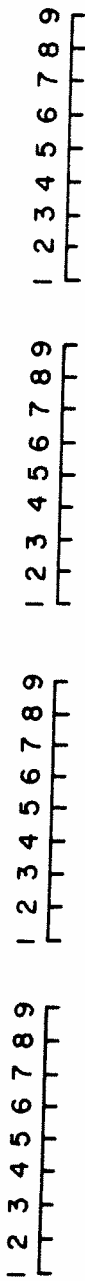
In general, the quality of the computed stiffness information can be improved by eliminating random system errors and other extraneous noise by averaging many data samples. This is successful only up to a point, since this same averaging process may smooth out the very variations that the system is designed to detect. An optimum averaging technique must be established that will minimize extraneous noise but still be capable of resolving the physical phenomena.

The data shown in Figure C-3 is based on whole section averages of the KTT involving many data samples per section. In the case of the KTT, this is meaningful because there should not be much variation within a section and a whole section average is valid. However, in more typical track systems this is not the case and it is not valid to average as many points. As a means for determining the optimum averaging technique, track data obtained under Test RM-176 on the Southern Railway was utilized. Several filter "window widths" for the averaging technique were applied. Filter 10 had a window of 10 points, Filter 32 had 32 points and Filter 100 had 100 points. The filters were also applied to KTT data and the results obtained applying these different filters (termed Mode 2 processing) are shown in Figure C-4. Curve (d) is the raw difference between the sensor gap value and the equivalent profilometer value. Curves (a), (b) and (c) show the effects of increasingly larger averaging intervals.

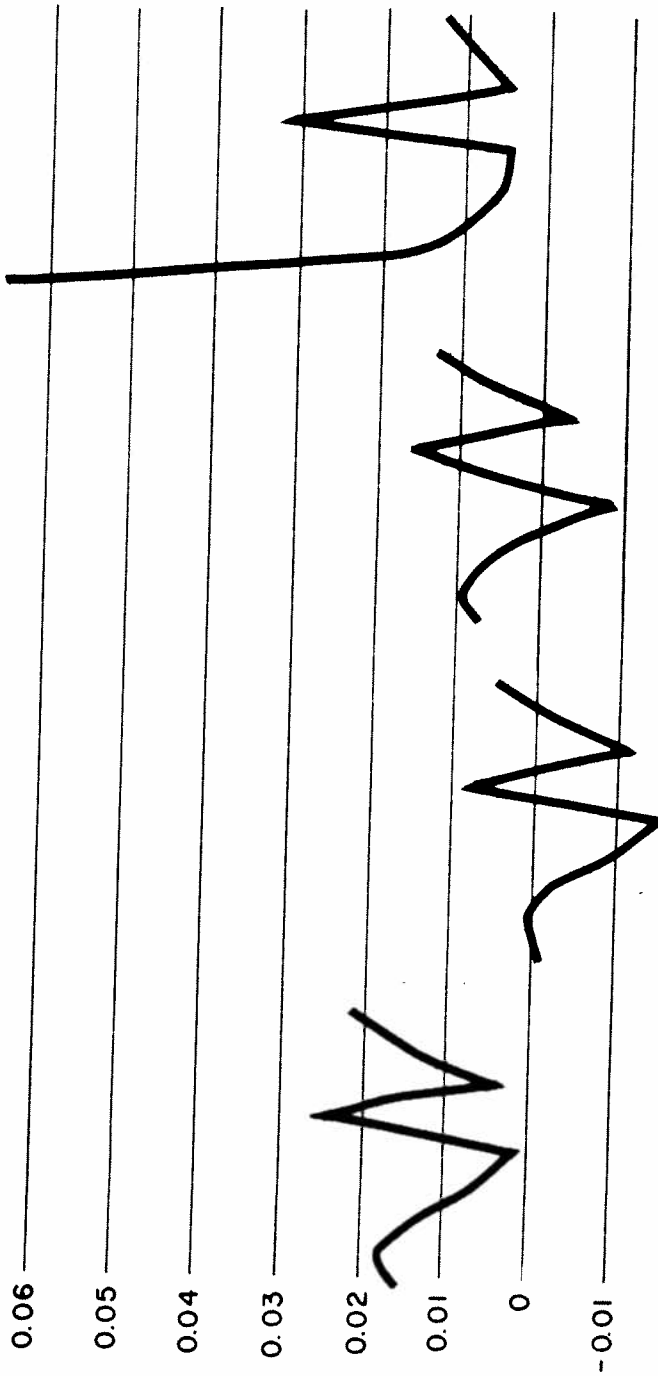
The results in Figure C-4 show:

- Profilometer prediction of sensor gap is quite good, being limited in this case by the digitizing resolution of 0.04-inch.

TRACK SECTION NUMBER



EQUIVALENT SENSOR OFFSET (INCHES)
(RELATIVE COMPLIANCE)



i) AVERAGE, FOUR
PASSES FRONT

j) AVERAGE, FOUR
PASSES REAR

k) AVERAGE, ALL
FOUR PASSES,
FRONT AND REAR

l) WATERWAYS
EXPERIMENTAL
STATION DATA
(SIX)

Figure C-3. Comparison of Average Compliance Values
With WES Data on the Kansas Test Track.

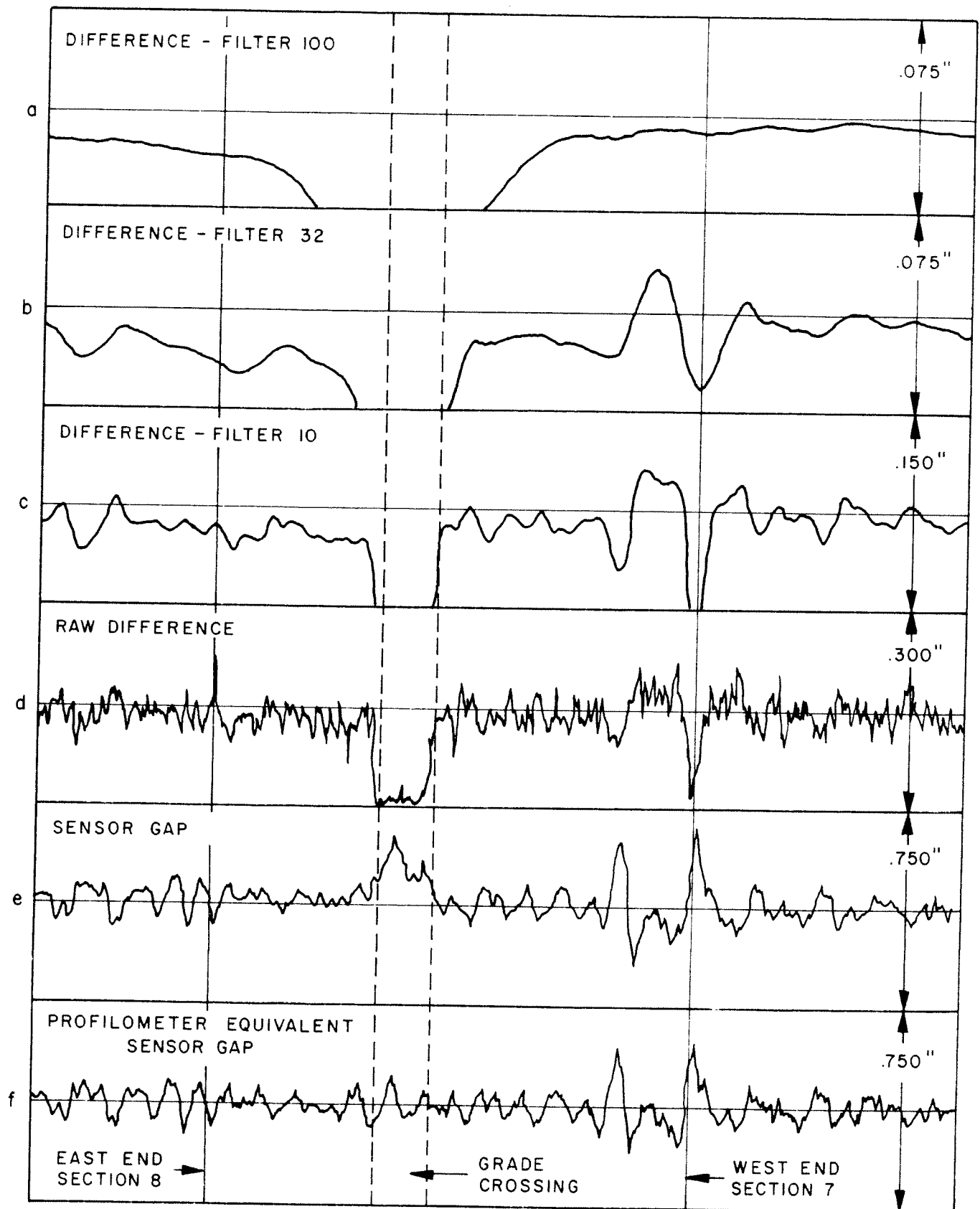


Figure C-4. Mode 2 Processing Showing the Effects of Averaging for Extracting Meaningful Stiffness Information

- The raw difference signal is jagged, reflecting the generally random character of the 0.04-inch resolution cited above.
- Filter 10 and Filter 32 are becoming progressively more reproducible. However, the influence of the profilometer resolution noise still shows through.
- Filter 100 completely eliminates the profilometer noise, leaving a signal that is reproducible from run to run.

(NOTE: The dashed lines indicate the existence of a grade crossing. The capacitive sensors do not function properly in the vicinity of grade crossings, so that the data within the neighborhood of the crossing should be ignored.)

From this investigation it was concluded that given the noise floor conditions of the KTT instrumentation, Filter 100 was the best compromise between feature extraction and error reduction. Improvements in the noise floor are expected in the design of the final stiffness measurement system.

C.1.4 APPLICATION OF OPTIMUM AVERAGING TECHNIQUE TO KANSAS TEST TRACK DATA

Having determined the optimum averaging filter, it was decided to reprocess the entire set of KTT data and make a careful comparison of the derived compliance or stiffness data with the known physical conditions at the site. This was to be a final check on the complete data processing package which now had been substantially updated and improved by incorporation of the advanced Mode 1 and Mode 2 processing techniques. Figure C-5 shows this reprocessed data for the entire KTT for all four passes using front and rear sensor configurations. It is evident that the compliance variations are very reproducible and at the same time distinct section-to-section variations are easily detectable.

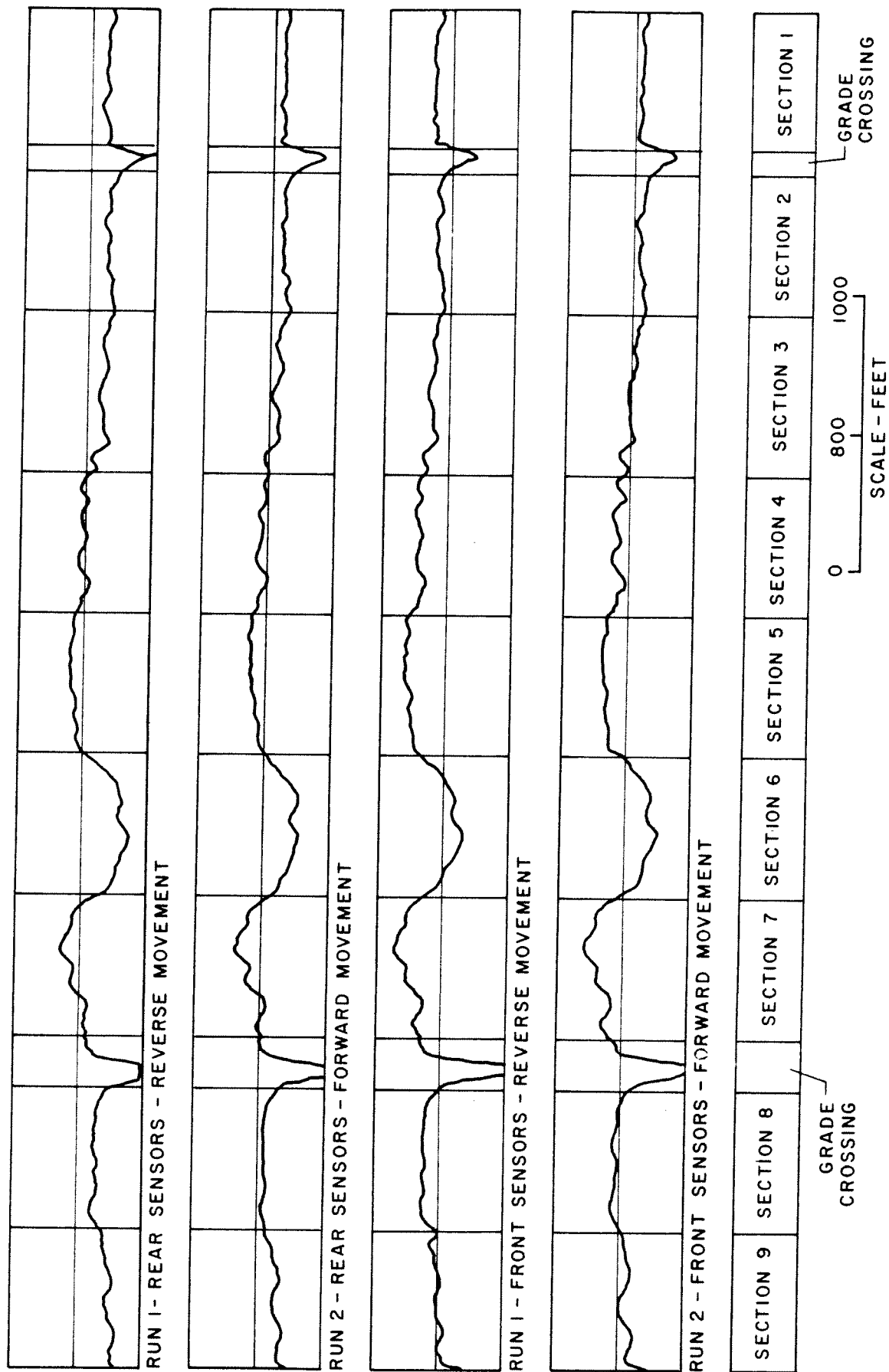


Figure C-5. Graph of Compliance Results Showing Repeatability for Different Sensor Positions and Direction of Travel on the KTT.

In Figure C-6, a profile of the test track embankment [7] is displayed against one of the derived track compliance characteristics. Both are to the same longitudinal scale for ease of comparison. The correlation of the derived compliance with the actual physical phenomena is very good and provides substantial validation for the proposed track-stiffness-measurement technique. Significant points are:

- There is a noticeable decrease in compliance in passing from Section 9 to Section 8. On the actual track, there is a transition from a fill to a cut condition. Also in Section 8, concrete ties spaced 27 inches on-center with 15-inch ballast are being used. This together with the compacted condition of the soil and the proximity to bedrock probably accounts for the increased stiffness of Section 8.
- Section 7 is particularly interesting. It is a zone in which there are intermittent transitions from cut to fill, and vice versa. In spite of the use of rigid precast beam construction, stiffness variations are quite evident and are coincident with the cut-fill variations. The precast beam in this section had developed negative moment cracks, and the compliance data suggested that the softer fill areas were responsible for these cracks.
- Section 6 and its surroundings present another interesting facet of the KTT. It is the only zone which is effectively unsupported by bedrock. The only support is by the red-brown clay indigenous to the area. Correspondingly, Section 6 is the softest of the KTT zones.
- Section 5 has a uniformly low value of compliance throughout. This is consistent with the concrete slab construction.

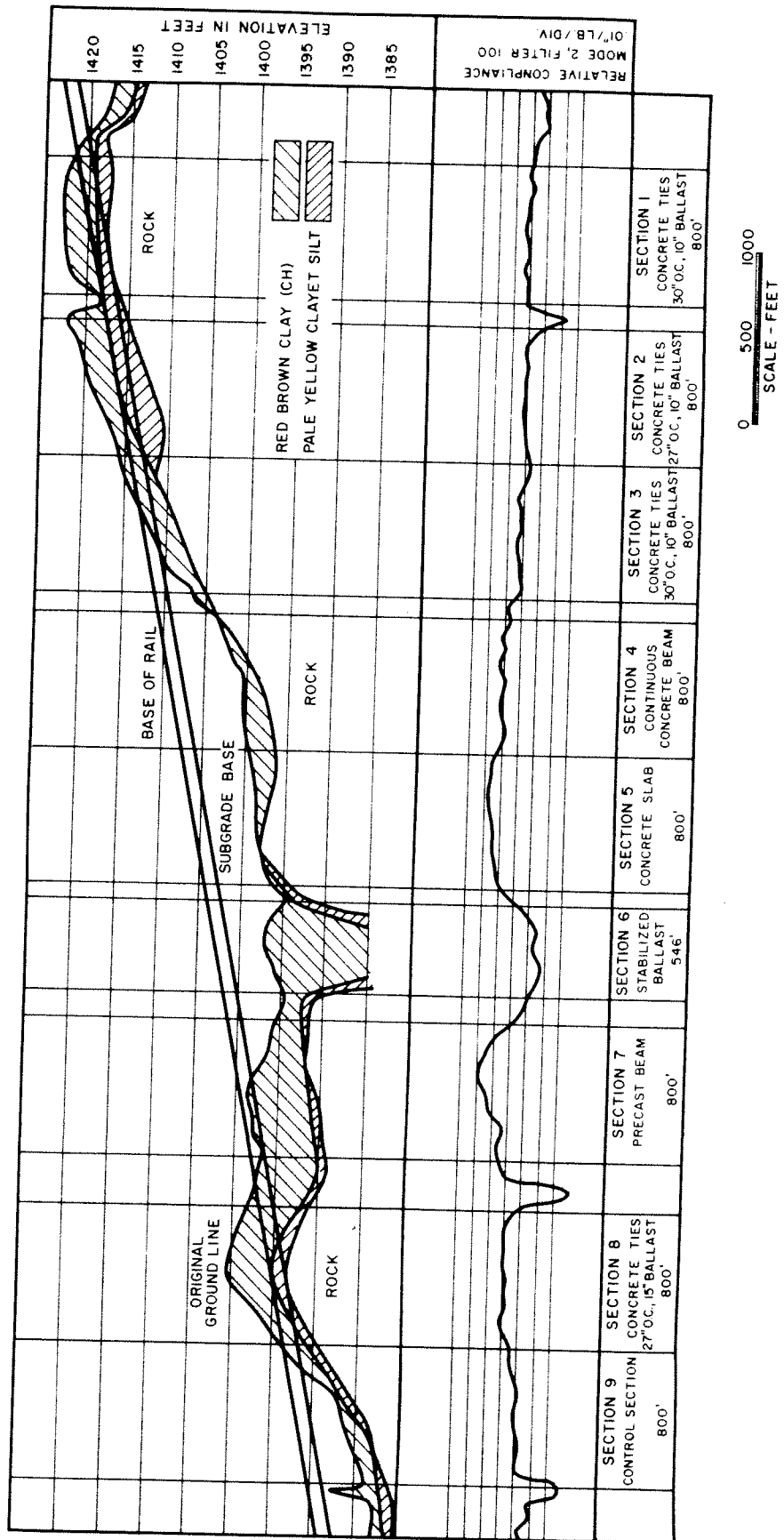


Figure C-6. Comparison of Computed Compliance with Physical Conditions on the KTT

- One would expect the same situation for Section 4. However, the continuous concrete beam construction experienced considerable negative moment cracking which is probably responsible for the variations between very stiff and moderately stiff values.
- Passage from Section 4 to Section 3 is accompanied by another transition from fill to cut. The decrease in calculated compliance is consistent with this change.
- Section 2 shows up as slightly softer than Section 3. This is not surprising in view of the 27-inch on-center spacing of the concrete ties with roughly similar subgrade conditions.
- Section 1 shows up as slightly more stiff than Section 2. This is surprising since concrete ties spaced 30 inches on-center are used. WES results [6] and ENSCO findings in the previous report [8] also do not show this to be the case. Possible explanations are that compaction has taken place since the WES data was taken; and the nonlinear characteristic of the chord sensitivity characteristic used in the previous evaluation caused an improper ranking.
- The proximity of bedrock to the surface of Section 1 may be an overriding factor in causing the low compliance of this section. Note that 200 feet from the left end of the section, the rock comes closest to the surface. This corresponds to the stiffest value in the section.
- Two hundred feet to the right of Section 1 there is a cut-fill transition. This is reflected by a substantial increase in compliance.

C.1.5 DATA PROCESSING

Data processing was conducted in two phases:

- Software development and debugging.
- Data reduction.

The software development effort produced the following programs whose functions were as follows:

- Program T176D2 was created to select six channels of data from tapes generated on Southern's R-1. The digitization capability on R-1 produces a tape that has up to 16 channels of data packed into 2,048 16-bit words per record. Data is digitized using a 10-bit sign plus a magnitude miniverter. The six channels so selected are output to an intermediate tape for plotting using program RQPLOT.
- Programs TNGP3 and TNGP4 selected required channels from raw data tapes generated by FRA T-3 on the KTT and the B&LE, respectively. Sensor data were linearized in this process. The output is a data tape in a 15 x 256 record format suitable for programs T176P3 and T176P4.
- Programs T176P1 and T176P3 are tri-modal processors that are the crux of the track compliance measurements. In each mode, six channels plus event information were transcribed onto an intermediate tape in the 7 x 256 format required for RQPLOT. Additional programs T176P2 and T176P4 were generated as minor variants of these for processing data from tests RM-176.2 and RM-176.4, respectively.
- Program RGSZR is a regression and correlation analysis program that selects one or more pairs of channels from an RQPLOT input tape. Specific channels of data, i.e., from scan to scan or from event to event can be processed.

Some existing general-purpose programs that were used included:

- Program RQPLOT, a six-channel plus event plotting package suitable for output on the Gould plotter/printer.
- Program C1527 takes six of fifteen channels of a 15 x N channel tape and converts it to a 7 x 256 format. The option to carry a seventh event type channel is included.

Figure C-7 shows the data flow between program and intermediate data tapes.

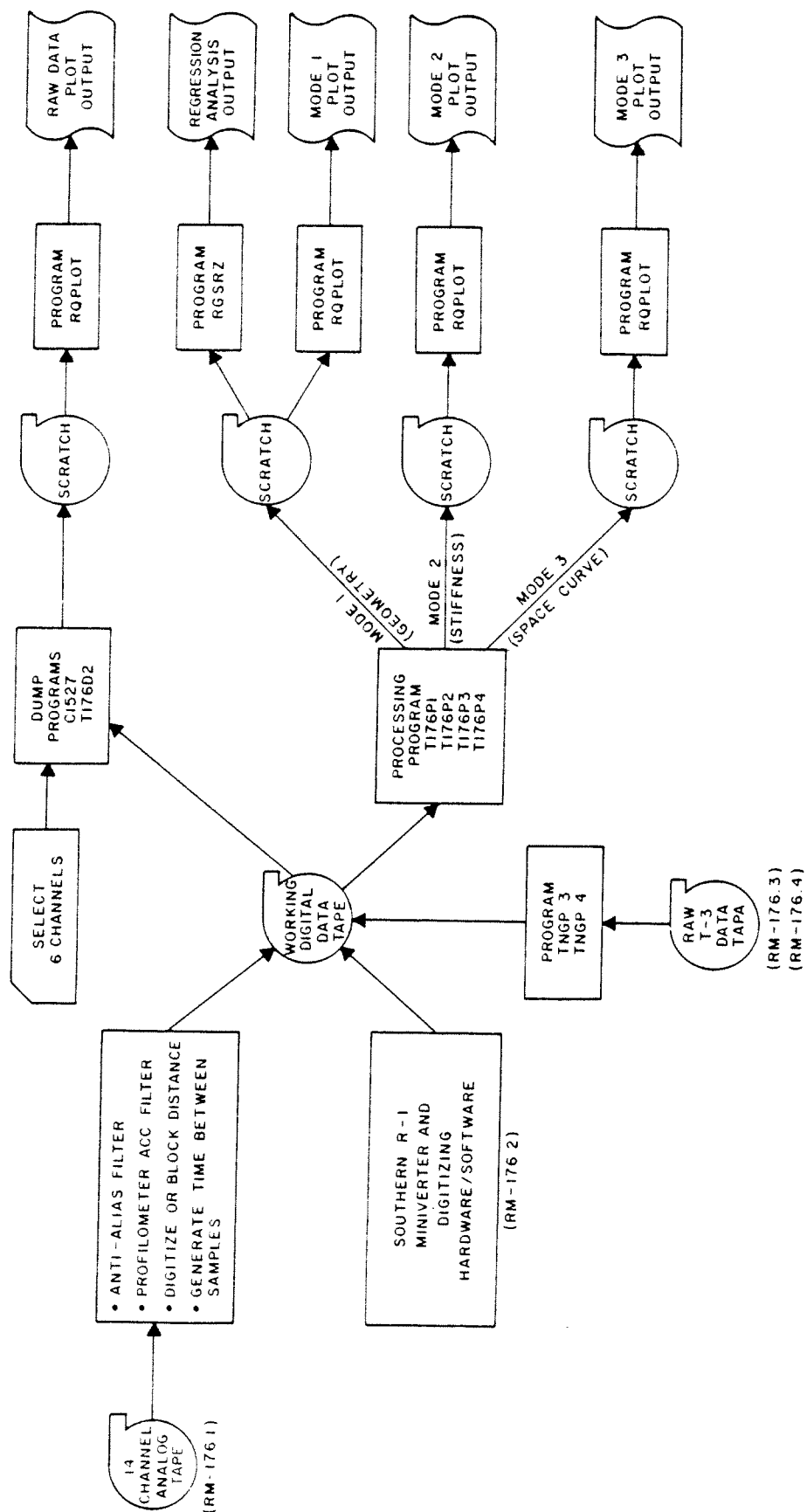


Figure C-7. Diagram of Data Flow

C.2 PHASE II

The main processing program was written to process the data scan-by-scan to simulate real-time, onboard processing.

It was necessary to perform three intermediate steps before the main processing.

- The 1600-bpi, 9-track magnetic tapes written by the onboard HP-2100 computer were delivered to the ENSCO computer facility in Springfield, VA and translated into 800-bpi, 9-track tapes for use at the ENSCO/FRA computer facility in Alexandria, VA.
- Each raw data tape was processed through the BACK432 program which generated analog charts of the raw data for the primary system channels.
- The dynamic calibration data were processed through the CAL432 program to determine the relative gains between the accelerometer and the linear-variable-differential-transformer (LVDT) of each profilometer.

Gains and bias for the various displacement transducers and the linear-variable-differential-transformers were derived from the field calibration data and were used as input to the main processing program (T432). This program produced a sixteen-channel tape of scan-by-scan rail geometry and rail stiffness information. A simple additional program (DMXSTIFF) was used to read this tape and select six channels for plotting on analog charts. Figure C-8 shows the data flow for post-test processing

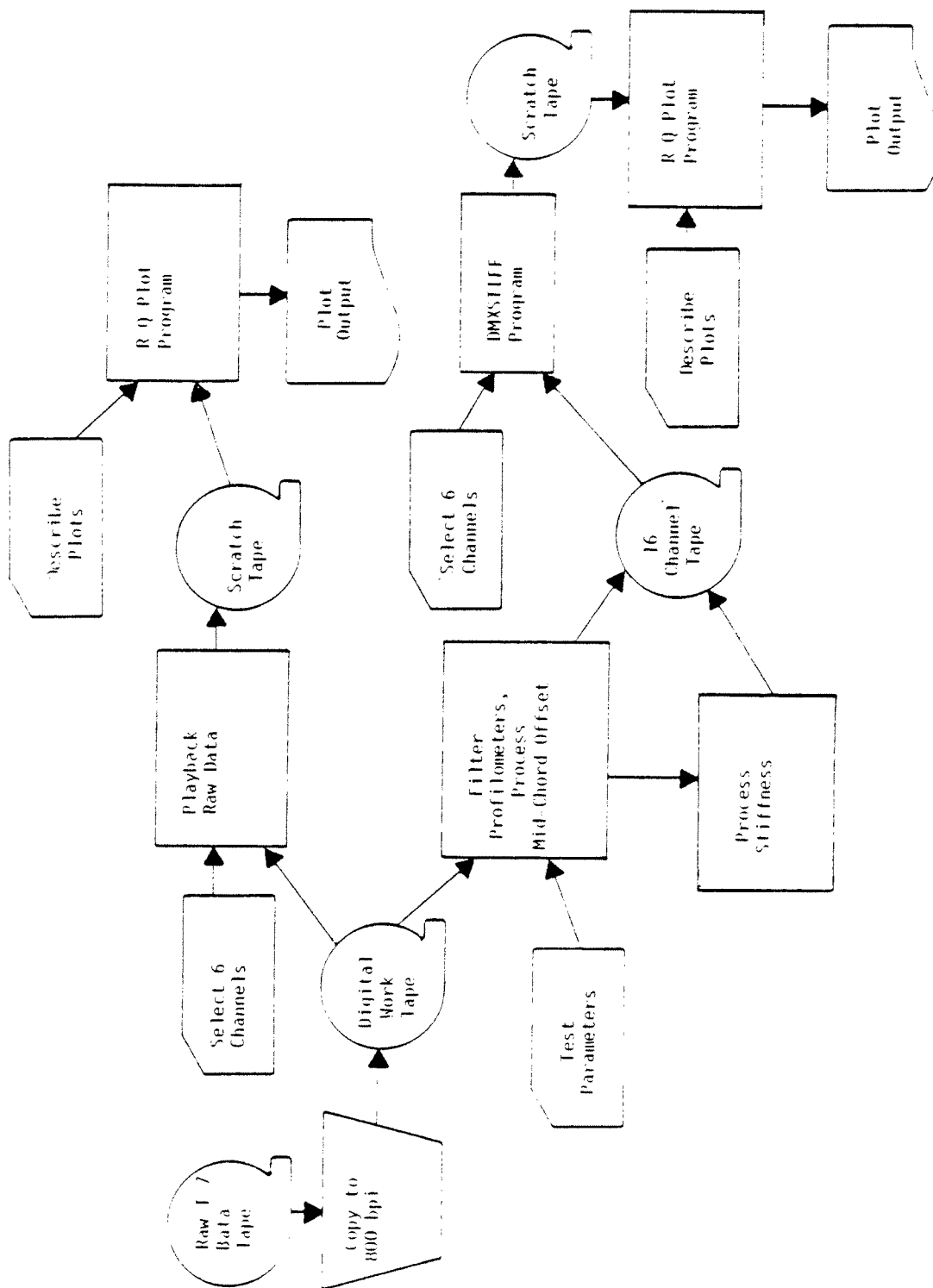


Figure C-8. Data Flow for Post-Test Processing

C.3 MAIN PROCESSING

The main processing program (T432), functionally illustrated in Figure C-9, is a real-time simulator. Data are read from a nine-track, 800-bpi, raw data tape and processed scan-by-scan. The signals from the accelerometer and the LVDT on each profilometer are filtered, corrected for gravity and velocity changes which affect the profilometer and combined to produce a phaseless, short, mid-chord-offset (one foot in length). These short, mid-chord-offsets are stored and can be used to generate simulated 11-foot, mid-chord-offsets or pseudo space curves. The signals from the paired, beam-mounted, displacement transducers (used to measure 11-foot, mid-chord-offset) are averaged to correct for rocking motion in the journal bearings.

Sixteen output channels were written on magnetic tape. These included events, time between samples, crosslevel, and for each rail, space curve, measured 11-foot, mid-chord-offset, profilometer generated 11-foot, mid-chord-offset and three rail stiffness channels. An auxiliary program was used to read the output tape and select any six channels to be output as analog strip charts, or to create track-averaged analog strip charts.

A segment of a typical set of profile charts is shown in Figure C-10. This figure shows plots of space curves and 11-foot, mid-chord-offsets both measured and profilometer generated for the left and right rails. These outputs are useful in providing accurate location information along the track as well as in the interpretation of stiffness variations.

A segment of a typical set of track stiffness charts is shown in Figures C-11(a) and (b). In Figure C-11(a), the track-averaged 11-foot, mid-chord-offsets both measured and profilometer generated are shown with their raw different curve.

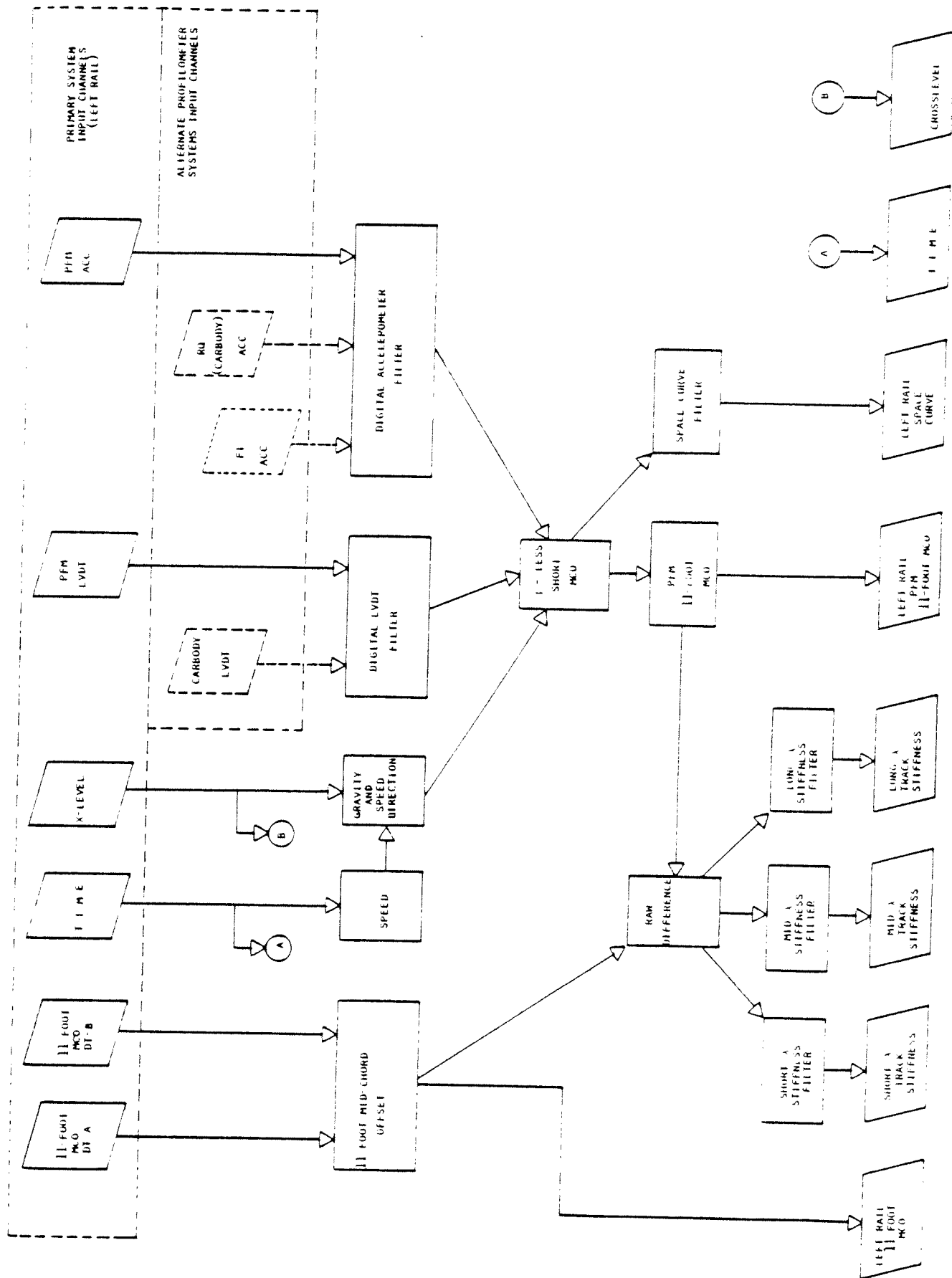


Figure 6-9. Program T432 - Functional Block Diagram

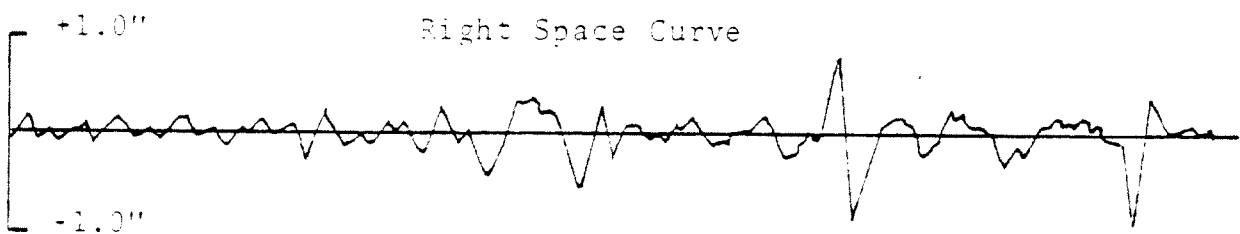
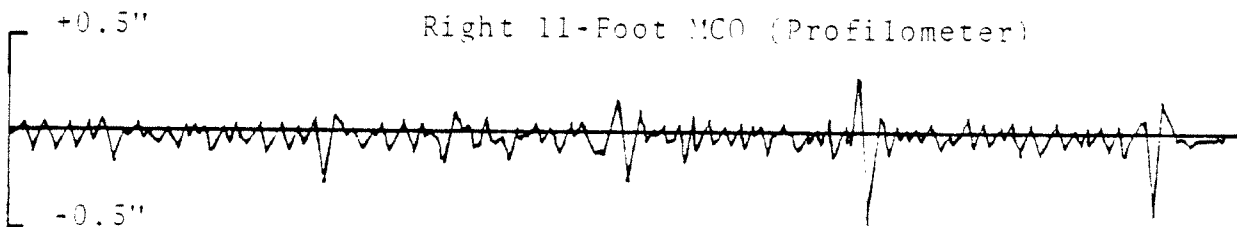
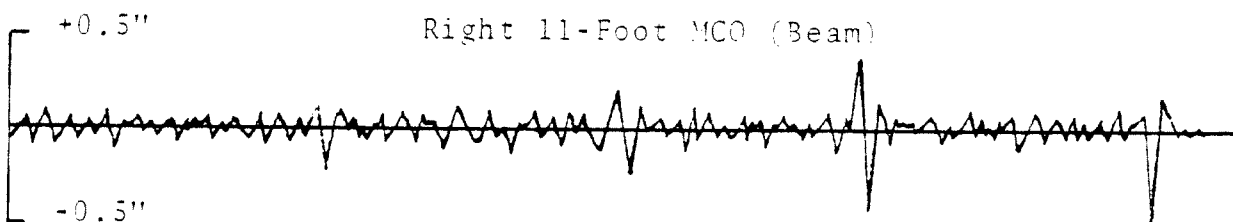
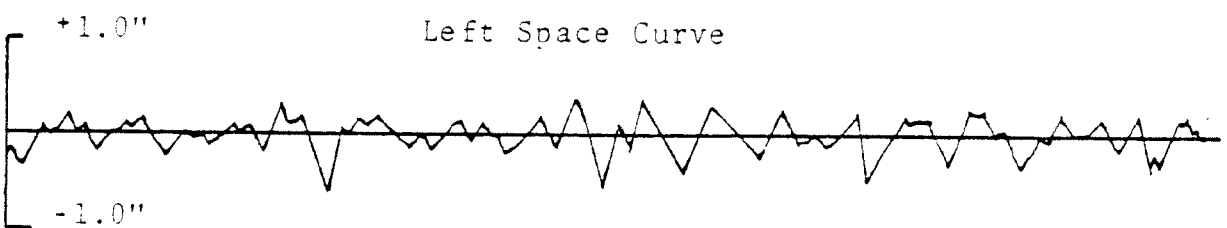
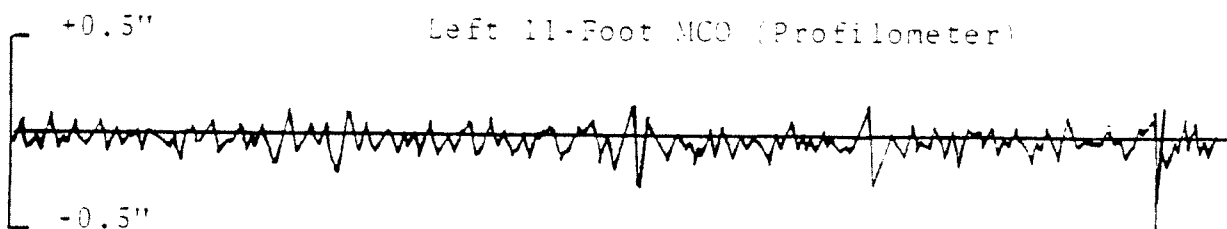
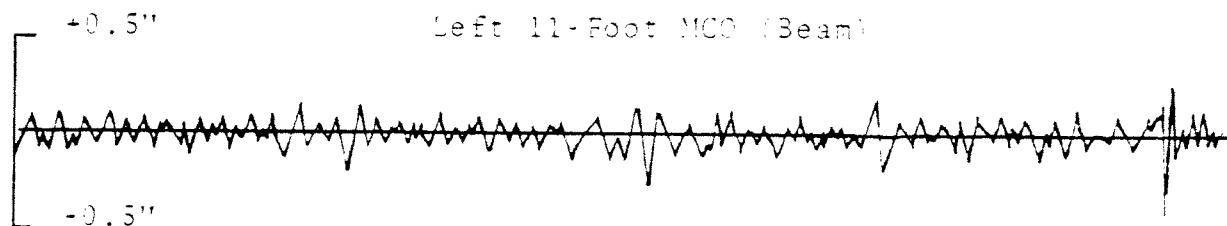


Figure C-10. Sample Analog Charts - Profile Mode

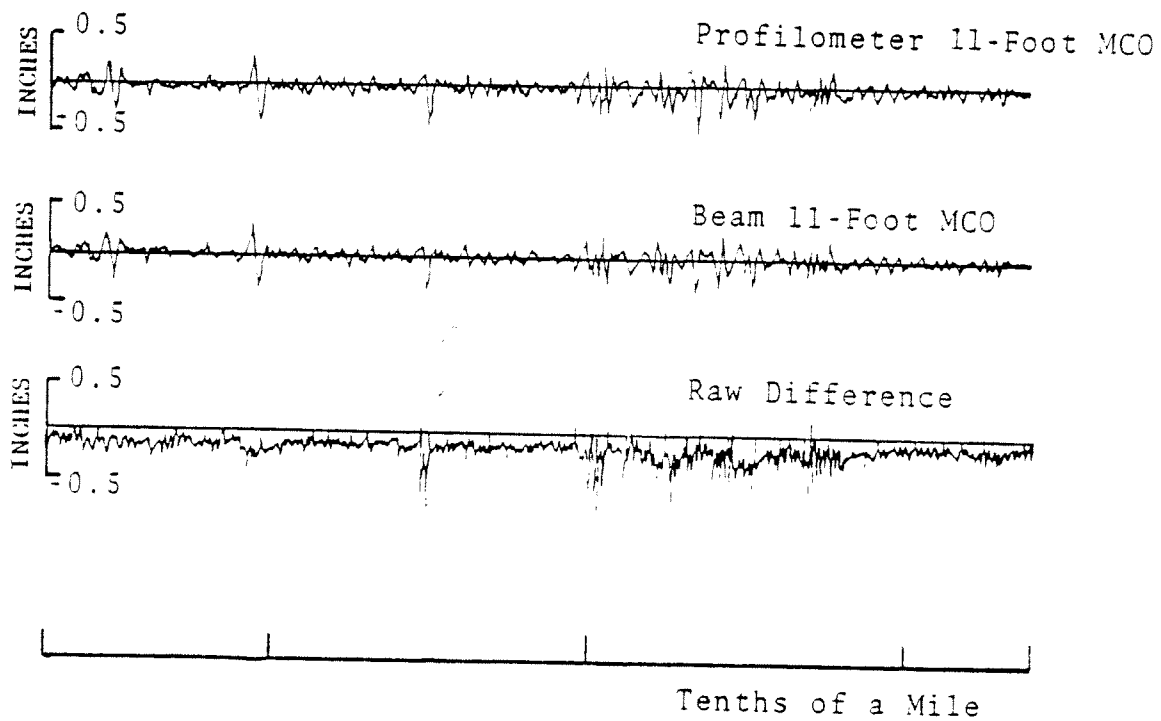


Figure C-11(a). Sample Analog Charts - Track Stiffness Mode

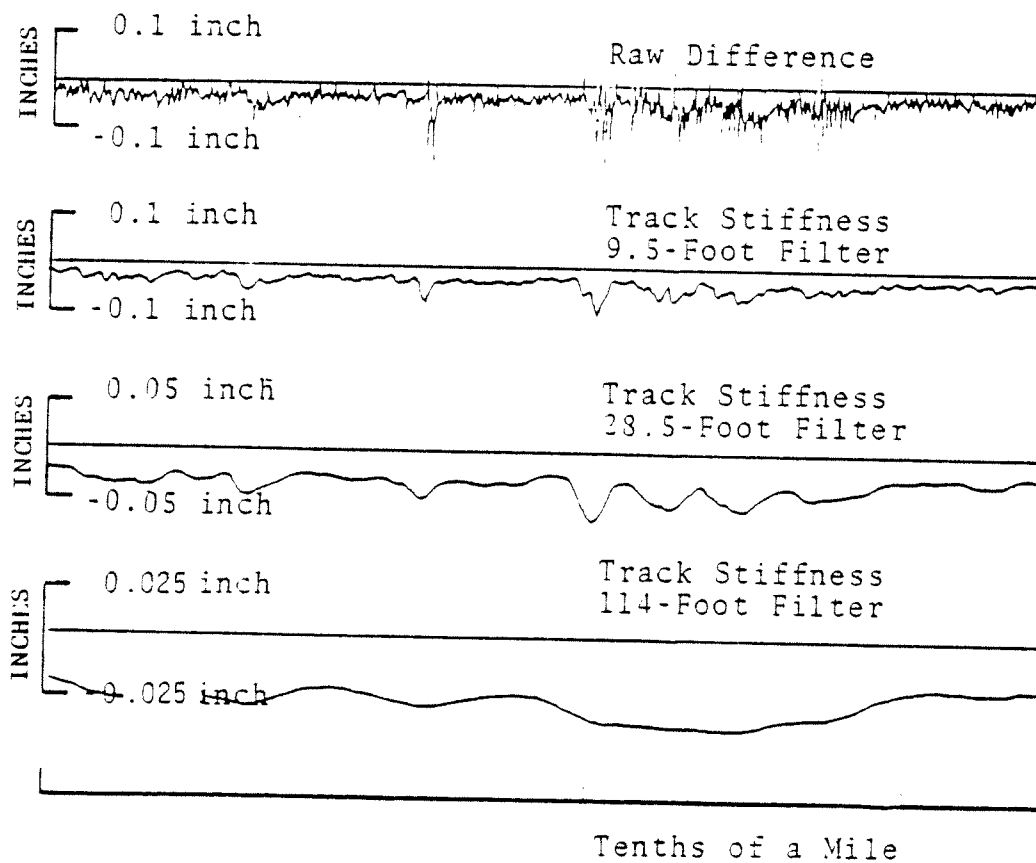


Figure C-11(b). Sample Analog Charts - Track Stiffness Mode

The high-frequency component in the raw difference data can be related to the 9.5-foot circumference of the R-1 wheels. This contribution results from small asymmetries in wheel diameters. To remove this periodic noise that is superimposed on the signal, a filter having a triangular impulse response was used to smooth the data. The frequency response of this filter is shown in Figure C-12. The filter was chosen for its nodes at 9.5 feet and multiples of that length. As shown in the graph, the 0.707 point is at a wavelength of 30 feet. To emphasize longer wavelengths, filters with nodes located at 28.5 feet and 114 feet were also used to process the data. The frequency response of these filters is also included on the graph in Figure C-12. The triangular impulse shaped filter was chosen for its simplicity in digital application, especially with regard to scan-by-scan processing.

The raw difference curve and its three filtered versions are shown in Figure C-11(b). The response for stiffer track (less compliant) will be close to the baseline; the response for track of less stiffness (more compliant) will deviate further below the baseline. Note that the amplitude scales for the 9.5-foot, 28.5-foot, and 114-foot filtered data are in progressively larger expansions by factors of two.

C.4 PHASE III

The data processing used in the third phase was the same as that utilized in the second phase. The only difference between the two systems was the computers. In Phase II an HP2100 was used while in Phase III an HP21MX was used in data collection. Off-line processing was accomplished with an RDS-500 at ENSCO's Huntington Avenue facility.

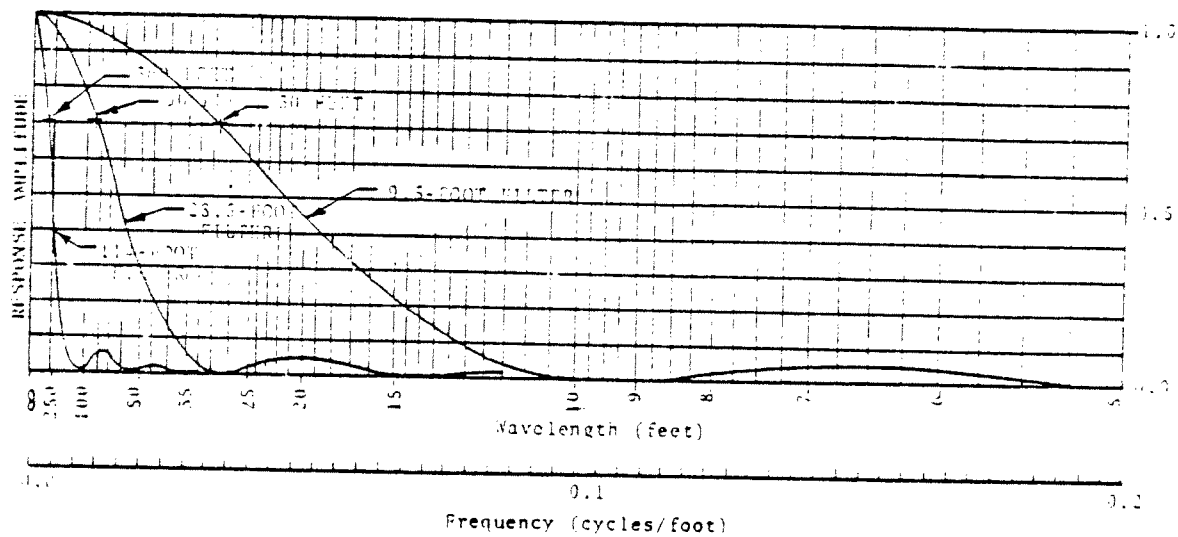


Figure C-12. Frequency Response of Triangular Filter

APPENDIX D

INSTRUMENTATION

D.1 PHASE I

D.1.1' INITIAL APPLICATION OF TRACK STIFFNESS MEASUREMENT TECHNIQUE TO KANSAS TEST TRACK (KTT)

The proposed track stiffness measurement system was first tested on the KTT under test objective RG-116 [5]. The test used track-geometry measurement consist, T-3/T-4 (this was a temporary configuration while T-1 and T-2 were being refurbished) with the combination profilometer/chord profile system. The test was successful and resulted in the following accomplishments:

- The nine KTT sections were ranked according to increasing stiffness using whole section stiffness averages. With the exception of Zone 4, these rankings agreed with those determined independently by the Waterways Experiment Station (WES) [6].*
- It was demonstrated that individual features such as zone transitions, culverts and some other soft spots were marginally identifiable.

From this initial application, it was concluded that the track stiffness measurement system showed promise and should be refined and developed further.

D.1.1.1 Alternative Sensor Configuration

Some alternate sensor configurations may be more effective for deriving compliance or stiffness information than the MCO configuration. However, just as with the MCO configuration, these sensor configurations will pick up geometric profile variations which are not stiffness related and must be removed.

* WES measurements were performed in advance of the KTT opening, while the stiffness measurement of RG-116 were performed after considerable KTT traffic. During the intervening period, the concrete slabs in Section 4 developed negative moment cracks.

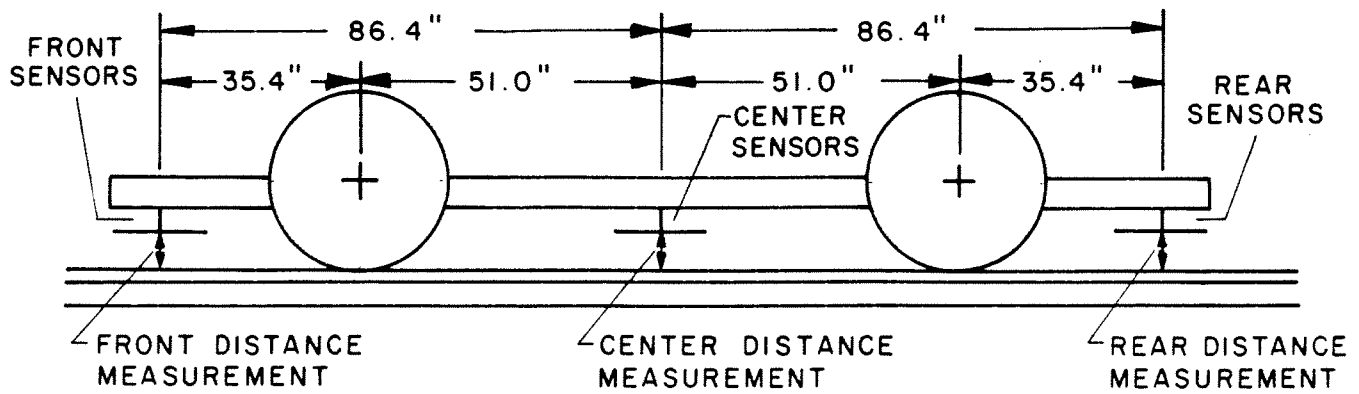
This is done in the same way as in the MCO case. An equivalent sensor gap value for the profilometer is generated and then subtracted from the actual sensor gap value.

Four possible configurations for the proximity sensors mounted on the measurement beam of T-3 are shown in Figure D-1. In Configurations (b), (c) and (d), the wheels provide two known point loads, and the proximity sensor provides a measurement of the spacing from sensor to railhead. While neither of these is quite as sensitive to higher compliances as the 14.5-foot MCO or the Southern 11-foot MCO, the response of the outside sensor has a higher sensitivity in the lower compliance region which makes it a more desirable candidate since track with low compliance is of greater interest. For the center sensor configuration, the higher nonlinear response makes it relatively ineffective for compliance or stiffness measurements.

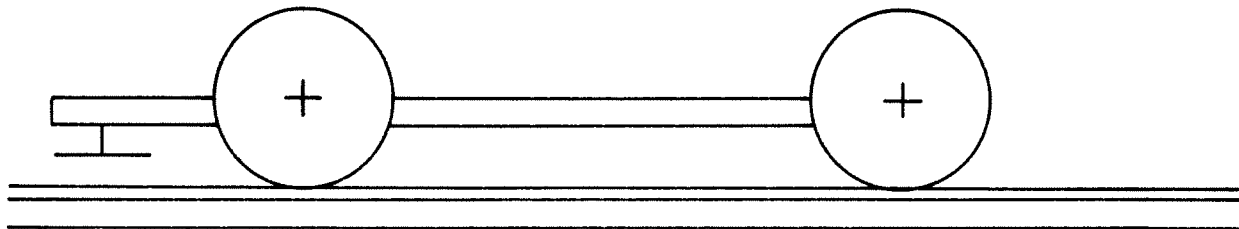
D.1.2 APPLICATION TO KANSAS TEST TRACK DATA

After validation, the Mode 1 processing technique was used to reprocess the KTT data to obtain track compliance information. Since the KTT is made up of nine sections which are constructed on uniform foundations, it is meaningful in this computation of track compliance or stiffness to work initially with whole section averages. Furthermore, since the Waterways Experimental Station had also made stiffness measurements on the KTT, a comparison of these whole section averages with the WES results provided a good means for gaining confidence in the reliability of the proposed stiffness measurement technique.

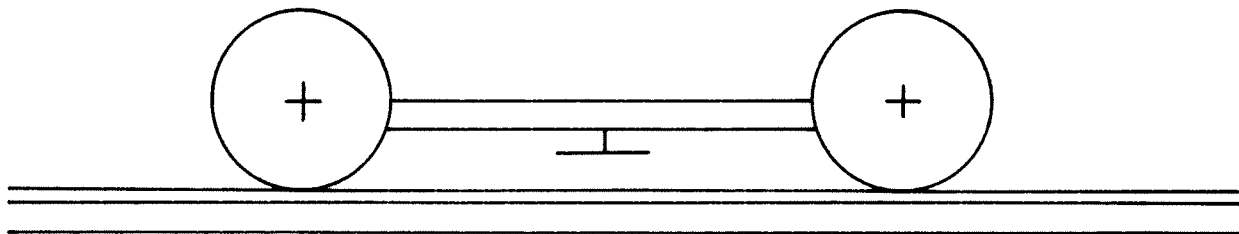
Figure D-2 shows the compliance results obtained using front and rear sensors for several different measurement passes. It is clear that the computed values for track compliance are all consistent. In Figure D-3, averages for all the passes are plotted against the experimental WES results.



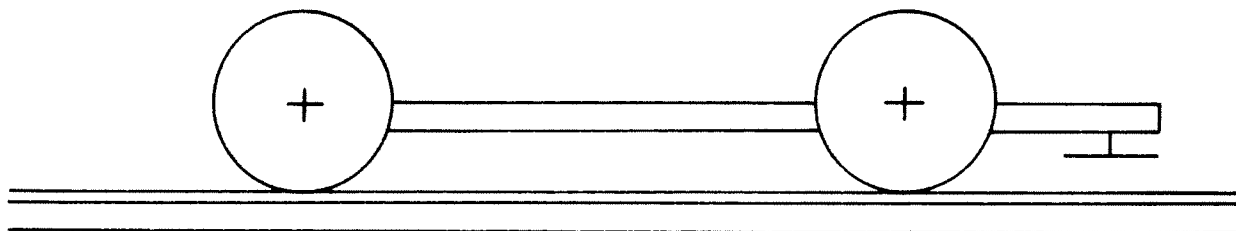
a) SENSOR CONFIGURATION & HEIGHTS MEASURED AND INCORPORATED IN FRA T-3 MCO.



b) EFFECTIVE CONFIGURATION WHEN USING FRONT SENSORS AND WHEELS AS SENSORS FOR CHORDAL MEASUREMENTS.



c) EFFECTIVE CONFIGURATION WHEN USING CENTER SENSORS AND WHEELS AS SENSORS FOR CHORDAL MEASUREMENTS.



d) EFFECTIVE CONFIGURATION WHEN USING REAR SENSORS AND WHEELS AS SENSORS FOR CHORDAL MEASUREMENTS.

Figure D-1. Sensor Configuration for T-3 MCO and Chordal Alternatives When Wheels are Used as Sensors

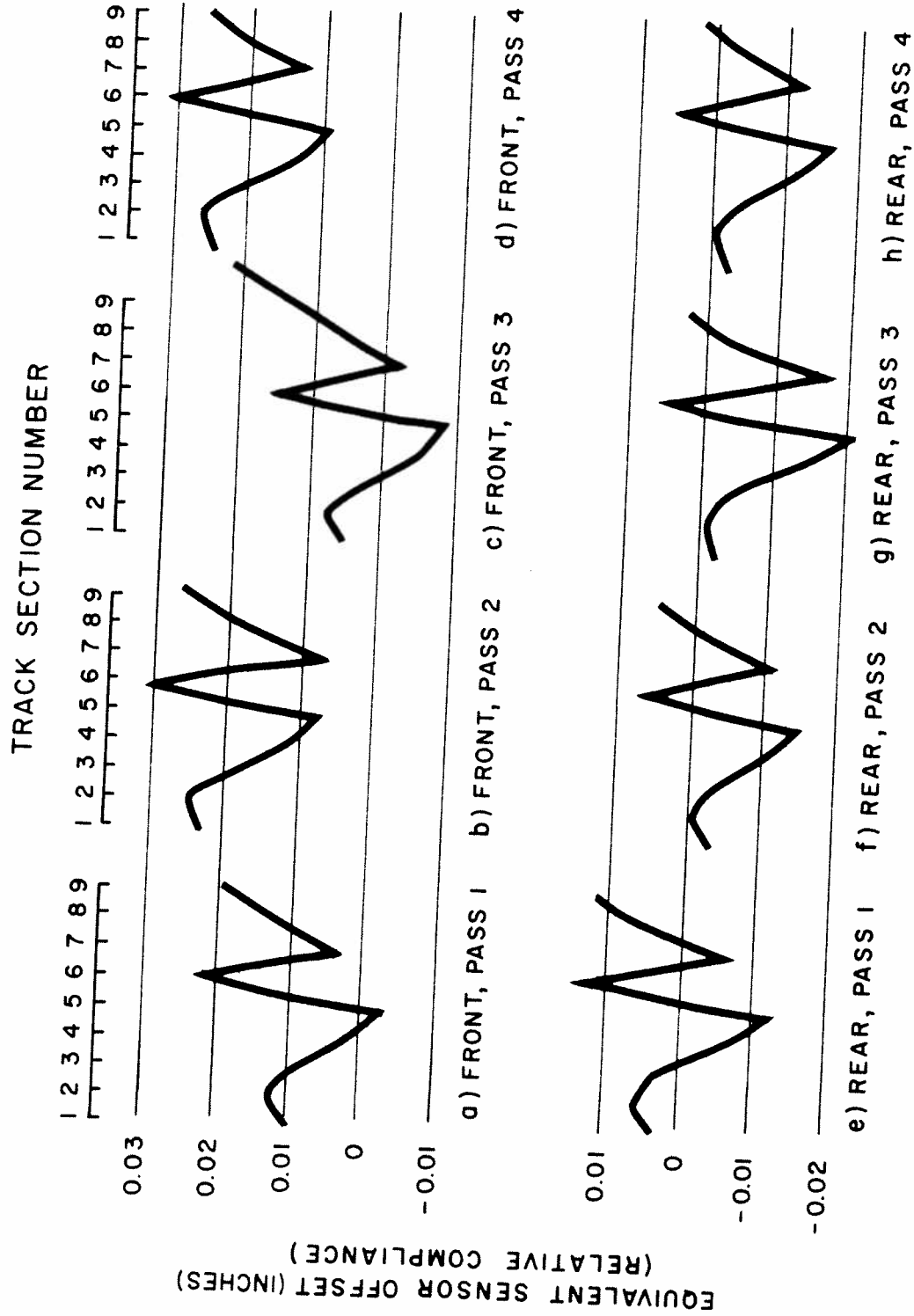
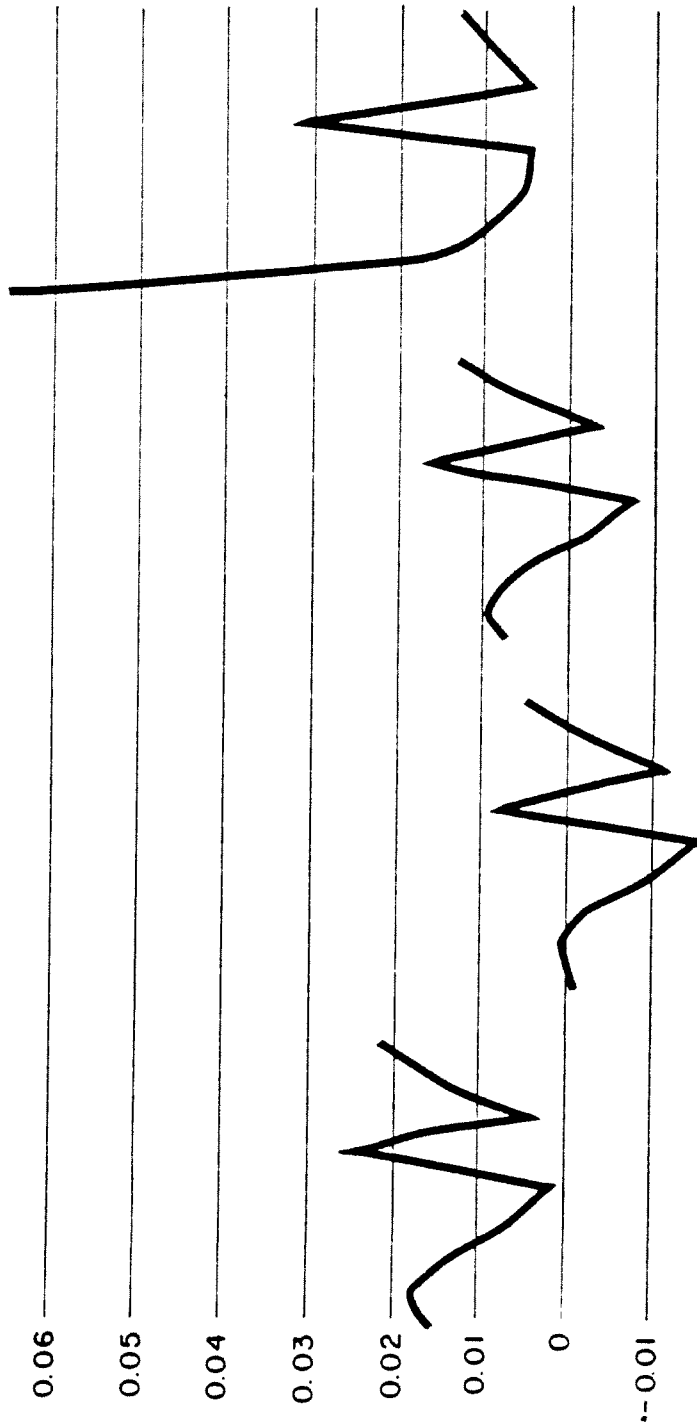


Figure D-2. Comparison of Compliance Values Obtained for Various Passes on the Kansas Test Track.

TRACK SECTION NUMBER

1 2 3 4 5 6 7 8 9 1 2 3 4 5 6 7 8 9 1 2 3 4 5 6 7 8 9

EQUIVALENT SENSOR OFFSET (INCHES)
(RELATIVE COMPLIANCE)



- i) AVERAGE FOUR PASSES FRONT
- j) AVERAGE FOUR PASSES REAR
- k) AVERAGE FOUR PASSES FRONT AND REAR
- l) WES DATA (6)

Figure D-3. Comparison of Average Compliance Values With WES Data on the Kansas Test Track

Figure D-2 shows that except for Section 1, the general shape of the computed compliance curves agree well with the experimental results. It should be noted that the WES data were obtained prior to the opening of the KTT, whereas the sensor data were taken after the KTT had experienced tonnage-included compaction. This is particularly important in the case of Section 1, which was an extensive fill area.

D.2 PHASE II

D.2.1 GENERAL

Accelerometers and displacement transducers were mounted on the instrumented truck of Southern Railroad Research Car R-1. The R-1 was used to take advantage of its three-axle trucks and cylindrical wheels. The analog signals generated by the instrumentation were cabled directly to the signal conditioning electronics aboard T-7. The signals were then recorded in digital form on magnetic tape using a computer-based data acquisition system. The 15 channels of collected data included six accelerometers, eight displacement transducers and one crosslevel signal. Time-between-scans, automatic location detector information, milepost numbers and message unit numbers were also recorded in the scan header. Figure D-4 is a block diagram of the data acquisition system. The locations of the instrumentation mounted on R-1 are shown in Figure D-5.

The instrumentation can be divided into the following groups:

- Primary
- Secondary
- Supplementary

The primary instrumentation consisted of the equipment required to collect and process the data needed to determine vertical track stiffness. This included:

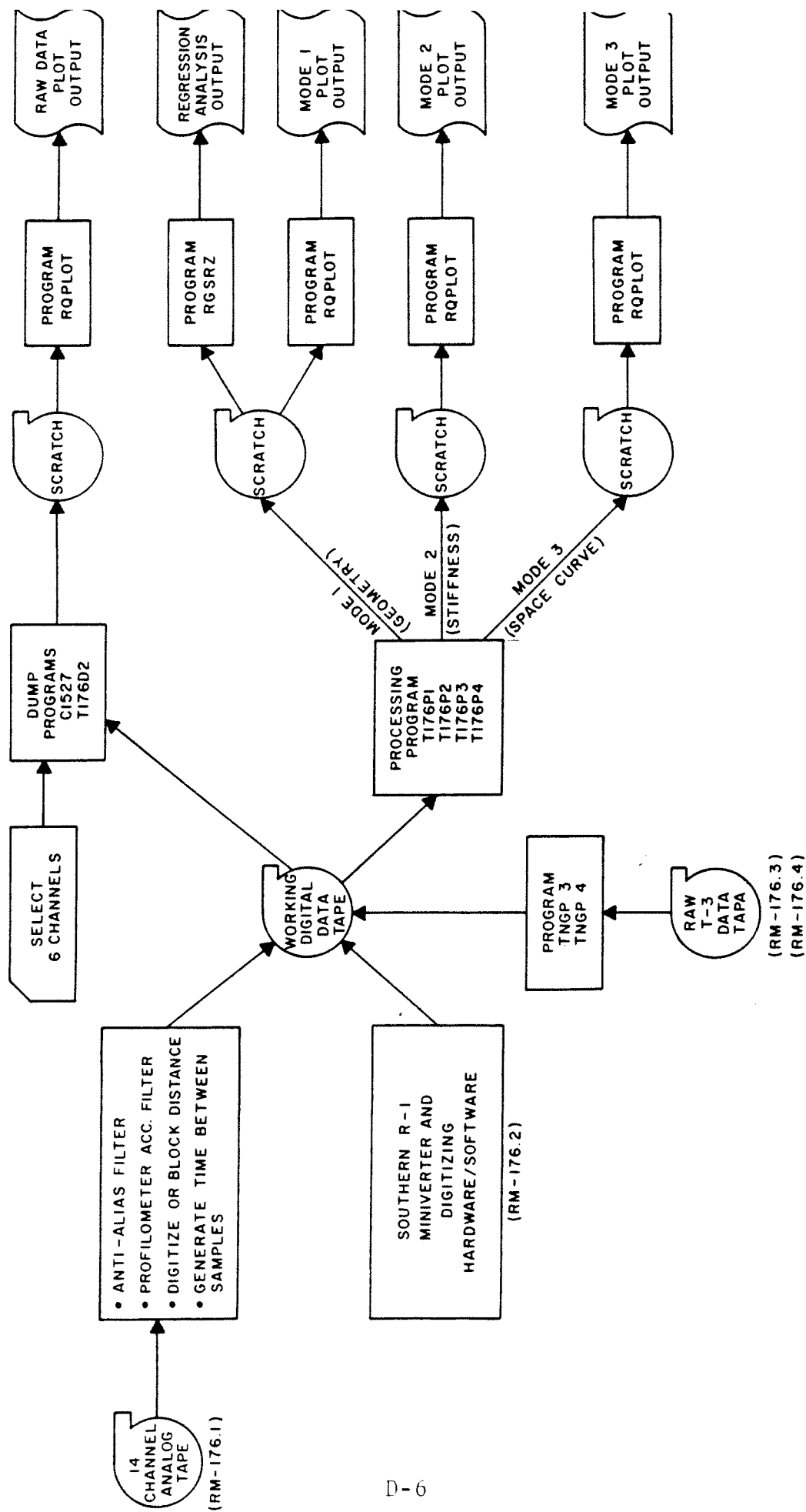


Figure D-4. Data Acquisition System--Block Diagram

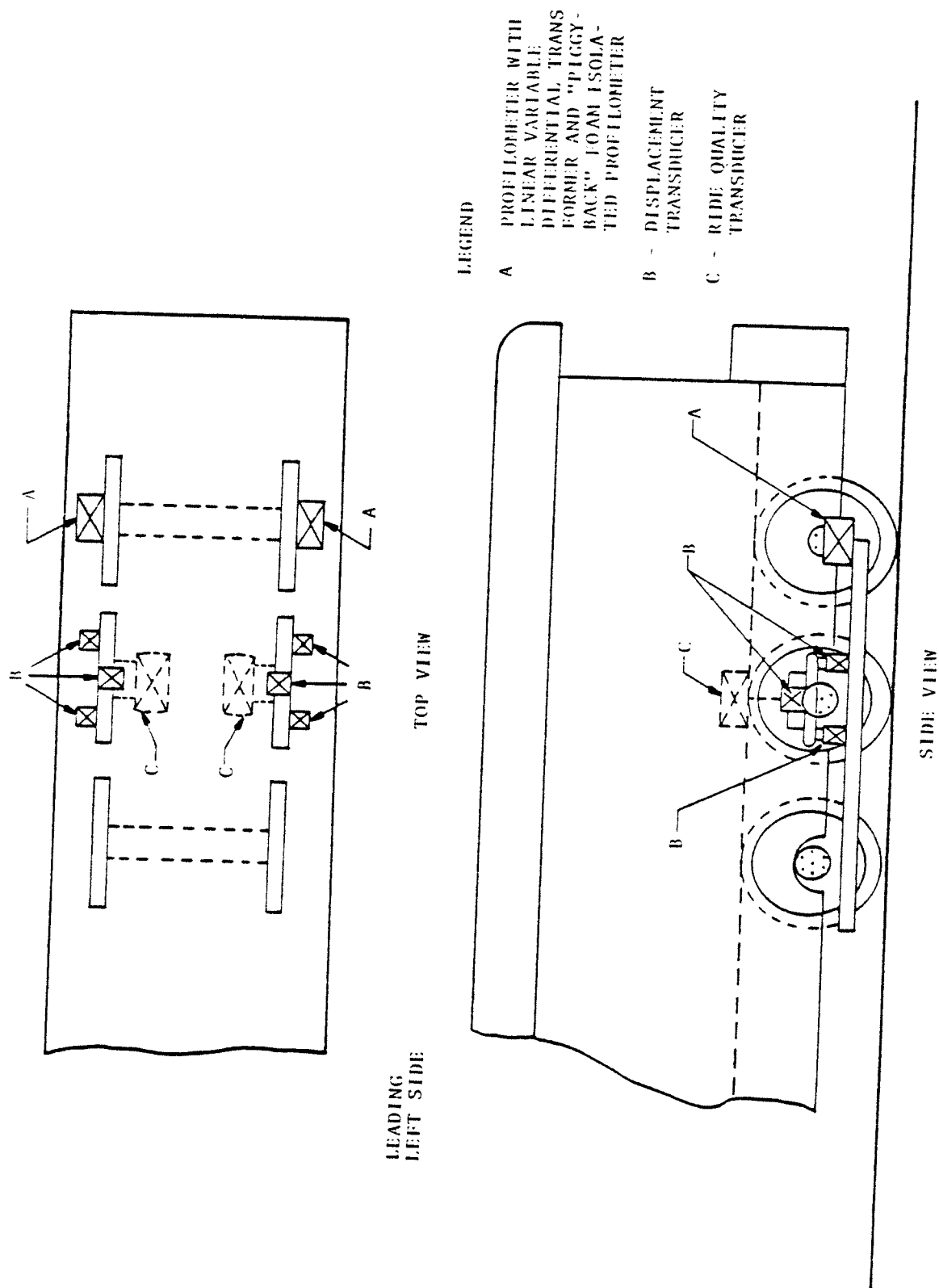


Figure D-5. Location of Test Instrumentation

- Four modified string-pot displacement transducers mounted on the instrumented truck of R-1 to collect 11-foot, mid-chord-offset measurements.
- Two inertial profilometers to measure track profile.
- The beam system on R-1 to measure cross-level and compensate for accelerometer inputs due to gravitational accelerations experienced on non-tangent track.
- Signal conditioning electronics to receive signals from the transducers, reduce noise, and provide proper signal levels to the analog-to-digital converter.
- The data acquisition system on T-7 to filter, digitize and record the conditioned signals.
- Cables, connectors, brackets, mounting plates and hardware.

The secondary instrumentation consisted of two piggy-backed profilometer systems which operated simultaneously with the primary system and were being independently tested for feasibility:

- A carbody profilometer system which consisted of displacement transducers connected between the carbody and the central-axle, journal bearing; and linear-ride-quality accelerometers located directly over the central axle as shown in Figure D-5.
- A foam isolated profilometer mounted with the primary profilometer on the rear axle of the instrumented truck as shown in Figure D-5.

The supplementary instrumentation included:

- The communications system between T-7, R-1 and the forward observer.

- Surveying equipment to measure static track-deflection (mid-chord-offset bias) which is required in the determination of absolute stiffness.

D.2.2 PRIMARY INSTRUMENTATION

D.2.2.1 Measurement of 11-Foot Mid-Chord Offset

The truck under the vestibule-end of R-1 is equipped on each side with a rigid beam attached to the journal boxes of the leading and trailing axles. The beam has a triangular cross section for maximum stiffness. Eleven-foot, mid-chord offset is measured by measuring the distance from the beam to the center of the middle axle.

Clearance problems made it impossible to attach a displacement transducer to the journal box over the center of the middle axle. It was necessary to use a pair of transducers, one on either side of the axle, to eliminate errors caused by the journal box shifting between the pedestal liners. The outputs of the paired transducers were recorded separately and averaged together during post-test, data processing.

Several modifications were made to the standard transducer design to bring its accuracy within the 0.02 inches required for this test. Special potentiometers were used which were screened for better than 0.1 percent linearity. The bearings chosen were of an improved type and grooves were machined into the take-up spool to prevent the wire from wrapping over itself and thereby changing the diameter of the spool. A resistor network was added to derive a differential signal at the output.

D.2.2.2 Track Profile Measurement

Two inertial profilometers (the same type used on Track-Geometry-Measurement Car T-6) were attached to the journal boxes on either side of the rear axle of R-1 (the axle nearest to the vestibule end).

Inside each profilometer, a fluid-damped, 10 g, servo-accelerometer (Terra Technology SA102-10) was mounted on a suspended mass; the mass acts as an inertial reference when deviations in track profile are small. In this case, a displacement transducer (linear variable differential transformer, Schaevitz LVDT Model 1002XS) was used to measure the displacement of the mass relative to the journal box. In the presence of larger inputs from the track, the output of the accelerometer was used to measure the extent of the deviation from a true inertial reference.

D.2.2.3 Crosslevel Measurement

The crosslevel signal was required to compensate for accelerometer inputs due to gravitational acceleration experienced on non-tangent track. This signal, produced by standard equipment on the R-1 car, was derived from carbody tilt relative to a reference furnished by a gyroscope compensated for track and speed irregularities between 5 and 80 mph.

D.2.2.4 Signal Conditioning

To keep noise levels low, displacement transducer signals were routed to a differential amplifier and then to a second stage where zero position and gain could be set during pre-test calibration. Scale factors are listed in Tables D-1 and D-2.

The linear-variable-differential transformer in the profilometer produced a voltage output proportional to the position of its primary coil. An oscillator/demodulator circuit was used to provide the necessary excitation and gain adjustment.

Accelerometer signals were transmitted in the current mode. At the signal conditioning chassis, these signals were converted to voltage signals and then routed through a two-pole, low-pass active filter ($f_c = 0.4$ Hz). The filter double-integrated the signals above the corner frequency and produced

TABLE D-1
FIELD CALIBRATION SUMMARY (22 AUGUST 1977)

ASSIGNED CHANNEL	CALIBRATION NUMBER				PERCENT STANDARD DEVIATION
	1	2	3	AVERAGE	
	SCALE FACTOR (VOLTS/INCH)				
No. 2 LVDT, Left at 0.994 Inch	7.98	7.96	7.97	7.97	0.1
No. 3 LVDT, Right at 0.991 Inch	7.90	8.07	8.07	8.01	0.4
No. 6 Carbody, Left at 1.665 Inch 2.451 Inch	3.98 3.99	3.93 3.96	3.96 3.95	3.96	0.4
No. 7 Carbody, Right at 1.665 Inch 2.451 Inch	3.98 3.99	3.97 3.97	3.96 3.98	3.98	0.2
No. 10 MCO-A Left at 1.665 Inch 2.451 Inch	4.01 4.00	3.97 3.98	4.00 3.97	3.99	0.4
No. 11 MCO-A Right at 1.665 Inch 2.451 Inch	4.02 4.04	4.02 4.01	3.99 4.00	4.01	0.4
No. 12 MCO-B Left at 1.665 Inch 2.451 Inch	3.99 4.01	4.01 4.00	3.98 3.98	4.00	0.3
No. 13 MCO-B Right at 1.665 Inch 2.451 Inch	4.01 3.98	4.02 4.00	3.99 3.97	4.00	0.4

a displacement output. The filter served a dual purpose by attenuating high frequencies so that low-frequency gain could be higher. This improved resolution at low frequencies without sacrificing dynamic range.

Regulated power supplies were used to provide required power for the transducers and the electronics.

TABLE D-2
FIELD CALIBRATION SUMMARY (26 AUGUST 1977)

ASSIGNED CHANNEL	CALIBRATION NUMBER				PERCENT STANDARD DEVIATION
	1	2	3	AVERAGE	
	SCALE FACTOR (VOLTS/INCH)				
No. 2 LVDT, Left at 0.994 Inch	8.10	7.95	8.02	8.02	0.8
No. 3 LVDT, Right at 0.991 Inch	7.61	7.59	7.66	7.62	0.4
No. 6 Carbody, Left at 1.665 Inch 2.451 Inch	3.97 4.00	3.94 3.97	4.01 3.98	3.98	0.6
No. 7 Carbody, Rt. at 1.665 Inch 2.451 Inch	3.99 4.02	4.02 4.02	3.99 3.99	4.00	0.4
No. 10 MCO-A Left at 1.665 Inch 2.451 Inch	4.03 4.00	3.98 4.01	4.00 4.00	4.00	0.4
No. 11 MCO-A Right at 1.665 Inch 2.451 Inch	4.04 4.04	4.02 4.04	4.02 4.03	4.03	0.2
No. 12 MCO-B Left at 1.665 Inch 2.451 Inch	4.04 4.04	4.00 4.03	4.01 4.01	4.02	0.4
No. 12 MCO-B Right at 1.665 Inch 2.451 Inch	4.02 4.00	4.03 4.02	3.99 3.97	4.00	0.5

D.2.2.5 T-7 Data Acquisition System

The conditioned analog signals were anti-alias filtered by four-pole, low-pass, Bessel-function filters with their corner frequency set at 100 Hz. The filtered signals were routed to a 12-bit Hewlett-Packard A/D converter for analog to digital conversion.

The T-7 digital interface was modified to change the data sampling interval from a time base to a distance base. One sample was taken every six inches of travel. The sampling interval was controlled by a tachometer signal routed to the speed and distance unit. The sampled data were then recorded on magnetic tape for subsequent processing.

Several other signals were recorded in the scan header with each sample: time-between-samples, automatic location detector information and milepost and message-unit numbers. The time between each sample, counted by a register in the digital interface unit, is necessary to relate the distance-sampled data to the speed at which it is acquired. The ALD aboard T-7 is a metal detector; it was adjusted to respond only to large metal objects between the rails. Metal targets are usually placed to provide reference locations but the presence of frequent switches and turnouts through the test zone, to which the detector also responds, made special targets unnecessary. The T-7 data acquisition system also provides for milepost numbers to be entered into the scan header via a remote milepost entry box. Special events such as road crossings and bridges were recorded in the handwritten log and indexed on the magnetic tape by entering the appropriate message number at the T-7 digital interface unit.

As a partial check on the integrity of the recording system, selected channels of the incoming digital data were reconverted to analog form by the digital-to-analog converter and displayed on a six-channel analog chart recorder. The digital-to-analog system also allowed recorded data to be monitored during playback.

D.2.2.6 Cables

The cables were multi-pair and individually shielded by aluminum-mylar foil. They were fabricated from No. 22AWG stranded conductors with polypropylene insulation and a chrome-vinyl jacket. The cables were terminated with carefully potted connectors at the transducers aboard R-1 and were run directly to receptacles at the signal conditioning chassis on T-7.

D.2.3 SECONDARY INSTRUMENTATION

D.2.3.1 Carbody Profilometer

In this system, the body of the car is used as an inertial reference similar to the function of the mass inside the type of profilometer used on T-6. Two modified displacement transducers, one on each side of the car, were attached between the middle axle of the instrumented truck and the carbody to serve the same function as an LVDT. In order to measure vertical accelerations on the carbody mass, two linear ride quality sensors were secured to the floor of R-1 over the middle axle, one sensor on each side of the car.

The displacement transducer signals and the accelerometer outputs were conditioned just as in the primary system. The accelerometer in the linear ride quality sensors is a fluid damped, 1.0g servo-accelerometer (Schaevitz LSVCS-1).

D.2.3.2 Foam Isolated Profilometer

Frequent high-amplitude, high-frequency accelerations present in the structural vibration of the vehicle are potentially damaging to accelerometers. When track profile or track stiffness data are being collected, these accelerations are of little interest. Through special mounting techniques, it is possible to attenuate these high frequencies, thus allowing the use of more sensitive accelerometers in an environment that would

otherwise saturate or destroy them. For example, the suspension of the inertial mass performs this function in a T-6 profilometer. The carbody suspension isolates the accelerometers of a carbody profilometer system.

Foam isolated profilometers were fastened to the profilometer brackets at the axle nearest the vestibule of R-1. Each foam-isolated profilometer employed open-cell, polyurethane foam in a specially designed enclosure to interpose a mechanical filter between the structural accelerations being measured and the servo-accelerometer. The filter attenuated frequencies above 150 Hz by approximately 12dB per octave. The servo-accelerometer was identical to that used in the T-6 profilometer (Terra Technology SA-102-10) and its current output was conditioned in the same way as the output of the accelerometers in the primary instrumentation.

D.2.4 SUPPLEMENTARY INSTRUMENTATION

D.2.4.1 Communications

The forward observer in the locomotive cab was provided with a microphone and headset which were cabled to the public address system on T-7 to maintain communication between the observer and the data acquisition crew. Communication between R-1 and the locomotive was maintained by the conductor who was in contact with the engineer via two-way radio. There was no radio or telephone communications between T-7 and R-1. Communication between these vehicles, when necessary, was via a message carried by a crew member.

D.2.4.2 Static Displacement Survey

A surveyor was hired to make the static displacement measurements which were required in the determination of absolute stiffness.

The measurements were made using a Wild-Heerbrugg N10 engineer's level; the procedure used was as follows:

- Both the wheels and the rail, on one side of the instrumented truck on R-1, were marked with chalk at the three points of contact.
- The entire consist was moved down the track until it was at least 30 feet past the measurement points, thus leaving the track unloaded.
- A special tool was used to make a scribe mark an equal distance below the rail head at each contact point.
- The engineer's level was adjusted to establish a reference horizontal plane and then a ruler was used to measure the position of the scribe mark relative to the horizontal plane. Unloaded mid-chord offset was calculated from these measurements.
- The train was then repositioned to align the chalk marks and mid-chord-offset measurements were made with the engineer's level, a stringline across the journal boxes and with the electronics.
- The procedure was then repeated for the wheels and the rail on the opposite side of the instrumented truck.

After the first survey, the static measurement procedure was modified to eliminate the need for scribe marks below the rail head and to increase accuracy; the measurement of unloaded, mid-chord-offset and the stringline measurement were also deleted.

On the first survey, a wooden folding rule was held against the scribe marks for the surveyor to use in sighting. In the modified procedure, a bubble level was placed against the bottom surface of the wheel extending over the rail. The level established the wheel/rail interface and served as a platform to

support a ruler against the wheel. At the direction of the surveyor, the ruler was marked with a fine point (0.015 inch wide). This mark defined the intersection of the rule with the horizontal reference plane. Three marks were made on each ruler, one for each wheel on the side of the instrumented truck being tested. These three points were accurately measured using a dial caliper and the measurements were used to calculate mid-chord offset. This procedure was repeated at least twice on each side of the instrumented truck.

The actual implementation of this static displacement was less than optimal. The purpose was to measure accurately the static displacement of the mid-point of the triangular beam. The accuracy required was not obtained and consequently the absolute mid-chord-offset of the beam could not be calculated. Without the absolute MCO measurement, the absolute stiffness measurement could not be accomplished. The relative stiffness of the track system was measured.

D.2.5 TRACK STIFFNESS SYSTEM CALIBRATION

D.2.5.1 General

Prior to field use, the signal conditioning electronics, the transducers and the field calibration techniques were tested in the laboratory so that scale factors, linearity and frequency response could be accurately determined. The inertial profilometer and the displacement transducers were also calibrated several times a day during the field tests to monitor variations in scale factors. After the field test was completed, the instrumentation was returned to the laboratory for a final check.

D.2.5.2 Displacement Transducers

The displacement transducers and the linear variable differential transformers on the profilometer were tested for linearity on a milling machine graduated in thousandths of an inch. The displacement of the mill and the voltage output of the signal

conditioning electronics were recorded as each transducer was operated over its range. Great care was exercised to minimize errors due to vertical misalignment and backlash in the gears of the mill.

Errors due to non-linearity in the transducers were less than 0.015 inch which is better than the required 0.020 inch in all but two cases. The exceptions were the No. 2 LVDT in the right profilometer and displacement transducer No. 3-106 (right carbody displacement). In each case, the accuracy of the transducer was within tolerance over 75 percent of its full range. The twin constraints of the test schedule and the fact that spare parts were not readily available prevented replacing these transducers before the test.

Field calibrations were performed to check the gain of each displacement transducer channel. The string pot displacement transducers were calibrated by wrapping the wire around a rod of known diameter. The output of the signal conditioning electronics was then recorded in a hand-written log and on magnetic tape. Calibration of the scale factor from this information takes into account the effect of the thickness of the wire.

The LVDT in the profilometer was calibrated in the field by moving a metal rod, screwed into the inertial mass, to each end of a slot. The output of the signal conditioning electronics was recorded at each position. To complete the profilometer calibration, the inertial mass was moved up and down vigorously and randomly while a speed signal representing 30 mph was simulated. During this dynamic calibration, the servo-accelerometer signals, the LVDT signals and the speed signal were recorded on magnetic tape for at least 60 seconds. Post-test processing applied to these signals, including fast Fourier transform, provided comparison of frequency spectra for gain and phase information.

The results of field calibration are listed in Tables D-1 and D-2. Variations in scale factor were less than one percent from one calibration to the next.

D.2.5.3 Accelerometers

The accelerometers were tested in the laboratory under static and dynamic conditions without the signal conditioning electronics. The resonant frequency of each foam isolator was also measured.

Gravitational acceleration was used to calibrate the scale factors of the accelerometers. Each accelerometer was placed on a level surface with its sensitive axis vertical. The output of the accelerometer was recorded in this position and again after turning the accelerometer through 180 degrees so that it was upside down on the same surface. The scale factors measured in this fashion were within 0.5 percent of the manufacturer's specification. To test dynamic operation, each accelerometer was mounted on a shaker table and its output was compared with the output of a reference piezo-electric-crystal accelerometer. Frequency response was plotted over the range from 25 to 60 Hz to check corner frequency. A spectral analysis was made and the waveform was monitored by oscilloscope to detect any distortion.

One accelerometer failed post-test calibration. Output from this unit, serial number 342 in the right foam-isolated profilometer, stopped suddenly after the interlock near MP 65 during the return trip.

A broken suspension wire inside the accelerometer was identified as the source of the problem. All the other accelerometers operated normally during post-test calibration.

The signal conditioning electronics for each accelerometer were tested in the laboratory to check the corner frequency of the filter associated with each profilometer and to measure the gain of each channel. The frequency response of each channel was plotted between 0.1 and 1.0 Hz. In each case, the corner frequency was close to 0.45 Hz, as expected.

The d-c gain measured in each case is listed in Table D-3. Prior to August 26th, the gains were adjusted to be nearly equal. After reviewing the data collected on August 22nd, the gain of the accelerometers in the two secondary systems was reduced to avoid possible saturation problems.

The low-pass characteristics of the foam isolators, used on the secondary system, were checked by performing a shock test on each unit. With a piezo-electric-crystal accelerometer attached to the servo-accelerometer inside the isolator, this system was subjected to an impulse of acceleration. A solid steel ball, suspended from the ceiling, was allowed to swing and strike one end of a solid steel cylinder which was suspended in the same manner. The unit under test was mounted on the opposite end of the cylinder as shown in Figure D-6.

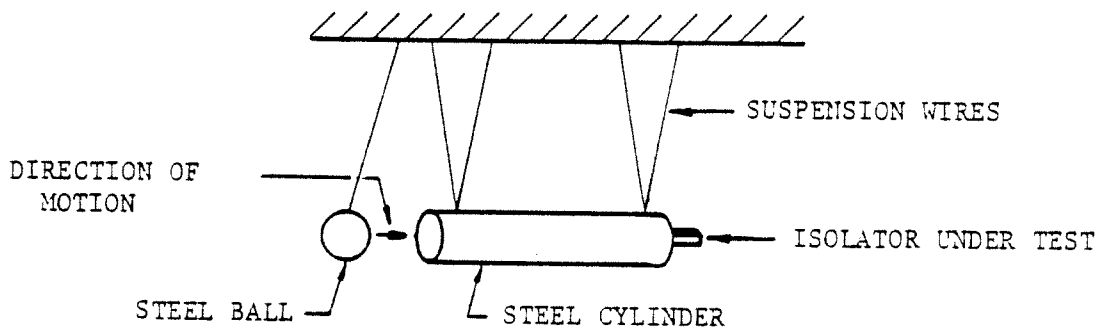


Figure D-6. Shock Test Assembly

The resonant frequency, which corresponds to the corner frequency, was recorded on polaroid film as the output of the piezo-electric transducer made a trace across an oscilloscope screen.

Initially, three isolators were tested. They were found to have resonant frequencies of 133, 90, and 112 Hz, respectively. Although it had no adverse effect on accelerometer data, it should be noted that the second isolator showed a much higher corner frequency (145 Hz) during post-test calibration. Since the initial corner frequency was lower than normal, it is possible that some of this difference could be attributed to additional hardening of the glue that held the foam.

TABLE D-3
ADJUSTED GAINS
ACCELEROMETER-SIGNAL-CONDITIONING ELECTRONICS

ASSIGNED CHANNEL	ADJUSTED GAIN (8/19/77)	ADJUSTED GAIN (9/7/77)
No. 1 Left Profilometer Accelerometer	159.7	155.9
No. 2 Right Profilometer Accelerometer	165.1	165.0
No. 5 Left Linear-Ride-Quality Accelerometer	150.1	15.6*
No. 6 Right Linear-Ride-Quality Accelerometer	150.0	15.6*
No. 9 Left Foam-Isolated-Profilometer Accelerometer	160.0	79.4*
No. 10 Right Foam-Isolated-Profilometer Accelerometer	160.2	78.5*

*Gains for accelerometers in the two secondary instrumentation systems were reduced after review of the data collected on 22 August 1977 to avoid possible saturation problems.

D.3 PHASE III

D.3.1 INSTRUMENTATION AND ELECTRONICS

The third phase instrumentation was identical to the second phase instrumentation except for the omission of the piggy-back profilometer systems. All calibration information was essentially the same. The same transducers used in the second phase were utilized in the third phase. For specific information, refer to Section D.2.

REPRODUCED FROM THE NATIONAL ARCHIVES AT COLLEGE PARK, MARYLAND